

Conceptual Design of High Temperature Superconducting Toroidal Field Coils for Future Fusion Power Plants

Zur Erlangung des akademischen Grades eines
DOKTOR-INGENIEURS
von der KIT-Fakultät für
Elektrotechnik und Informationstechnik
des Karlsruher Instituts für Technologie (KIT)
genehmigte

DISSERTATION

Von

M.S. Pattabhi Vishnuvardhan Gade

geb. in: Jamshedpur, India

Tag der mündlichen Prüfung: 25.07.2019
Hauptreferent: Prof. Dr.-Ing. Mathias Noe
Korreferent: Prof. Marco Breschi

TO MY LATE *MOTHER* GADE MADHAVI

Acknowledgments

I am immensely thankful for this dissertation to the help and support of my seniors, colleagues and associated staff members of the Institute for Technical Physics (ITEP) of the Karlsruhe Institute of Technology (KIT). The time spent at the institute has been very gratifying and it enabled me to learn and improve upon my scholarly skills.

At the outset, I would like to heartily thank my principal supervisor, Prof. Dr.-Ing. Mathias Noe, for trusting me and providing the necessary support to overcome the ordeal of untimely demise of my mother and ensuing health problems. His guidance and support has been instrumental in overcoming all odds culminating in the fruitful completion of my study. I extend my gratitude to Dr. R Heller, who not only guided me academically, but also provided support and guidance on a personal level. I am also ever thankful to Dr. W. H. Fietz for his support and guidance during the course of theoretical studies and technical papers. I express my special gratitude to Dr. Klaus-Peter Weiss for showing compassion and providing necessary academic assistance to further the dissertation process.

I further extend my heartiest thanks to all my friends/colleagues at KIT for both professionally and on a personal level, during the course of my dissertation.

Kurzfassung

Aus der langjährigen Forschung im Bereich der magnetischen Eingrenzung sind Stellaratoren und Tokamaks entstanden, die starken und ungleichmäßigen Magnetfelder zum Einfangen der Plasmapartikel nutzen und es ihnen ermöglichen, sich frei auf bestimmten Wegen zu bewegen. Die Tokamaks haben durch ein einfacheres Spulendesign, verschachtelte magnetische Oberflächen und die Fähigkeit, mit positiver magnetischer Scherung zu arbeiten, an Bedeutung gewonnen. Derzeit plant die Europäische Union (EU), ihre Studien über Tokamak auf Demonstrationskraftwerke (EU-DEMO) auszudehnen, die Strom erzeugen können. Ziel dieser Studie ist es, ein Konzept für die Ringkernfeldspule (TF-Spule) für zukünftige Kraftwerke mit dem Systemcode PROCESS zu entwickeln. Ziel dieser Studie ist es, ein Konzept für die Toroidalfeldspule (TF-Spule) für zukünftige Kraftwerke mit dem Systemcode PROCESS zu entwickeln.

Der PROZESS-Code gibt bestimmte Informationen wie die ungefähre Form der TF-Spule, die Fläche des Wickelpakets, das Magnetfeld an der Plasmaachse. Ausgehend vom Eingang wird das Wickelpaket der TF-Spule entworfen. Zum Beispiel, wenn die Pancake-Wicklung gegenüber der Lagen-Wicklung bevorzugt wird. Zum Beispiel, wenn die Pancake-Wicklung gegenüber der Lagen-Wicklung bevorzugt wird. Die erste Lage, die der Plasmawärme zugewandt ist, wird angesammelt, da sie sich im Hochfeldbereich befindet, wodurch der Magnet mit einer geringeren Betriebsmarge arbeitet. Der Leiter der Pancake-Wicklung ist jedoch in Umfangsrichtung und nicht entlang der Achse eines Magneten gewickelt und jedes Modul ist separat gewickelt und elektrisch in Reihe geschaltet. Der wesentliche Vorteil bei diesem Verfahren ist, dass die Temperatur im Hochfeldbereich am niedrigsten ist, da sich der Heliumeinlass im Hochfeldbereich des Wickelpakets und der Auslass im Niederfeldbereich befindet. Das Wicklungspaket mit der elektrischen Schaltung ist in Reihe geschaltet und die hydraulische Schaltung ist parallel geschaltet.

Aus dem PROZESS-Code wird überprüft, ob das Magnetfeld an der Plasmaachse gleich dem erforderlichen Magnetfeld ist. Das Spitzenmagnetfeld wird auch zur Bestimmung des Arbeitspunktes des Leiters berechnet. Die 3D Elektromagnetische Simulation wird mit dem Präprozessor TOKEF und dem Code EFFI durchgeführt. Codes zur Magnetfeldberechnung einer allgemeinen dreidimensionalen Stromverteilung, die

Formulierungen verwenden, die auf einer fadenförmigen Annäherung und der endlichen Leitergröße basieren. Diese Codes werden durch eine Reihe von verteilten Filamenten unter Verwendung der EFFI-Formel, die aus dem Bio-Savart Gesetz für die Volumenstromverteilung abgeleitet wurde, approximiert.

Die Statik der TF-Spule bestimmt die Spannungen im Spulengehäuse und im Wickelpaket. Der Bereich mit den höchsten Spannungen liegt in der Mittelebene des inneren Schenkels, was durch eine ähnliche Analyse mit dem Spulenmagnetsystem JT-60SA TF bestätigt wird. In der EU DEMO führt die TF-Spule hohe Ströme (in MA) und erzeugt hohe Felder. Die TF-Spule ist daher hohen magnetischen Drücken und Kräften ausgesetzt. Um die Spannungen im Wickelpaket und am Gehäuse zu untersuchen, werden in COMSOL und ANSYS verschiedene Methoden zur Analyse der Spannungen am Gehäuse, des Lösens des Wickelpakets und der Spannungen in Isolationsbauteilen betrachtet.

Ein wichtiger Fehler, der bei der Konstruktion supraleitender Magnete zu berücksichtigen ist, ist der Übergang von der supraleitenden zur normal leitenden Phase, dem sogenannten Quench. Da im normal leitenden Modus der elektrische Widerstand des Supraleitermaterials hoch ist, erzeugt die Einführung von Kupfer als elektrischer Ableiter für den Stromfluss eine Joule-Erwärmung. Der Magnet muss durch Anschluss eines externen Widerstandes parallel zum Magneten entladen werden, um einen übermäßigen Temperaturanstieg zu vermeiden. Die maximal zulässige adiabatische Hotspot-Temperatur, wie sie vom International Thermonuclear Experimental Reactor (ITER) festgelegt wurde, ist auf 150 K begrenzt, wobei alle Materialien im Leiter berücksichtigt werden, d.h. Supraleiter, Kupfer, Helium, Edelstahlmantel und Isolierung. Um die Quenchausbreitung zu simulieren, wird eine externe Heizung in den Supraleiter eingesetzt und überprüft, wie die Ausbreitung ist und welche maximale Temperatur sie während der Entladungszeit erreicht.

Abstract

Sustained research in magnetic confinement has given rise to Stellarators and Tokamaks, which utilise strong and non-uniform magnetic fields for trapping the plasma particles and enables them to move freely along specified paths. The Tokamaks have gained prominence due to simpler coil design, nested magnetic surfaces and ability to operate with positive magnetic shear. Currently, European Union (EU) is planning to extend its studies on Tokamak towards demonstration powerplant (EU-DEMO) that can generate electricity. The aim of this study is to develop a conceptual design for the toroidal field coil (TF coil) for future power plants using PROCESS system code.

The PROCESS code gives certain output like, the approximate shape of TF coil, area of winding pack, magnetic field at plasma axis. From the input, winding pack of the TF coil is designed. For example, in case where pancake winding is preferred over the layer winding. The first layer facing plasma heat is accumulated since it is in high field region, as a result of which, the magnet operates at lower operating margin. However, the conductor of pancake winding is wound in a circumferential direction rather than along the axis of a magnet and each module is wound separately and jointed electrically in series. The basic advantage in this method is that the temperature is lowest in the high field region since the helium inlet is located in the high field region of the winding pack and the outlet at the low field region. The winding pack comprising the electrical circuit is connected in series and hydraulic circuit is connected in parallel.

From the PROCESS code it is checked whether the magnetic field at plasma axis is equal to the required magnetic field. The peak magnetic field is also calculated for defining the operating point of the conductor. 3D Electromagnetic simulation is carried out using the pre-processor TOKEF and the code EFFI. Codes for magnetic field calculation of a general three-dimensional current distribution, that use formulations based on a filamentary approximation and the conductor finite size. These codes are approximated by set of distributed filaments using EFFI formula derived from Bio-Savart law for volume current distribution.

The structural analysis of the TFC determines the stresses in the coil casing and in the winding pack. The area with the highest stresses occurs in the midplane of the inboard leg that is confirmed by a similar analysis done with the JT-60SA TF coil magnet system. In EU DEMO, the TFC carries high currents (in MA) and produces high fields. The TFC is hence subjected to high magnetic pressure and forces. To examine the stresses in the winding pack and at the casing, various methods are considered in COMSOL and ANSYS to analyse stress at casing, debonding of the coil winding pack and stresses in insulation components.

One important failure that has to be taken care of in the superconducting magnet design is the transition from the superconducting to normal conducting phase known as quench. Since, in normal conducting mode, the electrical resistance of the superconductor material is high, introducing copper as an electrical diverter for the flow of current, generates joule heating. The magnet has to be discharged by connecting an external resistance parallel to the magnet to avoid excessive temperature rise. The maximum allowable adiabatic hotspot temperature as laid by International Thermonuclear Experimental Reactor (ITER) limits to 150 K, considering all materials in the conductor, i.e., superconductor, copper, helium, stainless steel jacket, and insulation. To simulate quench propagation, an external heater is placed in the superconductor and checked how the propagation is and what is the maximum temperature that it attains during discharge time.

Contents

1. Introduction and Motivation.....	1
2. Introduction to TF Coil	4
2.1. Magnetic Confinement	4
2.1.1. Basic Features of a Stellarator	4
2.1.2. The TOKAMAK Concept.....	6
2.2. Evolution of TOKAMAK.....	8
2.3. Superconductivity.....	12
2.3.1. Introduction to Superconductivity	12
2.3.2. Classification of Superconductors.....	13
2.3.3. High Temperature Superconductors	15
2.4. LTS Cable concept for TF coil.....	17
2.4.1. Pool-Boiling Conductor	19
2.4.2. Cable-In-Conduit Conductors (CICC) Cooled	20
2.5. HTS Cable Concepts for TF Coil.....	23
2.5.1. Roebel Assembled Coated Conductor (RACC)	23
2.5.2. Conductor on Round Core (CORC)	24
2.5.3. Twisted Stacked Tape Cables (TSTC)	25
2.6. Winding pack and casing for TF coil	25
2.7. Material consists for TF Coil	27
2.8. Pre-Conceptual Demo Design Using Process Code	28
3. Conceptual Design of a TF coil for EU DEMO	29
3.1. Introduction to the Conceptual Design of a TF Coil.....	29
3.2. Identifying the Parameters from the PROCESS Code	29
3.2.1. Shape of TF Coil from the PROCESS Code.....	30
3.2.2. HTS conductor for TF Coil	30
3.2.3. Winding pack.....	32
3.2.4. Electromagnetic Field Calculation.....	35
3.2.5. Result of Electromagnetic Analysis.....	36
3.2.6. Conductor Operating Point	38
3.2.7. Hotspot Calculation.....	40
3.3. Electromagnetic Analysis Conclusion	42
4. Structural Analysis of the TF Magnet for EU DEMO	44
4.1. Structural Analysis	44

4.1.1. Introduction to Mechanical Analysis	44
4.1.2. Constant Tension Coil and Hoop Force.....	45
4.1.3. D Structural Analysis of the Inboard Leg in the Midplane	50
4.1.4. Modeling	50
4.1.5. Modeling Criteria	51
4.1.6. Introduction to various models simulated in COMSOL	52
4.1.7. Material Properties	54
4.1.8. Boundary Conditions	55
4.1.9. Results of the Structural Analysis	56
4.2. Structural Calculation Conclusion	67
5. Thermal Hydraulic Modeling of the HTS Conductor	69
5.1. Introduction to the Conductor Quench Modeling.....	69
5.2. Hydraulic Analysis	70
5.2.1. Friction Factor Co-relation	70
5.2.2. Heat Load Imposed on the Conductor	74
5.2.3. Hydraulic Analysis Results	75
5.3. Quench Analysis	77
5.3.4. Model and Boundary Conditions.....	77
5.3.5. Material Properties	83
5.3.6. Quench Analysis Results.....	84
5.4. Summary on Conductor Modelling.....	89
6. Summary and Conclusion	91
Bibliography.....	96
Appendix A.....	103
Appendix B: Designations and abbreviations.....	133
Appendix C: Index of Symbols.....	135

List of Figures

Figure 2.1: Schematic diagram of the superconducting stellarator Wendelstein 7-X [Walk00].	5
Figure 2.2: Schematic of the current and magnetic fields within a TOKAMAK [Magn00]	7
Figure 2.3: A 3D view of ITER TOKAMAK [Iter00b].	11
Figure 2.4: Critical-current surface for a commercial superconducting alloy of NbTi [Bart13].	13
Figure 2.5: H and T Phase diagram of type II superconductor [FoSu04].	14
Figure 2.6: A cross section view of a NbTi, Nb ₃ Sn and MgB ₂ strand, from left to right [NoGo15].	15
Figure 2.7: Schematic representation of layers of HTS superconducting tape. [Bart13]	17
Figure 2.8: A selection of pool boiled (or bath) cooled conductors [Bruz06].	20
Figure 2.9: ITER Toroidal field coil conductor and ITER Central solenoid conductor showing as an example for cable in conduit conductor or internally cooled conductor [Sana00a][Sana00b].	22
Figure 2.10: Schematic drawing of RACC.	24
Figure 2.11: Five CORC are twisted together to form a CICC [Corc00].	25
Figure 2.12: Single strand and cabling of TSTC [BFMN18].	25
Figure 2.13: A cross section of ITER TF coil with radial plates, casing and conductor [MiSF08].	26
Figure 3.1: Left: D- shaped tori given from PROCESS code.	30
Figure 3.2: Cross sections of different materials in the HTS conductor surrounded by a stainless steel jacket with high voltage insulation. [GBBF14]	32
Figure 3.3: Schematic diagram representing the winding pack and bus bar.	33
Figure 3.4: Proposed HTS winding pack cross section which has 2 outer pancakes and 14 inner pancakes with casing	34
Figure 3.5: Variables for the general coil element used to define equation (3.1) and (3.2)	36
Figure 3.6: Magnetic field plotted along the center of torus. X is the radial dimension along the torus.	37
Figure 3.7: Magnetic field plotted at winding pack cross section of the inner leg of TF coil. X is radial dimension and y is axial dimension.	38
Figure 3.8: Magnetic field vs critical current at different temperatures. The operation point is indicated as black star	39
Figure 3.9: Critical current vs temperature at 13.5 T magnetic field. The operation condition is indicated as asterisk.	40
Figure 3.10: Time vs adiabatic hotspot temperature. The operation condition is indicated as asterisk.	42
Figure 4.1: Ideal D shaped toroid and the magnetic field inside the toroid as a function of the radius.	44
Figure 4.2: Ideal thin shell tori composed of a current sheet uniformly distributed on a surface which has non-circular cross section.	45
Figure 4.3: Segment of a thin-shell torus with total current I. The magnitude of the field within the torus at this location is B and the local radius of curvature is ρ .	46
Figure 4.4: Example of an ideal constant tension toroidal coil shape.	48

Figure 4.5: Exploded view of the straight and curved segments of the upper half of the constant tension shape.	48
Figure 4.6: The left figure illustrates the plane strain and plane strain models. The displacement in the mid plane is denoted by U_z	51
Figure 4.7: a: Cut sectional view of the TF coil in the mid-plane of the inboard straight leg with the geometrical parameters as taken from the PROCESS code. b: shows the cut sectional view of TC coil in the mid-plane of the inboard straight leg with the winding pack.	53
Figure 4.8: Cut sectional view of the modified TF coil in the mid-plane of the inboard straight leg.	54
Figure 4.9: Boundary conditions applied in COMSOL (red lines denote sliding boundary condition).	55
Figure 4.10: Boundary conditions applied in COMSOL (red line denotes sliding boundary condition; green dotted line denotes debonding of winging pack from case and black dash-dotted line denotes symmetry).	56
Figure 4.11: Von Mises stress (N/m ²) of the casing in the mid-plane of the inboard leg of TF coil for study 1. The region where the peak stress is located is shown in a marked rectangle.....	57
Figure 4.12: Total displacement (m) in the mid-plane of the inboard leg of TF coil along with deformation (scaled by a factor 10)	58
Figure 4.13: Shear stress (N/m ²) in the turn insulation of the side pancake.....	58
Figure 4.14: LHD shear criteria for the turn insulation of the side pancake.....	59
Figure 4.15: Von Mises stress (N/m ²) in the mid-plane of the inboard leg of TF coil for study 2. The region where the peak stress is located is shown in a marked rectangle	60
Figure 4.16: Total displacement (m) of the mid-plane of the inboard leg of TF coil along with deformation (scaled to 10 times) for modified geometry.	61
Figure 4.17: Shear stress (N/m ²) in the side pancake turn insulation of the mid-plane of the inboard leg of TF coil for modified geometry.	61
Figure 4.18: LHD shear criteria for the turn insulation of the side pancake.....	62
Figure 4.19: Von Mises stress (N/m ²) in the mid-plane of the inboard leg of TF coil for study 3 and debonding of the winding pack from the case (scaled to 10 times).	62
Figure 4.20: Total displacement (m) of the mid-plane of the inboard leg of TF coil along with deformation (scaled to 10 times) for study 3.	63
Figure 4.21: Shear stress (N/m ²) in the side pancake turn insulation of the mid-plane of the inboard leg of TF coil for study 3.....	63
Figure 4.22: LHD shear criteria for the turn insulation of the side pancake for study 3.	64
Figure 4.23: Von Mises stress (N/m ²) for both the casing and the winding pack in the mid-plane of the inboard leg of TF coil for study 4. The region where the peak stress is located is shown in a marked rectangle	65
Figure 4.24: Von Mises stress in both the casing and the winding pack for the ideal elastic model. The zoomed picture shows the maximum stress in the jacket area calculated with the ideal elastic-plastic model.....	66
Figure 4.25: Total displacement (m) of the mid-plane of the inboard leg of TF coil along with deformation (scaled to 10 times) for study 4.....	66

Figure 4.26: Shear stress (N/m^2) in the side pancake turn insulation of the mid-plane of the inboard leg of TF coil for modified geometry.	66
Figure 4.27: LHD shear criteria for the turn insulation of the side pancake for study 4.	67
Figure 5.1: The event tree for the evolution of an initial thermal disturbance in a superconducting cable.	70
Figure 5.2: The figure shows EURATOM LCT Coil conductor. Picture is from Kernforschungszentrum Karlsruhe.....	73
Figure 5.3: ITER TF coil conductor. Reference: ITER Newlines #141, 23 July 2010	73
Figure 5.4: Friction factor of the helium flow in a CICC, from the various correlations. The correlation of Katheder has been evaluated for a cable void fraction of 40%.	74
Figure 5.5: left side: figure represent the schematic representation of plasma and TF coil. right side: figure represents the cross section of AA with TF coil case winding pack and neutron flux due to plasma	75
Figure 5.6: Temperature increase and pressure drop of the inner pancake conductor for different nuclear heat loads Q_{nucl} . 200 W/coil is the reference [Boni14].	76
Figure 5.7: Thermal link between Helium, conductor and jacket for 1D analysis.	78
Figure 5.8: Effect of the temperature increase on the critical current and on the operating position: the current in the superconductor remains constant at the I_{op} value as long as the temperature is below T_{cs} , then decreases along the I_c curve. At T_c the current carried by the superconductor is zero, and all the current I_{op} flows in the shunting copper.	80
Figure 5.9: Critical current density data of REBCO as a function of magnetic field parallel to c-axis and fitting function.	84
Figure 5.10 : Development of resistive voltage of the HTS conductor as a function of time.	86
Figure 5.11: Conductor, jacket and helium temperature evolution during quench of 39 m long HTS conductor for the delay time $t_{del,1}$	87
Figure 5.12: Conductor, jacket and helium temperature evolution during quench of 39 m long HTS conductor for the delay time $t_{del,2(right)}$	87
Figure 5.13: Evolution of the normal zone length with respect to time. The figure also shows a zoomed section of normal zone length for the first 10 seconds. ...	88
Figure 5.14: Evolution of the massflow with respect to time.....	89

List of Tables

Table 2.1: Comparison between Stellarator and TOKAMAK.....	8
Table 2.2: Comparison of Toroidal Field Coils (Non-Tritium Operation) [WeCa11].....	9
Table 2.3: Comparison of Toroidal Field Coils (Full Deuterium & Tritium Operation) [WeCa11]	12
Table 2.4: List of some of the conductors used for TF coil [Bruz06].	23
Table 3.1: TF coil Parameters for EU DEMO	29
Table 3.2: Various Materials in HTS Conductor for TF coil	32
Table 3.3: Summary.....	43
Table 4.1: Comparison of hoop forces and stress for selected TOKAMAK systems.....	49
Table 4.2: Material properties used in simulation	54
Table 4.3: Comparison of various studies used for structural analysis.....	67
Table 5.1: Collection of parameters used in the hydraulic analysis.....	75
Table 5.2: Fit parameters for the critical surface of REBCO	83
Table 5.3: Parameters used in the THEA input.....	85
Table 6.1: summary of the results	94

1. Introduction and Motivation

Commercial applications of nuclear fusion are being explored due to its endless resources, appreciable environmental and safety advantages that it has over other ways of producing energy on a large scale [OnOg16]. While natural resources for non-renewable energy are depleting rapidly, fusion fuels such as Deuterium is abundantly available, and Tritium is extracted from minerals. Today, a majority of the pollution is being caused due to the by-products of power plants, however, the major by-product during a fusion reaction is just an inert gas (Helium). Additionally, in a fusion device, accidents that typically occur in nuclear power plants can easily be avoided. Since fusion has to be incessantly fueled as in the event of a disruption in the system, the plasma cools within seconds and the reaction stops, henceforth negating the risk of any ensuing chain reaction [ArPi08a].

Plasma is comprised of ionized particles that are heated to a high temperature. In a magnetic confinement, nuclear fusion is initiated by electrons and ions in the plasma that are confined by means of magnetic fields. This balances the pressure with the forces exerted by a magnetic field produced by currents flowing in circuits surrounding the plasma [ArPi08a]. Experiments with toroidal configurations started in the mid-fifties and a small toroidal device with a porcelain chamber was fabricated that was progressively improved. By late 1957, a device called TOKAMAK (Ivor Golovin [Shaf01]) having a stainless-steel liner inside a copper vacuum chamber was built that is deemed as a beginning for toroidal coil concept. TOKAMAK has electromagnets oriented in the form of a torus or ring to shape the plasma; a term first enunciated by Irving Langmuir to describe a positive column of gas discharge [BrSt02]. A consortium of countries one of them being the European Union, has embarked towards building a nuclear fusion experiment on a large scale, based on TOKAMAK design named ITER which in Latin means “the way” and its full form stands for International Thermonuclear Experimental Reactor [BrSt02]. This attempt is to demonstrate that a burning plasma with an energy output 10 times the power input can be sustained over a time period of several seconds to minutes.

There were several challenges in commercializing nuclear fusion. For example, to overcome the electrostatic repulsion between the Hydrogen nuclei, the temperature has to exceed 2×10^8 K [Wood06]. To produce heat for reaching temperature of that magnitude, the heating current in central induction coils need to exceed millions of

amperes [ArPi08a]. Several technological advancements in this field made it possible to conduct fusion reaction with the assistance of strong magnetic fields. These strong magnetic fields are generated using large electromagnets made up of superconducting cables in a toroidal configuration termed as Toroidal Field Coil (TFC or TF coil). The Toroidal Field coil is one of the major components of the EU DEMO [FKWB14] project.

The aim of the initial DEMO conceptual studies is to demonstrate the feasibility for the generation of electricity by means of nuclear fusion [CFBL17a]. The inputs for the conceptual design for the EU DEMO TF coil were derived from the PROCESS [KKLK14] System Code. Based on this a preliminary geometry of the coil is determined. Subsequently, electromagnetic, structure and thermo-hydraulic analyses are performed to arrive at the final geometry of TF coil. This thesis provides a detailed treatment of each of these analyses and proposes the solutions to the conceptual design of EU DEMO TF coil with HTS as discussed in below chapters.

Chapter 2 begins with the general concept of a TOKAMAK in more detail followed by the requirements of the magnetic field to be generated by the TF coil. This is followed by how superconductors can help to generate such high magnetic fields. Two different kinds of superconductors, namely, low temperature superconductors and high temperature superconductors, their types and properties are explained. This proceeds with the motivation of usage of high temperature superconductors based on a more suitable cabling design being possible with them. It then explores into the pre-conceptual demo design of the TF coil based on the output of the PROCESS code.

Chapter 3 introduces the conceptual design of the TF coil for EU DEMO and defines its parameters and shape utilizing the PROCESS code. The subsequent discussion is on an iterative process that is required to determine the volume of the HTS, the geometry of the winding pack and the type of winding of the winding pack. These are determined by optimizing the electromagnetic field calculation, the conductor operating point and the hotspot calculation.

The structural analysis of the TF coil for the EU DEMO is presented in Chapter 4. The structural and mechanical analysis is explained to define stresses in the coil casing and the winding pack. A mathematical analysis is presented to determining the hoop stress in the winding pack and the case. Structural analysis of the inboard leg in the midplane is conducted by using the conductor current and the magnetic field that is

generated by the torus. Plane strain, stress, material properties and boundary conditions are discussed and analyzed, and structural calculations are derived.

Chapter 5 explains the quench modelling of the HTS. The study is made on the behavior of the coolant using a simplified set of mass, momentum and energy conservation equations. A hydraulic analysis of the friction factor co-relation is shown to determine the pressure drop and temperature rise in the conductor. The heat load imposed on the conductor is analyzed considering the steady heat load by conduction and heat deposited from the neutrons generated in the plasma. The hydraulic analysis is presented by considering the conductor length, wetted perimeter, Helium cross-section, inlet pressure and temperature. Finally, the quench analysis of model and boundary conditions, quench propagation and temperature are formulated.

A brief discussion of the proposed solutions along with outlook of the work is revisited as a summary in Chapter 6.

2. Introduction to TF Coil

2.1. Magnetic Confinement

The concept of controlled fusion originated from Hans Albrecht Bethe in 1939 who stated that fusion is the power derived from the stars [Baye16]. When two hydrogen isotopes, deuterium and tritium fuse together, helium nucleus is produced whereby a neutron and energy are released. To achieve fusion in a real world, several methods were developed. One of the methods suitable for large-scale implementation is magnetic confinement.

The concept of magnetic confinement deals with interaction of charged particles within magnetic fields. Strong and non-uniform magnetic fields are utilised for trapping the plasma, which enables them to move freely along specified paths keeping them away from material walls. These paths are achieved by the poloidal magnetic field that revolves around the minor cross section of the torus [GhMe17].

Magnetic confinement utilizes equilibrium between plasma pressure and magnetic forces to have a rotational transformation of the toroidal magnetic field to prevent drift of the plasma particles towards the wall. Based on evaluated research activities of Spitzer and Mercier the magnetic field may be twisted by [Xu16].

- creating a poloidal field by a toroidal electric current;
- rotating the poloidal cross-section of stretched flux surfaces around the torus
- making the magnetic axis non-planar.

As a result of the sustained research in nuclear fusion, two types of devices known as Stellarator relying on the latter two methods and TOKAMAK based on the first method came into prominence [Xu16].

2.1.1. Basic Features of a Stellarator

Stellarator is a toroidal device having a magnetic configuration to confine the plasma without using the effects of symmetry [Booz02]. Its name is derived from Latin “stella” meaning “star” [Baye16]. The concept of a Stellarator was conceived by Layman Spitzer at Princeton University in 1951 as a toroidal configuration with a rotational transformation providing a steady state field without an induced current. He envisaged

that when a steady-state plasma came in contact with the cylinder walls it would show constant pressure at all radii and the toroidal diverter would help reduce the wall interaction [BrSt02]. In a closed system, the field lines form a set of nested toroidal surfaces to attain a stable confinement [BrSt02]. Stellarator is one of the earliest fusion power devices that confines hot plasma with magnetic fields to sustain a controlled nuclear fusion reaction

Stellarator has a distinct advantage over toroidal machines of not having plasma instabilities. In a Stellarator, the magnetic fields evolve which enable the particles circulating around the long axis of the machine to follow twisting paths that neutralize the instabilities. The magnetic fields vary as a function of the toroidal angle using non-axisymmetric coils. One of the largest Stellarators, Wendelstein 7-X built in Greifswald, Germany and operational since 2015, has a major radius of 5.5 m and a minor radius of 0.52 m with a magnetic field of 3 T [BrSt02] as shown in Figure 2.1 below.

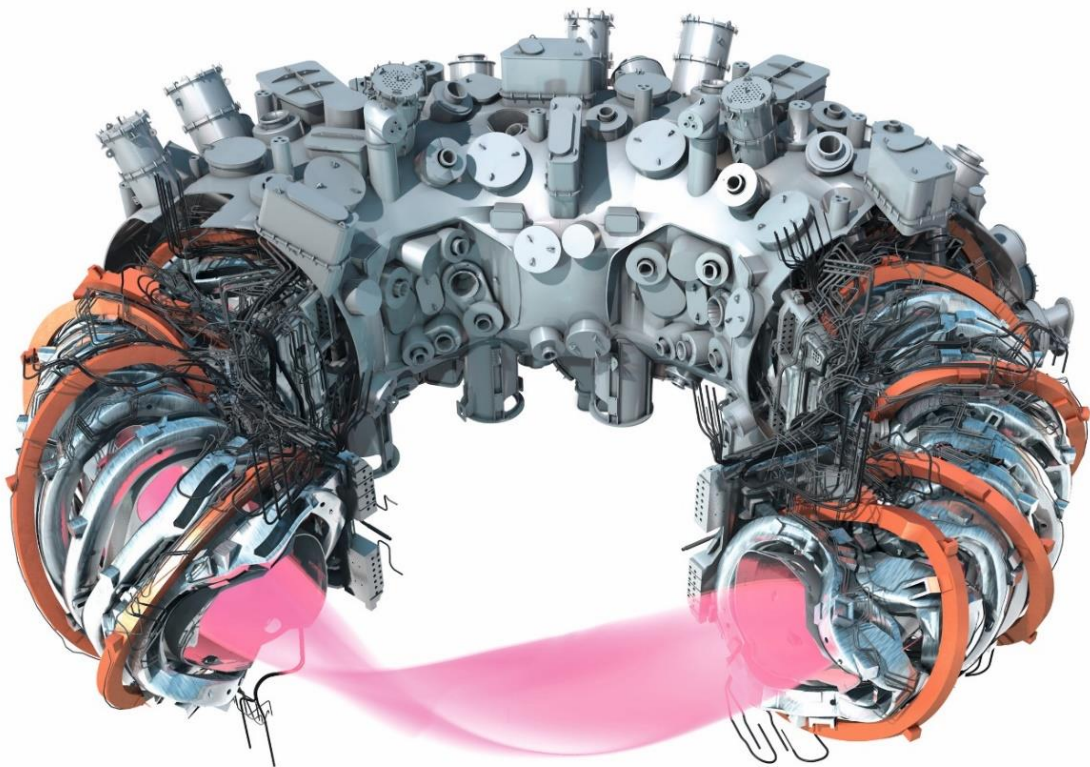


Figure 2.1: Schematic diagram of the superconducting stellarator Wendelstein 7-X [Walk00].

One of the main disadvantages of a Stellarator is that it requires several large asymmetric electromagnets of various shapes. This delayed the advance of this technology, compared to TOKAMAK geometry.

2.1.2. The TOKAMAK Concept

TOKAMAK is a magnetic confinement device with a toroidal geometry. It has three different main coil systems: the toroidal field coil, poloidal field coil and central solenoid coil. The toroidal field coil is made up of several individual coils that are distributed symmetrically in a toroidal form [ArPi08b]. The plasma confinement by the toroidal magnet is placed vertically around the torus. The primary of the transformer is the central solenoid that is located at the centre of the torus and initiates the intensive heating of the plasma due to joule effect. The poloidal coils configured horizontally around the torus are located so, to enable the low intensity magnetic fields to control the position and shape of the hot plasma flowing inside the vacuum vessel. This would prevent the hot plasma from touching the walls and prevent them from being harmed because of its intense heat. [GhMe17].

The coils shaped around the torus produce a magnetic field whose lines of force lead to a charge separation due to toroidal shape of the configuration. However, to confine the plasma particles, a poloidal magnetic field forms an additional component turning around on the minor cross section [GhMe17].

The toroidal direction refers to the path around the circumference or axis of the torus, whereas the poloidal direction running orthogonal to the toroidal direction. The interaction of these fields produces a resultant magnetic field that moves in a helical orientation about the center of the torus that causes the plasma particles to spin in a helical pattern. This spinning effectively confines the plasma by keeping the particles in a constant motion towards the center of the toroidal field and away from the vessel walls. A representation of this process can be seen in Figure 2.2.

The magnetic field at the center of the plasma is limited to around 6-8T or even less as the toroidal magnetic field is inversely proportional to the major radius [WeCa11]. The TOKAMAK creates a poloidal field by a toroidal electric current. Thus, in TOKAMAKS twisting is produced by asymmetrical plasma [GhMe17] resulting in better plasma confinement.

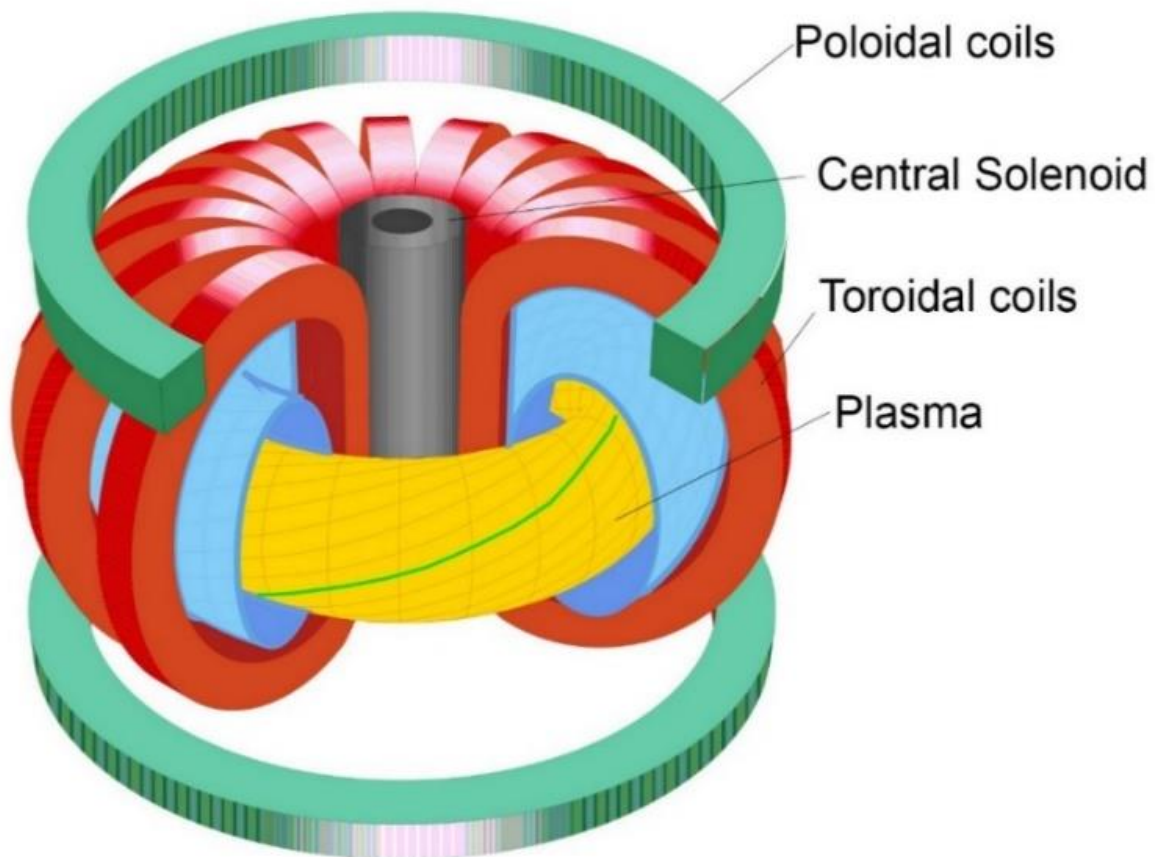


Figure 2.2: Schematic of the current and magnetic fields within a TOKAMAK [Magn00]

The main advantage of the TOKAMAK over stellarator is all the components are better accessible and hence the construction and maintenance is less sophisticated [McSt12]. This leads to increased plasma confinement and ohmic dominated ignition, increased fusion power density, improved drive scenario as well as increased flexibility in selecting operating scenarios [Schw92].

For TOKAMAKS it was successfully demonstrated that present designs were practically implementable and performance levels were better than any other device. Due to its rotationally symmetric magnetic chamber, construction and maintenance of the TOKAMAK becomes easier and more accessible [Baye16].

Today, TOKAMAK being adopted universally and in 1986 an agreement of the International Thermonuclear Experimental Reactor (ITER) in 1986 between European Union, Japan, the Soviet Union and the USA. It will be the largest TOKAMAK ever built [Baye16]. The concept of TOKAMAK is discussed elaborately in the section below.

The comparison of the Stellarator and TOKAMAK is given in Table 2.1 below.

Table 2.1: Comparison between Stellarator and TOKAMAK

	Stellarator	TOKAMAK
Geometry	Complex Coils	Planer* Coils [Prag05]
	Helical Symmetry within Plasma	Symmetry around Axis [Prag05]
Confinement and operation	No need for Plasma Current	Current Carrying Plasma [Prag05]
	Operate plasma in a steady state	Pulsed system due to induced plasma current by central solenoid [Xu16]
	Asymmetric particle orbits	Axisymmetric particles [Xu16]
	Twisting field is produced entirely by external non-axisymmetric coils	Rotational transform formed by a toroidal field [Xu16]
	No plasma current, hence does not have a poloidal field	Poloidal field generated by plasma current [Xu16]
	Provides a steady state field without an induced current [IOP, 2.4; 58/341]	Poloidal field determines plasma confinement and while toroidal field provides stability

2.2. Evolution of TOKAMAK

The acronym “Tokamak” is developed from Russian which means “toroidal chamber with magnetic coils” [ArPi08b]. The Tokamak designs enunciated at Kurchatov, USSR, demonstrated improved performance by the mid-1960s. Independent measurements taken by the UK delegation confirmed the Soviet results, and publication of the findings in 1969 resulted in a great leap in Tokamak construction. These machines attained all of the conditions needed for practical fusion and a new series of machines were designed in the 1970s to run on a fusion fuel of deuterium and tritium.

TOKAMAK machines may be broadly classified “Non-Tritium” and “Deuterium and Tritium” type as per their mode of operation. The “Non-Tritium” type was used in the initial TOKAMAKS configuration being initially “Circular” in the 1st TMP /T-1, then became “Circular Limiter” from T-2 of Kurchatov, USSR to CASTOR, Prague, Czech Republic. TOKAMAK ASDEX built at Garching, Germany used “Circular Diverter” while UK used the “D shaped Diverter” for its COMPASS-D TOKAMAK at Culham. The basic features used in “Non-tritium” type is given in Table 2.2 below.

Table 2.2: Comparison of Toroidal Field Coils (Non-Tritium Operation) [WeCa11]

Item	T-1	T-3	T-10	CASTOR	ASDEX	COMPASS D
Year of Operation	1958	1962	1975	1985	1980	1989
Country	USSR	USSR	USSR	Czech.	Germany	UK
Location	Kurchatow	Kurchatow	Kurchatow	Prague	Garching	Culham
Major Radius(m)	0.67	1.0	1.5	0.4	1.54	0.56
Minor Radius(m)	0.17	0.12	0.37	0.09	0.4	0.21
Configuration	Circular	Circular limiter	Circular limiter	Circular limiter	Circular Diverter	D-shape Diverter
Peak Magnetic Field (T)	1.5	2.5	4.5	1.5	3.0	2.1

T-1 is the first working TOKAMAK designed by Natan Yavlinskii [Robe08] and began operation in 1958. The stability features of the Russian TOKAMAK device were much stronger and the magnetic and toroidal fields persisted for a longer time duration for times of the order of milliseconds as compared to the British ZETA device lasted for less than around five milliseconds [Shaf01]. T-2 was the first MHD stable regime with the concept developed of the complicated TOKAMAK magnetic structure. It was later known as magnetic island that was demonstrated when modified to become TM-3 that was built in the 1960s.

T-3 had a minor radius of 0.15 m and a major radius of 1 m. It had a toroidal magnetic field of 3.8 tesla and carried a plasma current of 150 kA [Smir09]. The main features comprised an iron cored transformer, vacuum system having a stainless-steel wall, refractory metal aperture and a thick copper shell. Its main purpose was to explore the stable operating conditions with limited interaction with the walls of the vacuum vessel.

TOKAMAK CASTOR [Bals00], a first-generation machine with a metal vessel was operational in Czech Republic from 1985 – 2007. It was a former Russian TM1-VCh/TM-1MH 1960 machine that was refurbished with vacuum vessel

The first TOKAMAK in Germany was built at Garching called ASDEX(Axially Symmetric Diverter Experiment) and became operational in 1980 [Keil85]. It had a major radius of 1.54 m, a minor radius of 0.4 m and peak magnetic field of 3.0 tesla. It

was upgraded and operational in 1991 to prepare a base for the ITER by matching the plasma density, plasma pressure and the wall load to the specified conditions.

TOKAMAK having “Deuterium and Tritium” was first used by USA in 1982 in the fusion reactor TFTR at Princeton that used the “Circular Diverter” shaped TF coil. However, the EU initially made JET with “D-shaped Limiter” at Culham and later used “D-Shaped Diverter” in its later configuration TOKAMAK that became operational in 1992.

The International Thermonuclear Experimental Reactor (ITER) initiative began with the collaboration of US, European Union, Russia and Japan as a nuclear fusion project confined to plasma physics research envisaging the development of a 500 MW fusion power plant. The construction began in 2005 at Cadarache facility in Saint-Paul-lès-Durance, in Provence, southern France and it expected to have deuterium and tritium operation by 2035 [Iter00a]. Through an official agreement signed in 2006 [Afp06], 35 countries have joined the ITER movement. The TOKAMAK has a major plasma radius of 6.2 m and a minor plasma radius of 2.0 m [ShSp04]. The image of the ITER TOKAMAK is as shown in Figure 2.3.

ITER envisages to demonstrate that the fusion power output to be 10 times the given input. In-line with objectives laid out, ITER has planned for duration of plasma pulse for less than 300 s [ShSp04]. Although ITER is a collaboration of numerous countries, European Union, formed EUROfusion, a Consortium for the Development of Fusion Energy and embarked upon its own demonstration model for the commercial use of fusion power plant called EU-DEMO [CFBL17b].

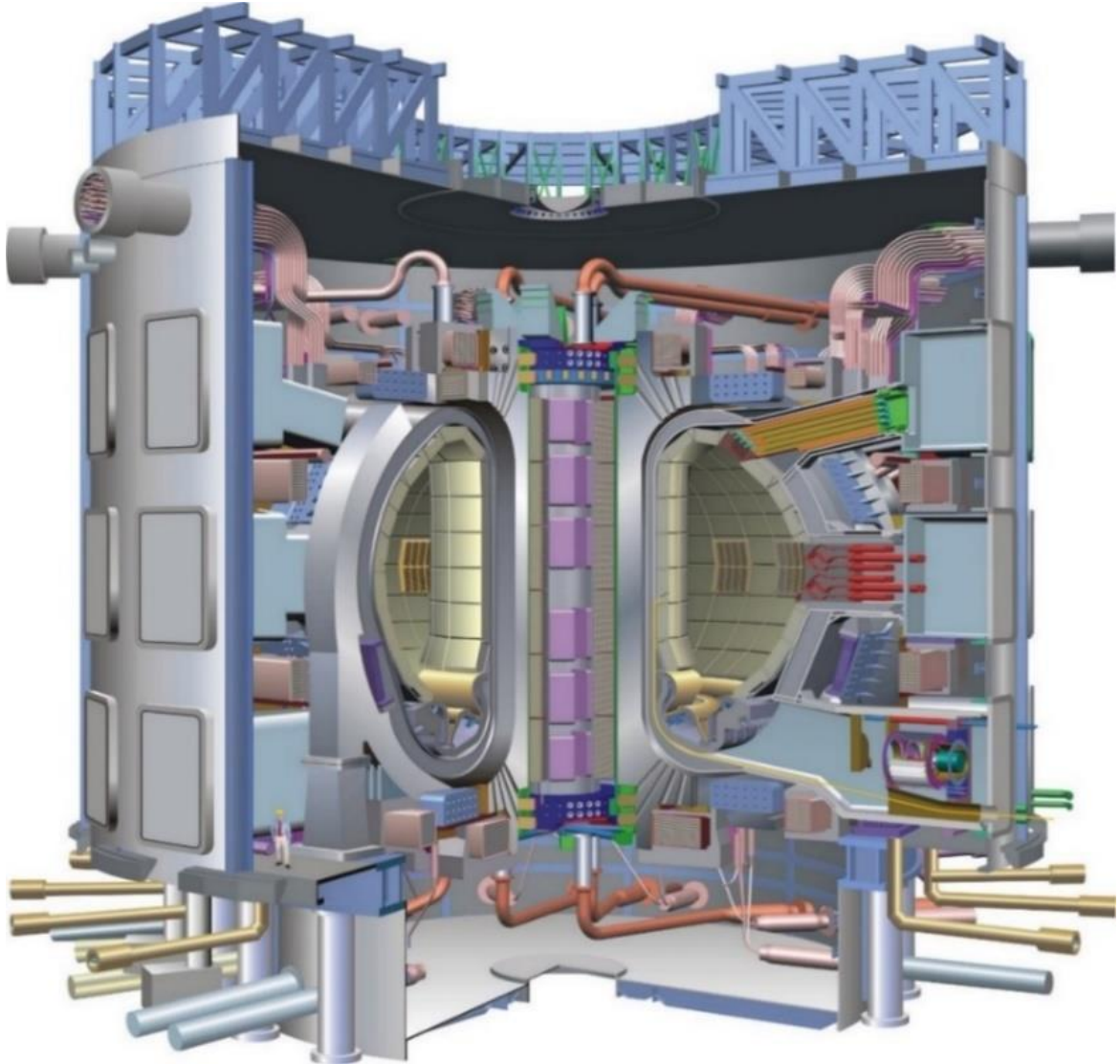


Figure 2.3: A 3D view of ITER TOKAMAK [Iter00b].

To assess the viability of a hypothetical fusion station including all reactor sub-systems from basic plasma physics to the generation & transmission of electricity, computer programmed system codes are well suited for studies and identification of reactor operating regimes. The computer intensive modelling methods facilitate thorough investigation using the PROCESS code [Knig13] as a computational tool. It is aimed to provide the design guidelines for the EU-DEMO model involving the PROCESS code to establish that pulse plasma mode would be 1.8 times [GBBF14] of plasma volume compared to that of ITER.

The movement of mass and energy towards the TOKAMAK boundary depends on the strength and intensity of the magnetic field. The fusion reactor design intends to take advantage of highest fields available till date, as the power density of a fusion reactor increases with B^4 times [ThTa82] while the cost of the magnet increases at

somewhat lower rate (somewhere between B and B^2) consistent with other mechanical constraints such as stress limits of structural materials.

Table 2.3: Comparison of Toroidal Field Coils (Full Deuterium & Tritium Operation) [WeCa11]

Type of TOKAMAK	TFTR	JET	JET	ITER
Year of Operation	1982	1983	1992	2018
Country	USA	EU	EU	France
Location	Princeton	Culham	Culham	Cadarache
Major Radius (m)	2.4	3	2.96	6.2
Minor Radius (m)	0.8	1.25	0.96	2
Configuration	Circular Diverter	D-Shape Limiter	D-shape Diverter	D-shape Diverter
Peak Magnetic Field (T)	5	3.5	4.0	5.3

Such high magnetic fields (to the order of 8T-14T) can only be achieved by employing superconductors [Wils87]. This is because superconductors are capable of conducting high current densities resulting in high magnetic fields while maintaining low resistance. In addition to the high magnetic fields, TF coils also require larger working volumes (by several order of magnitude). The combination of high field and large working volume leads to a special design for the superconducting magnet.

2.3. Superconductivity

Superconductors are materials that exhibit the flow of electric current with zero resistance when they are cooled below a critical temperature. The phenomenon of superconductivity is that a superconducting element expelled a weak magnetic field when cooled below the critical temperature while when the magnetic fields are strong, the superconducting effect disappeared and the material exhibited properties prevalent in its normal state [Schm00].

2.3.1. Introduction to Superconductivity

First experiments of Kamerlingh Onnes revealed that as the temperature of an extremely pure mercury thread was reduced to 4.2 K, its electrical resistance dropped by a factor of about 10,000 due to a temperature drop of 0.02 K and this led to the discovery of superconductivity [RoRh78].

Superconductors are characterized by three threshold variables, namely critical temperature (T_c), critical current density (J_c) and critical magnetic field (B_c), which determine the region in the BJT [Wils87] space is shown in Figure 2.4.

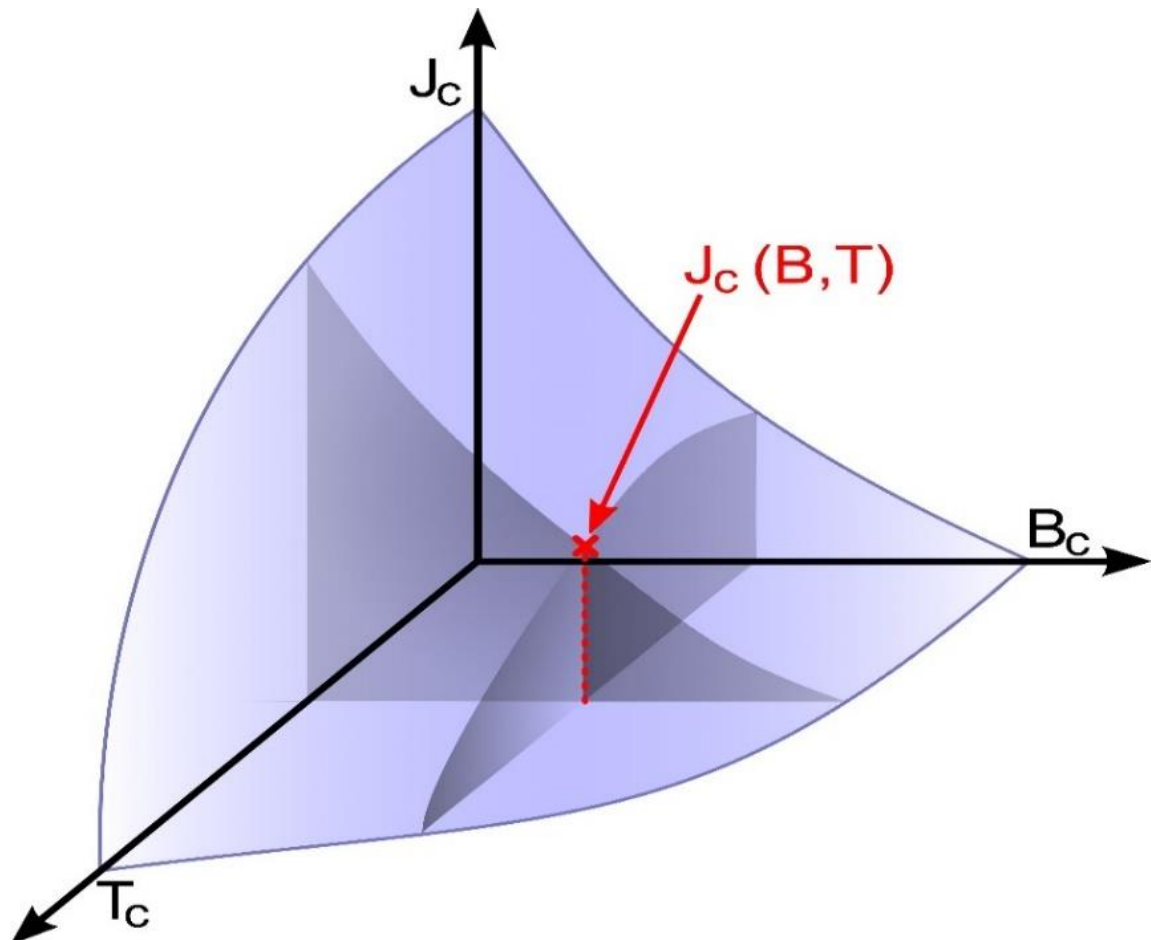


Figure 2.4: Critical-current surface for a commercial superconducting alloy of NbTi [Bart13].

The discovery of Meissner and Ochsenfeld that below the critical magnetic field, the magnetic flux density inside a single tin crystal was zero [RoRh78] led to the generalization that superconductors are perfectly diamagnetic.

2.3.2. Classification of Superconductors

Low temperature superconductors are classified as type-I and type-II superconductors, based on their magnetic properties. The essential difference between the two types is, type-I superconductors have only a single critical magnetic field H_c , below which they are superconducting. They are perfectly diamagnetic and the magnetic field cannot penetrate inside the material. Type - I superconductors are also called soft superconductors since they lose the superconducting state even with a low-intensity magnetic field and the transition is sharp and abrupt.

Type-II superconductors have two critical magnetic fields, and their magnetic behavior is identical to type-I superconductors only below the lower critical magnetic field, H_{c1} [FoSu04]. Type-II superconductors are not perfectly diamagnetic for external field values between the lower critical magnetic field intensity H_{c1} and the higher critical magnetic field intensity H_{c2} , although, they continue to have zero DC resistance. Type-II superconductors, have two distinct magnetic states. For applied field intensities below H_{c1} , they display a Meissner state similar to type-I superconductors, but for field intensities between H_{c1} and H_{c2} they are in a mixed state (shown in Figure 2.5), wherein the magnetic flux inside the superconductor is not zero but it remains superconducting.

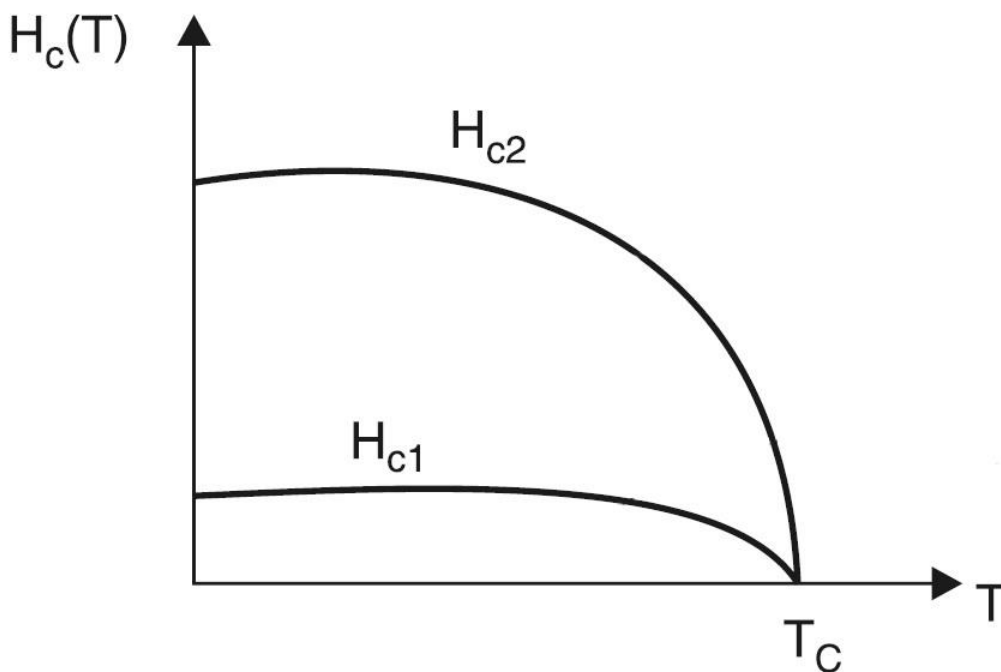


Figure 2.5: H and T Phase diagram of type II superconductor [FoSu04].

The critical field for most type-I superconductors is less than a few milli-hundred tesla [Wils87]. The lower critical field of most type II superconductors is of the same order, but the upper critical field can be of the order of tens of tesla which present a larger range of superconducting operation.

The flow of electric current through type-II superconductors, operating in a mixed state, creates impediments in the movement of the current vortices due to the resulting Lorentz forces. This Lorentz forces can move fluxoids (magnetic field penetrated in the superconductors) causing an electrical resistance called flux flow resistance, which is proportional to the normal resistance of the superconductor. However, in the mixed

state, if the type-II superconductor has impurities or structural imperfections and dislocations, the movement of the vortices is halted due to their pinning into these imperfections (also referred to as pinning centers). Consequently, the critical currents of imperfect type-II superconductors are much higher because, a greater amount of current is required to create Lorentz force strong enough to unpin the vortices from the pinning centers [WaNM87].

Type-II superconductors also called hard superconductors, are of importance in the construction of high-field high-current superconductors due to their high upper critical field and high critical current values. In general, hard superconductors exist in the form of an alloy or a compound, and the most prominent ones in use in the industry are NbTi [Wils87], Nb₃Sn and MgB₂ as shown in the figure below.

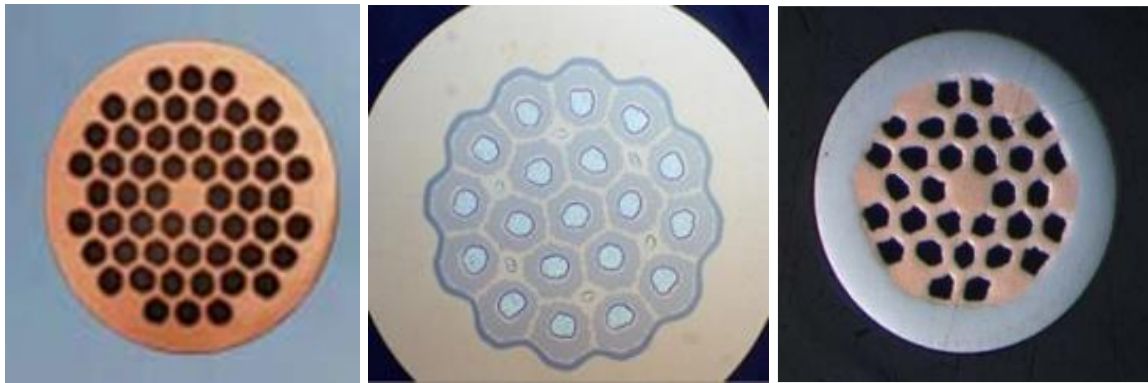


Figure 2.6: A cross section view of a NbTi, Nb₃Sn and MgB₂ strand, from left to right [NoGo15].

However, amongst these low temperature superconductors, both NbTi and MgB₂ have low critical magnetic fields with 14.5 T and 17 T respectively. Nevertheless, Nb₃Sn meets the requirements for the usage with a critical magnetic field of 27.9 T, but has low critical temperatures of 18.3 K [NoGo15]. In comparison to Nb₃Sn, high temperature superconductors like REBCO has critical magnetic field more than 100 T and critical temperature more than 90 K [NoGo15]. For these reasons, this work explores the possibility of use of HTS material as a possible candidate for TF coil.

2.3.3. High Temperature Superconductors

In 1986, Bednorz and Müller discovered a set of materials that could be used as superconductors with liquid nitrogen to cool them [BeMü86]. The materials mostly used is Yttrium-Barium-Copper oxide (YBCO) at a critical temperature of 100 K [BCCC87] and are classified as High temperature superconductors (HTS) [FoSa04]. These Rare-Earth-Barium-Copper-Oxide (REBCO) materials are ceramic in nature. The critical

current depends on the oxygen concentration in the copper oxide layer and the orientation of the ceramic crystals (known as grain boundaries) [Rao91]. In theory, best current density can be achieved by a single grain, but it is not possible to create such a grain across several meters of length of the conductor. Therefore, the alignment of the grains is done such that the loss of current density is minimized [GMPG04]. Most of the commercial manufacturers develop REBCO superconductors in the form of tapes.

Despite being available from several manufacturers across the world, these coated conductors are restricted to a tape type geometry as illustrated in Figure 2.7. According to [Selv11], their thickness varies between 50 μm to 200 μm , up to 40 mm with and are available in up to nearly a kilometer single piece length commercially. A substrate made of Hastelloy[®]C276 or stainless steel with a thickness between 50 μm and 120 μm acts as the base material of REBCO superconductor [Bart13]. This substrate is coated with several buffer layers to compensate the lattice mismatch between substrate and REBCO layers. The buffer layers are composed of metal-oxides or ceramics Ytria (Y_2O_3), Magnesium Oxide (MgO) and Ytria-Stabilized Zirconia (YSZ) [Baye16]. Rolling Assisted Biaxially Textured Substrates (RABiTS) achieved a good alignment of the grains with high critical current densities and critical magnetic fields. Buffer layers can alternatively be patterned by Ion-Beam-Assisted-Deposition (IBAD), Alternating-Beam-Assisted-Deposition (ABAD) or Inclined-Substrate-Deposition (ISD) [Baye16]. High performance tapes are required to determine the orientation of the grains and reduce the angle between the grain boundaries. A very thin film of REBCO layer is coated on the topmost buffer layer. Almost all the current within the tape is carried in superconducting layer of 1 μm to 3 μm thickness. The super conducting layer has a current density as high as 10 kAmm^{-2} at 4.2 K in a 19 T background magnet field [Mond16]. To improve the distribution of the current and heat, the super conducting layer is layered with a very thin (few micro meters thick) silver cap which stabilizes the superconductor. There are also versions of REBCO available that are electro-plated with copper with thickness ranging between 20 μm and 100 μm for increased electrical stabilization.

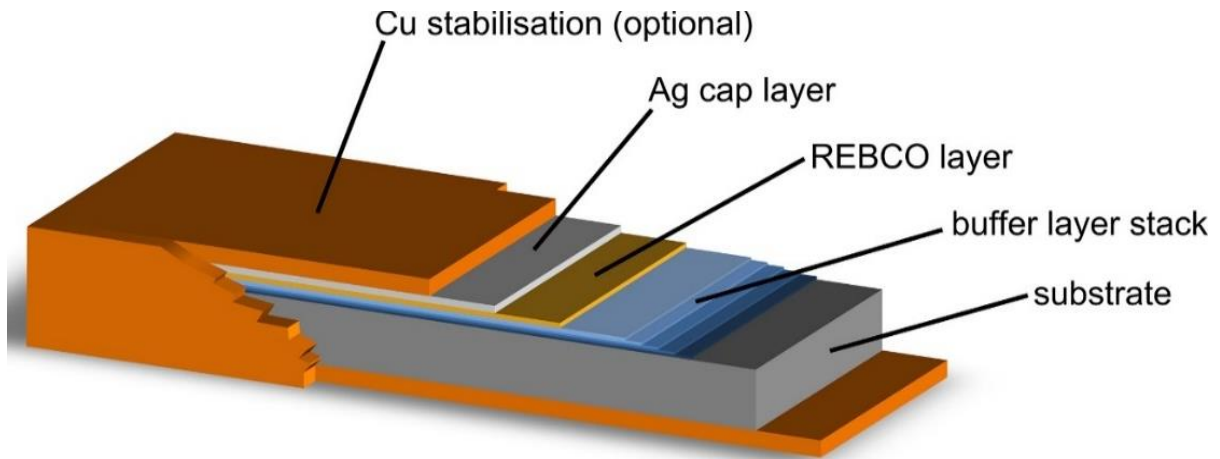


Figure 2.7: Schematic representation of layers of HTS superconducting tape. [Bart13]

Different compositions of various rare earth elements are used by the manufacturers of REBCO. Manufacturers like American Superconductor (AMSC), Fujikura SWCC, Brucker EHTS and Super Power use Yttrium, whereas Gadolinium is used by Furukawa, Sumitomo Electric, Fujikara and ISTEK. KERI uses Samarium. Additionally, the used thin film depositing methods or the thickness of the layers also differ. Various methods are used to grow REBCO layers : Metal Organic Decomposition (MOD), Metal Organic Chemical Vapour Decomposition (MOCVD), Pulsed Laser Decomposition (PLD), Chemical Solution Deposition (CSD), Physical Vacuum Deposition (PVD), Reactive Co-Evaporation and Cyclic Deposition Reaction (RCE-CDR) or the faster Reactive Co-Evaporation and Deposition Reaction (RCE-DR) [Moon14] [IOFT93] [Cond00] [FBCC09] [Amel15] [NZBS15]. Hence, manufactured superconducting REBCO tapes possess varying mechanical, thermal and electrical properties due to differences in the substrate material, layer thickness and the manufacturing process.

2.4. LTS Cable concept for TF coil

Superconducting cables are widely in use in high-current and high-field magnet applications [Seeb98]. Presently, type-II superconductors are used in the manufacture of wires or tapes for such high current carrying cables. The fabrication of these cables is carried out with extreme care, as a lot of degradation in performance is attributed to defective manufacturing process [Seeb98]. The fundamental requirement of such cables during their operation, in the presence of external disturbances, is stability [Wils87].

External disturbances deposit energy within the volume of the superconductor in the form of heat. If the resulting heating of the superconductor is greater than its ability to remove heat deposited locally then the temperature of the superconductor increases. This increase in temperature reduces the material properties of superconductor i.e. critical field and critical current density and eventually loses the superconductivity. Quenching is a term used to describe the transition of a part of a superconductor from the superconducting state to the normal resistive state without recovering the superconducting state. Quenching of a superconducting magnet is a very undesirable process as it results in releasing all the energy stored in its magnetic field into the superconducting cable in the form of heat, which can cause structural damage to the magnet and its surroundings [Wils87]. For the safe operation of superconducting magnets, it is imperative that they should be stable against physical disturbances and perform under quench-free conditions.

Quenching can be prevented by improving the heat removal efficiency (or ameliorating the cooling conditions) or by reducing the possibility of sudden energy inputs into the superconducting cable volume. One of the main sources of production of heat in the superconducting cable is the internal and external Lorentz forces on it. External Lorentz forces move the wires and wire motion generates heat due to friction while internal Lorentz forces disengage fluxoids from the pinning centers and the resulting flux motion dissipates heat. Initially, if the heat is not promptly removed by the available cooling conditions, a small heat pulse is deposited in the cable due to undesirable imperfections, which raises the temperature of the cable [Wils08][BoZi92a][BoZi92b]. Due to the increase in temperature, the critical current density of the cable decreases.

This causes flux motion that generates more heat, which raises the temperature even more. This positive feedback causes an avalanche of heat generation and flux motion, called a flux jump, which quenches the superconductor. Flux jumps can be avoided by reducing the available physical region for flux motion, and by conducting the heat generated before it can lead to the positive feedback. Both these methods for obviating flux jumps require a fine subdivision of the superconductor [Wils08].

Fine filaments of superconducting material are embedded in a normal metal matrix called stabilizer, usually made of copper. Such a composite structure of many filaments in a matrix is termed multifilamentary zone. As mentioned earlier, superconductors in general have a much higher electrical resistivity when operating in the normal regime

than conventional conductors such as copper or aluminum. Annealed electrical copper at 4.2 K operating in 6 T has an electrical resistivity $\sim 3 \times 10^{-10} \Omega\text{-m}$ and a thermal conductivity of $k \sim 350 \text{ W m}^{-1} \text{ K}^{-1}$, which is higher than that of NbTi [Wils87]. Copper also is very ductile, which helps in the fabrication process of the composite. The good electrical conductivity of the stabilizer provides an alternative low-resistance path to the current. In case a part of the superconductor becomes normal due to a disturbance and thus promotes the dynamic stability of the superconducting wire against flux jumping. Copper also protects the superconductor in the event of a quench. The high thermal conductivity of the stabilizer enhances heat removal capacity and improves stability. Therefore, the stabilizer not only prevents a quench from occurring, but also protects the superconductor during a quench. Usually, the multifilamentary zone is enclosed in a cladding of normal material, which augments the functionality of the stabilizer [Wils08].

However, the stabilizer in the multifilamentary composite has a serious disadvantage; its low-resistivity allows the filaments to be coupled together in changing magnetic fields. Coupling between the filaments is undesirable because it causes flux jumping and losses. Instead of the filament size being the characteristic flux jump size, the composite radius becomes the size of the flux jump, which is usually much larger than that allowable under stability concerns. Coupling can be reduced by twisting [Taká97] the composite with a short enough twist pitch which ensures that the distance between point of reversals is insufficient for transverse currents to build up and the filaments to stay decoupled. Such a multifilamentary composite wire twisted in the final stages of drawing the wire with the appropriate twist pitch is called a superconducting strand. Two kinds of conductors utilizing multifilamentary composites have been developed for fusion applications: pool-boiling cooled conductors and forced-flow cooled Cable-In Conduit Conductors (CICC) [Bruz06]

2.4.1. Pool-Boiling Conductor

Pool-boiling conductors are superconducting strands (Figure 2.8) placed in a liquid helium bath and were used to construct the first truly stable magnets by Stekly [StZa65]. These magnets recover their superconducting state irrespective of the size of the thermal perturbation they are exposed to. This stable behavior is achieved by immersing the magnet cables in pools of liquid helium and reducing the current density by adding stabilizer to the conductor until the Joule power generation on the conductor surface, in the normal state, is less than the minimum film boiling heat flux. This form

of stability is called cryostability. Cryostability reduces the limiting current density which gets translated into bulkier magnets for the same operating parameters ($< 3 \text{ kA cm}^{-2}$ at 8 T for NbTi magnets) and thus results in higher costs [Dres02a].

Stekly's cryostabilizing condition is conservative while Maddock, James, and Norris [StZa65] demonstrate that cryostability can be preserved at higher current densities than those allowed by Stekly's criterion. Maddock [MaJa68] introduced the concept of cold-end recovery in which recovery starts at the end of the normal zone and proceeds inward, the center of the disturbance being the last point to recover. In contrast, according to Stekly's criterion, the whole normal zone recovers instantaneously and all parts of the normal zone disappear simultaneously.

Cryostability, even with Maddock's criterion, limits the current density to unacceptably low values. After many efforts to increase the current density of pool-boiling magnets by trying to improve heat transfer between Helium and conductor or using superfluid Helium for example, this concept was abandoned in favor of internally forced-flow cooled conductors [Hoen80].

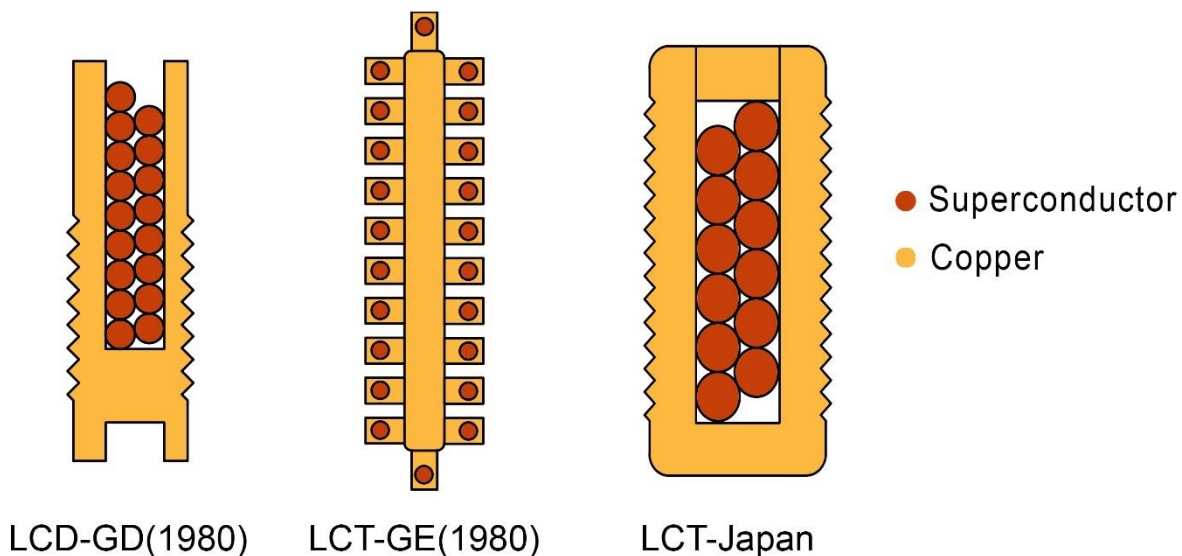


Figure 2.8: A selection of pool boiled (or bath) cooled conductors [Bruz06].

2.4.2. Cable-In-Conduit Conductors (CICC) Cooled

Cable-In-Conduit Conductors (CICCs) which are internally forced-flow cooled conductors have become the primary choice of superconducting cables for use in large-scale high-field superconducting magnet applications such as Magnetically Levitated (MAGLEV) high-speed trains [LeKL06], Superconducting Magnetic Energy Storage

(SMES) [NiMo10], high energy particle physics detectors, Magneto Hydrodynamic (MHD) generators [KrKa13] and most notably, in magnetically-confined fusion power generation. Reasons are structural robustness, relatively low AC losses, low inventory of helium coolant and high voltage integrity, which enables them to support high electrical currents with minimal energy losses and produce high magnetic fields.

Cable-In-Conduit Conductor consists of a twisted, multistrand cable wound in many stages and enclosed in a structural alloy conduit (as shown in Figure 2.9). The strands are multifilamentary composites with many superconducting filaments embedded in a normal metal stabilizer matrix, usually copper. Good heat removal is facilitated by pressurized supercritical liquid helium flow through the conduit. The helium flow area is about 35% of the total cable cross-sectional area, also termed as void fraction [ZaGM06]. The conduit serves as a structural support and as a channel for the liquid Helium coolant. Wrapping the conduit with electrical insulation gives it electrical integrity. Unlike pool-cooled conductors, the Helium flow path inside a CICC can be quite long (up to a kilometer for ITER magnets) and the frictional forces can be substantial due to forced-flow of Helium through the constricted space available in the conduit.

Cable-In-Conduit Conductors consequently, have a high inlet pressure to overcome the frictional drag. Due to the mechanical strength of the conduit material, CICC can handle high quench pressures easily. In CICC, each strand is in direct contact with the coolant, resulting in very efficient heat transfer. In contrast, monolithic conductors, which use epoxy (or similar material) to hold the superconducting strands together, have a much lower heat transfer capability because of the low thermal conductivity of epoxy [ScSc93]. The idea of subdividing the superconductor into thin strands dates to Chester [Ches67], who remarked, "another important parameter in the stability condition is the thermal capacity of the superconductor.... the superconductor may be combined with another material of high thermal capacity.... the most effective material would clearly be liquid helium or high-pressure helium if this could be retained in close thermal contact with the superconductor, perhaps by using a hollow tubular conductor with the helium trapped inside. Clearly, excellent thermal contact is desirable between the superconductor and the thermal ballast.... this is achieved by subdivision of the superconductor to present greater interfacial area."

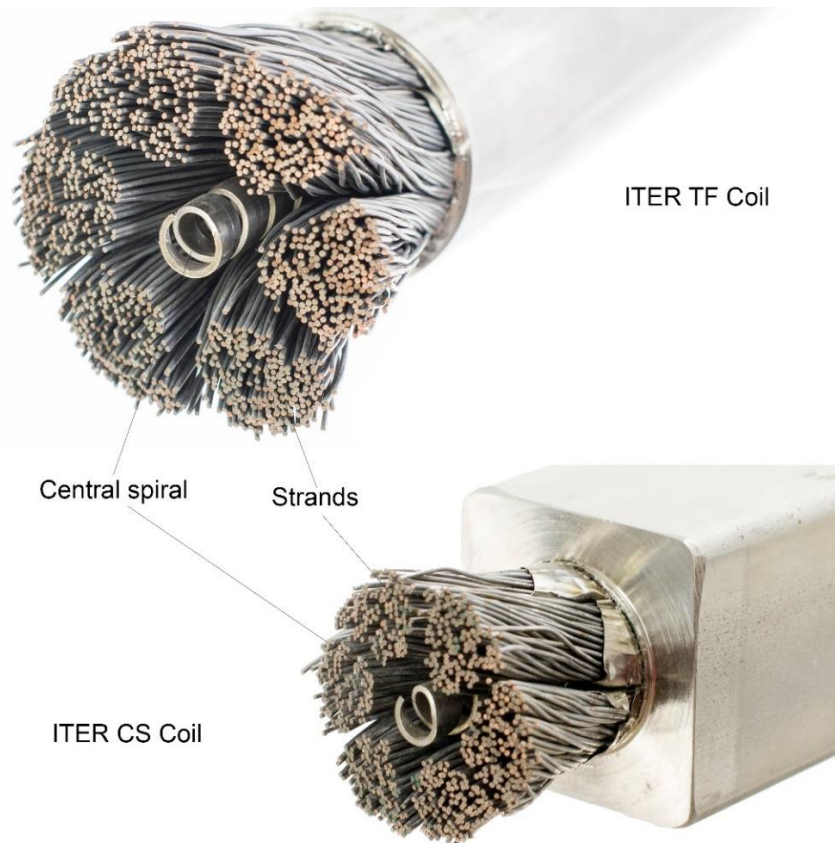


Figure 2.9: ITER Toroidal field coil conductor and ITER Central solenoid conductor showing as an example for cable in conduit conductor or internally cooled conductor [Sana00a][Sana00b].

Cable-In-Conduit Conductors gained popularity due to the work by Heonig, Iwasa and Montgomery who demonstrated the advantages [IwHM77]. As far as stability is concerned, CICC's are not cryostable but metastable due to the nature of helium residence in them. Recovery from a thermal disturbance takes to the order of tens of milliseconds but the residence time of helium in a coil can be a few minutes even at high flow rates, which limits the inventory of helium available for recovering from the disturbance [Dres95]. Depending on the magnitude of the disturbance enough heat might be deposited into the surrounding helium at fast-enough rates to raise its temperature above the current-sharing threshold. In this situation, the helium will not be able to take away more heat and the cable temperature will increase until the cable finally quenches. To understand different kinds of CICC's used in TF coils, a list of some of the conductors are shown in the table below.

Table 2.4: List of some of the conductors used for TF coil [Bruz06].

Tokamak	Superconductor / Cooling	Peak field (T)	Operating current (kA)	Year
Tokamak T-7	NbTi / Forced flow	5	6	1974
LCT (6 coils)	NbTi+ Nb_3Sn / Pool - Forced flow	8	10-18	1980
Tokamak T-15	Nb_3Sn / Forced flow	9.3	5.6	1981
EAST	NbTi / Forced flow	5.8	14.5	2001
KSTAR	NbTi+ Nb_3Sn / Forced flow	8	35	2002
SST - 1	NbTi / Forced flow	5	10	2002
ITER	Nb_3Sn / Forced flow	11.8	68	2008

2.5. HTS Cable Concepts for TF Coil

The HTS cable concepts relate to the mechanical properties and performance of the cables at various temperatures and magnetic fields. In order to study the adaptability for of fusion magnets, the HTS cable concepts are set up in various field, force and current. REBCO tapes tend to be suitable alternatives in high and strong magnetic field applications with better mechanical properties, higher critical temperature and higher densities [Bart13]. Copper is used for HTS tape stabilization since it has low ohmic resistivity, solder joints have low specific joint resistance and have high thermal conductivity that enables good heat exchange between the REBCO layer and the conducting medium [Baye16]. The HTS cable concepts investigated so far are Roebel Assembled Coated Conductor (RACC), Conductor on Round Core (CORC) and Twisted Stacked Tape Cables (TSTC).

2.5.1. Roebel Assembled Coated Conductor (RACC)

Ludwig Roebel, in 1912 patented [Roeb12] the Roebel assembling technique to reduce alternating current losses in copper stator windings of AC generators. Based on this, the RACC is characterized by multilayer REBCO tapes that consists of meander shaped coated conductor tapes resulting in cables of rectangular geometry with a flat cable design that facilitates the cable's c-axis inside the magnetic background field. The RACC cable has the lowest alternating current losses and has a flat cable design that has been proven. The cable is vulnerable to Lorentz forces and transverse

pressure, but it is possible to reinforce the cable inside a stainless-steel conduit with appropriate pre-compression and prevent damage at magnetic background fields.

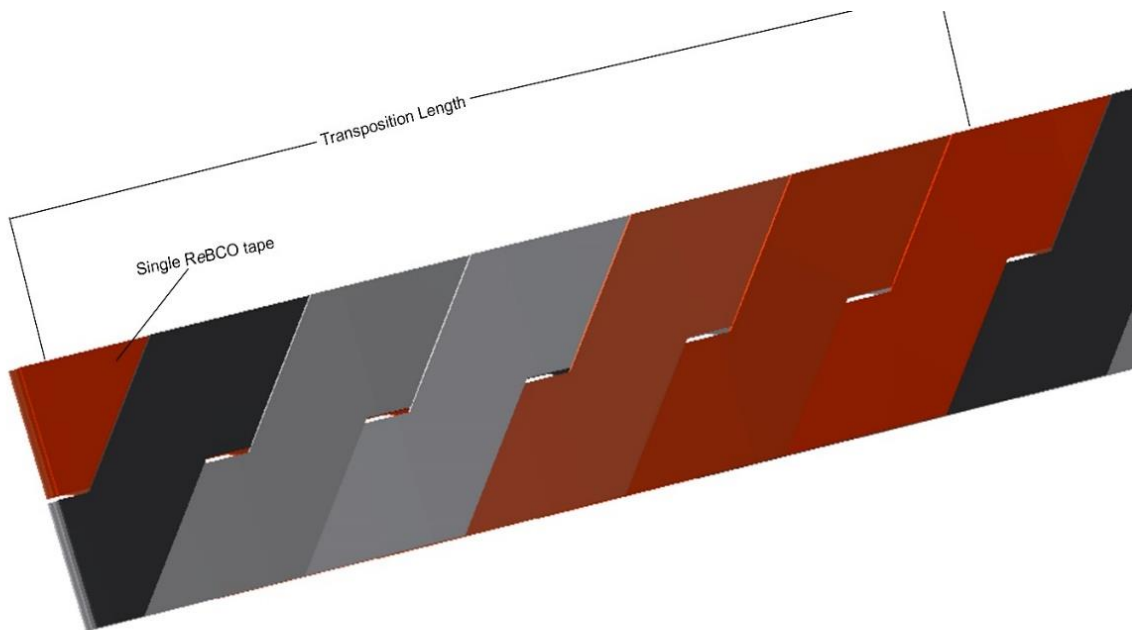


Figure 2.10: Schematic drawing of RACC.

2.5.2. Conductor on Round Core (CORC)

D.C. van der Laan in 2009 [Cvan09] proposed and published the concept of Conductor on Round Core (CORC) cables as shown in Figure 2.11. These cables have arrangement of the REBCO tapes, that is an arrangement similar to REBCO or BiSSCO (bismuth-strontium-calcium-copper oxide) power cables. They are tightly wound around a central former, usually a copper tube. The layers are wound in alternative directions, that is, each layer is wound in the opposite direction as the layer below. The CORC cable is flexible and it can be bent to a radius of few centimeters. It can be fit with a jacket of structural material such that it provides additional mechanical stabilization and extends possibility of forced air cooling with hollow formers. With increase in the REBCO tape layers, a thermal shield at the center of the cable is formed which sequentially leads to a strong radial temperature gradient leading to a higher current level.



Figure 2.11: Five CORC are twisted together to form a CICC [Corc00].

2.5.3. Twisted Stacked Tape Cables (TSTC)

In order to provide a “simple, high current density and scalable cabling method applicable to a large-scale magnet”, M. Takayasu et al. in 2011 [TCBM11] proposed the concept of Twisted Stacked-Tape Cable (TSTC). The REBCO tapes are longitudinally stacked and twisted due to which the Lorentz forces act radially. The electrical and mechanical stabilization is provided by copper tapes that are inserted into a structural jacket as shown in the Figure 2.12. Since they are of circular configuration, TSTC are anisotropic in radial direction. Due to mechanical loads in parallel direction TSTC is a better choice in high field magnets. High copper content in TSTC facilitates increase in the movement of thermal energy along the length of the sample that leads to decrease in the average temperature near the heating section.



Figure 2.12: Single strand and cabling of TSTC [BFMN18].

2.6. Winding pack and casing for TF coil

Above discussed cable concepts (in section 2.4 & 2.5) were developed especially for high field and current magnet application such as TF coils. Forces generated due to high magnetic fields are compensated using additional re-enforcements like steel case outside the magnet, radial plates (used in ITER TF coil as shown in Figure 2.13) as well as steel or aluminum jacket around the conductor. The jacket also helps in encapsulating helium which flows to cool the superconductor. The current density across the cross section of a TF coil is constant. To determine the number of turns of the coil is an iterative process that depends on the discharge voltage and current carrying capacity of the conductor. The discharge voltage helps to evaluate the

insulation, but the insulation should also meet the mechanical requirement of the magnet. If the requirements are not met, the number of turns must be varied.

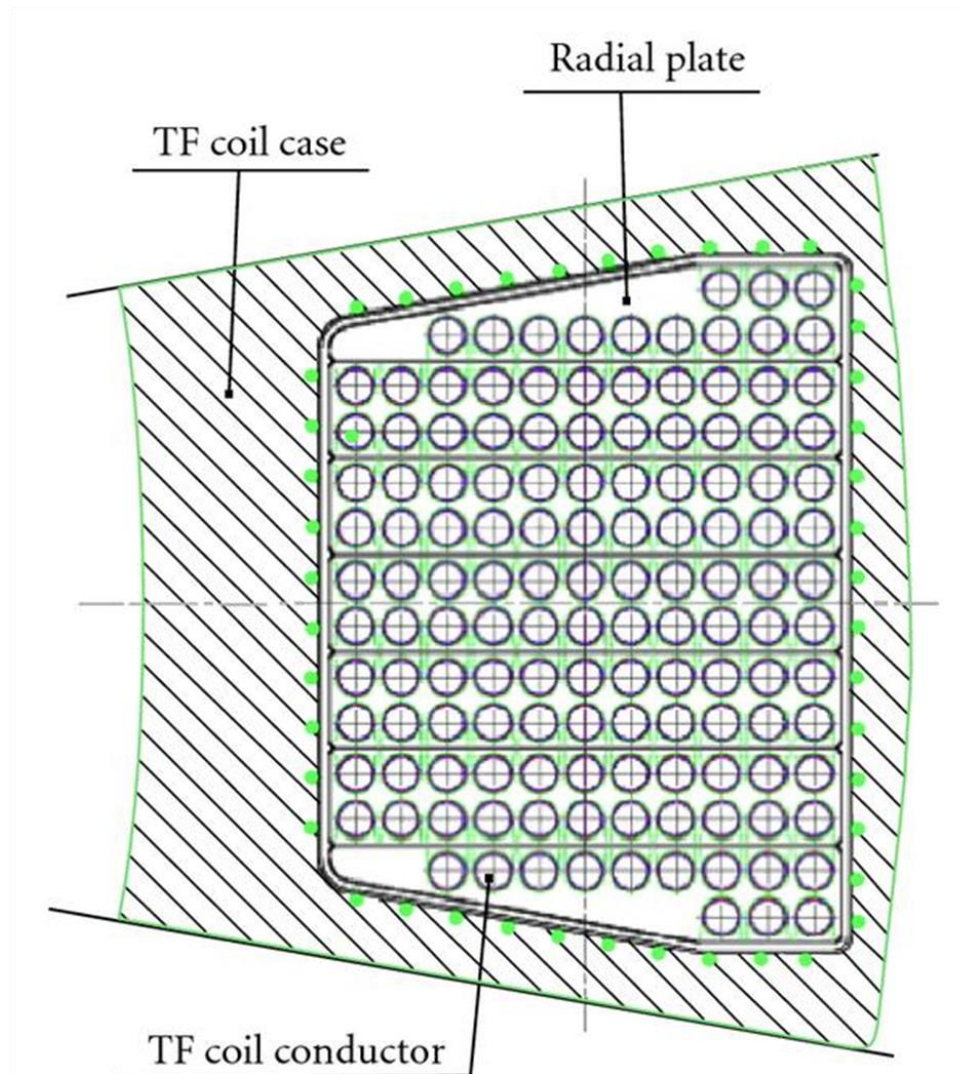


Figure 2.13: A cross section of ITER TF coil with radial plates, casing and conductor [MiSF08].

A toroidal field coil can be wound using a layer or a pancake winding. The advantages and disadvantages of a layer and pancake winding is discussed in section 3.2.3. It is evident from Table 2.4 that NbTi and Nb₃Sn are preferred low temperature superconductors for TF coil. Magnets made from NbTi conductor are simple because NbTi is a malleable alloy. The limitation of NbTi conductors comes with reduced current densities with high magnetic fields.

Nb₃Sn has been used for several years. Magnets made out of Nb₃Sn used techniques like “wind and react”. The former technique namely “react and wind” puts the magnet

at risk due to its brittle nature. Today, nearly all Nb₃Sn magnet use the “wind and react” method. Despite of being widely used techniques, great care must be taken while handling the conductor during the heat treatment process because of thermal expansions.

From section 2.5, high temperature superconductors can be a good fit for TF coils because

- High current density compared to NbTi and Nb₃Sn.
- No heat treatment is required.

2.7. Materials for TF Coil

The TF coil of superconducting materials like insulated cables or tapes that provide mechanical stabilization and fillvoids. The materials should be able to maintain their component structure and withstand thermal expansion due to temperature variations since operating temperature is 4K. In special scenarios like quench, the temperatures might rise as high as 250 K. Hence it is essential that the thermal co-efficient of materials used is in an identical range to prevent damage to the cables due to operating stresses. The materials are grouped into structured formats based on co-efficient of thermal expansion such as, superconducting tapes, structural stainless steel, aluminum or copper materials, plastics, composite materials, insulation and filling materials etc. to match specific application areas of activity.

The thermal expansion of structural materials like stainless steel 316-LN, stainless steel Nitronic® 40 etc., match that of REBCO tapes and are thus well suited for structural applications in HTS cable. Copper is used in superconducting cables for thermal and electrical stabilization for EU DEMO.

Composite materials are preferred in HTS cable since the pattern and thermal expansion can be adjusted as per requirements by adding e.g. glass fibers. Orienting the reinforced material in the direction of the superconducting tapes helps to avoid the differences in expansion along the length of the HTS cable.

Filling materials help to fill the voids and provide mechanical stabilization of high forces environments preventing movement of individual tapes. The filling materials should be mechanically strong and match the thermal expansion of REBCO tapes. Although materials such as, Stycast Black or Blue match the expansion of REBCO

tapes, they have been found unsuitable in high flux environment of fusion magnets, since they degrade when exposed to radiation. However, studies have shown that a mixture of Araldite epoxy resin with quartz powder is suitable for fusion applications [Bart13].

2.8. Pre-Conceptual Demo Design Using Process Code

PROCESS is a system code that self-consistently calculates the fusion power plant parameters with specific performance, provided that no operating limits are violated along with an option to optimize a given function of the parameters [Knig13]. The engineering and economic growth of a fusion power plants is assessed by PROCESS [KKLK14]. From the basic plasma physics to the generation of electricity, simple models of all parts of the reactor system are used for the assessment. Despite of being derived from many earlier system codes, PROCESS is based on the TETRA (TOKAMAK Engineering Test Reactor Analysis) code and its descendant STORAC (Spherical Torus Reactor Analysis Code). Although the code was written by personnel at Oak Ridge National Laboratory in Tennessee, USA, along with many other contributions, due to its evolution from a wide range of sources, the structure of the code is not considered ideal from the programmer's point of view. After many efforts put-in, to improve the code since early 1990's, in 2012 the whole program was upgraded to Fortran 90/95 along with benefits of modern software practices and several useful code management utilities.

Principally, PROCESS serves good mathematical evaluations of the available theoretical understanding and fits into the experimental data. The algorithms used in process are not oversimplified, instead, they do not possess enormous deal of complexity to present each and every model describing one of the component systems. This property facilitates to evaluate expressions, as the code's iterative approach to solve the optimization problem requires repeated evaluation involving a large number of expressions. This iterative approach turns to be incompatible with complex codes such as that of the fusion power plant design code. Therefore, PROCESS code is not a comprehensive fusion power plant design code, rather it forms a firm basis for the outlook of a conceptual and feasible power plant design.

3. Conceptual Design of a TF coil for EU DEMO

3.1. Introduction to the Conceptual Design of a TF Coil

The conceptual design of the TF coil for the EU DEMO starts from the output file of PROCESS code [KKKW11]. The TF coil system in EU DEMO consists of 16 coils, placed equidistant in the toroidal direction, carries high currents (in MA) and produces high magnetic fields. In this chapter, to understand the fields in the TF coil, the shape of the TF coil is modified from PROCESS code output. To perform an electromagnetic analysis, first conductor geometry and the winding pack have been defined using an iterative process. One of the outcomes of the electromagnetic analysis is the peak magnetic field. The peak magnetic field helps to determine the conductor performance.

During a quench the superconductor loses superconductivity and joule heat is produced. To protect the TF coil from the heat the current is discharged. A zero-dimensional adiabatic hotspot calculation is done to estimate the discharge time constant, in order to achieve an acceptable hot-spot temperature. The other outcome of the electromagnetic analysis is the inductance per coil. Using the inductance, the discharge time constant and the discharge voltage across the coil can be calculated.

3.2. Identifying the Parameters from the PROCESS Code

The input parameters for the design of the TF coil are taken from PROCESS System Code output dated 25th July 2012 [Demo00] and are summarized in Table 3.1.

Table 3.1: TF coil Parameters for EU DEMO

	DEMO July
Number of TF coil	16
Total current in one TF coil	19.2 MA
Toroidal field at plasma axis	6.823 T
Total available winding pack area	1.10 m ²
Overall steel cross section, inboard	1.34 m ²

3.2.1. Shape of TF Coil from the PROCESS Code

The approximation of the inner shape of the TF coil has been given by the output of the PROCESS System code. The design of D-shaped coil has to fulfill the requirement for plasma stability, plasma confinement and to reduce excessive mechanical stresses in a torus [FiSh71]. The detailed D-shape analysis will be discussed in chapter 4.1.2. As a consequence, the current centerline of the coil is composed of arc segments defined by center coordinates and the radius and angle of each arc. The criteria to define the geometry of the D-shaped coil are given below.

- i. the tangents of the successive arcs should match,
- ii. the sum of all angles of the arcs should be 180° for each the upper and lower half of the coil and
- iii. the inner leg of the TF coil has to be straight.

In Figure 3.1 the geometry of the TF coil as given in the PROCESS output is shown. It can be seen that the above-mentioned criteria are not fulfilled. The sum of the angles of the different arcs are not equal to 180° , at one point the tangents do not match and the straight leg is not straight.

Therefore, the shape of the TF coil has been modified in the frame of the EUROfusion work package [00b]. The improved shape is shown in right part of Figure 3.1. It is used in the further work.

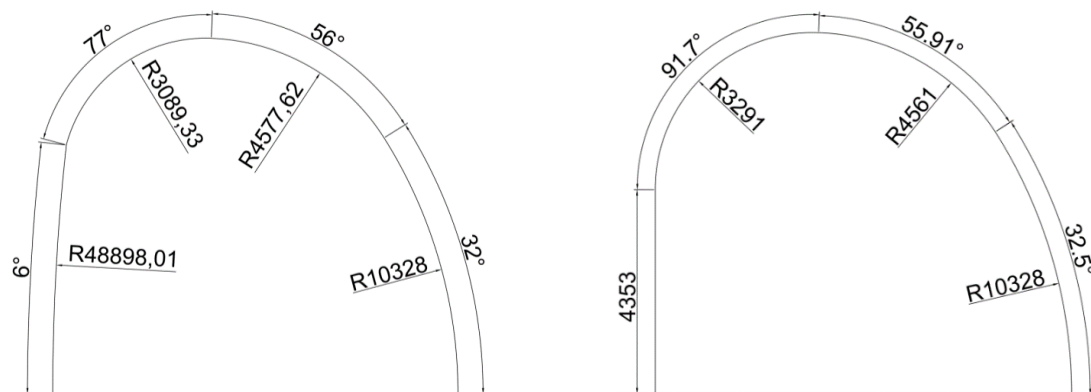


Figure 3.1: Left: D- shaped tori given from PROCESS code.

Right: Modified D-shaped tori to have consistent tangents, a sum of 180° and a straight inner leg for July 2012 design.

3.2.2. HTS conductor for TF Coil

Several concepts to form a high current conductor from HTS tapes have been discussed in chapter 2. In the TF coil conceptual design phase, the knowledge of a

3.2. Identifying the Parameters from the PROCESS Code

specific conductor design is not required. However, the cross sections of different materials in an HTS conductor used for the TF coils are necessary to come to an optimized conductor cross section.

In general, an HTS conductor consists of:

- i. *REBCO*-tapes which are mainly composed of the superconducting layer, the substrate, and a protective silver layer,
- ii. copper to protect the HTS conductor in case of a quench,
- iii. space for coolant flow (i.e. forced flow helium),
- iv. stainless steel for mechanical stabilization, and
- v. Electrical conductor insulation.

For example, HTS conductor must have sufficient copper to sustain the quench current and propagate quench, sufficient superconductor area to have a good operating margin and also have optimum area for flow of helium so as to ensure good cooling with less pressure drop.

The optimization of all the materials has to be done in an iterative process. Starting point is the operating point of the superconductor which is defined by the ratio of the operating current to the critical current. Taking the critical current of the superconductor at the peak magnetic field and the operation temperature as specified by the manufacturer the cross section of the HTS tapes is obtained. The amount of copper is optimized by limiting the maximum temperature of the HTS conductor using the adiabatic hot spot analysis. To withstand the Lorentz forces a stainless-steel jacket is added whose amount is determined by the structural analysis. Further investigation on the jacket thickness will be discussed in detail in chapter 4.1.9. For cooling enough space is allocated for helium flow. An electrical insulation of 1.5 mm thickness is taken for the conductor. The resulting area of various materials in the HTS conductor is shown in Figure 3.2 and summarized in

Table 3.2.

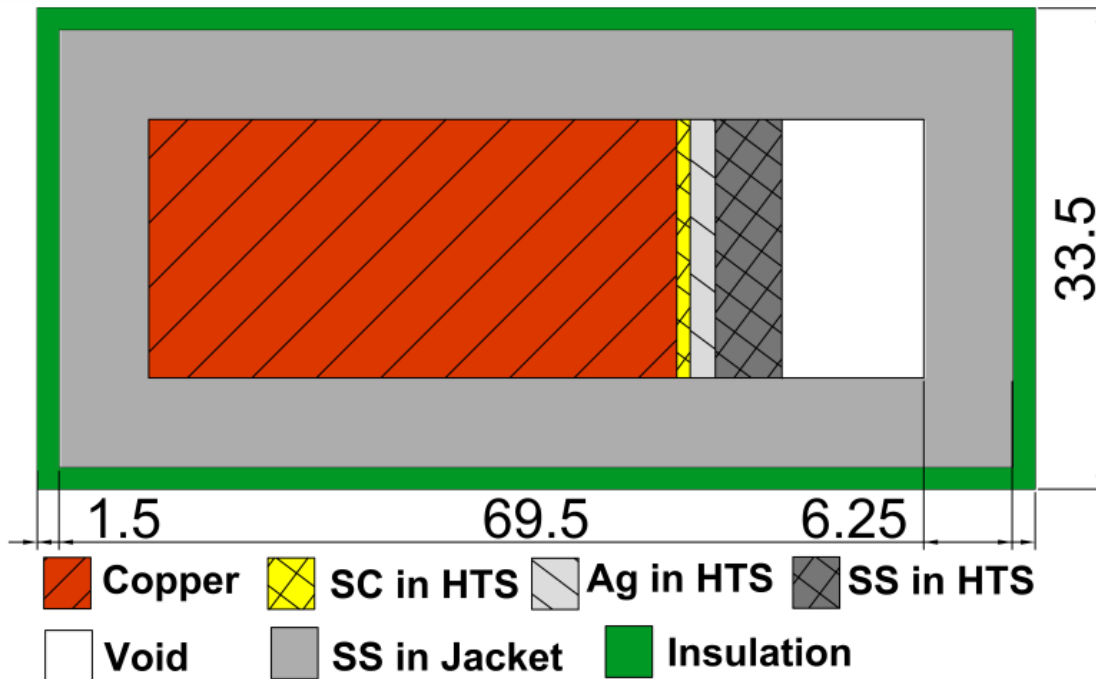


Figure 3.2: Cross sections of different materials in the HTS conductor surrounded by a stainless steel jacket with high voltage insulation. [GBBF14]

Table 3.2: Various Materials in HTS Conductor for TF coil

	Area in mm ²
Total Copper	553.2
Total Void	272.2
Total Hastelloy in HTS tapes	67.1
Total silver in HTS tapes	5.37
Total superconductor in HTS tapes	1.46
Total stainless steel in jacket	1056.25

3.2.3. Winding pack

Once the conductor geometry has been chosen, the selection of winding geometry and type is necessary. A TF coil can be wound using a layer or pancake winding. In a layer winding, the adjacent turns are laid evenly and side by side along the length of the coil and any number of additional layers may be wound over the first. The helium inlet connection is connected to each layer and the layer is connected in series electrically. The main challenge is in the first layer of the winding. This layer is facing plasma, the heat is accumulated, and the layer is in high field region. Therefore, the

3.2. Identifying the Parameters from the PROCESS Code

magnet operates at a lower operating margin. The advantage of having a layer winding is that one can have a different conductor in different layers.

A conductor is wound in a circumferential direction rather than along the axis of a magnet and forms a unit module like a pancake. 'Pancakes' are wound separately, stacked together, and then jointed electrically (pancake-to-pancake joint) in series. Locating the helium inlet in the high field region of the winding pack and the outlet at the low field region has the advantage that the temperature is lowest in the high field region. The warm helium flows from the low field region of the pancake winding. In the pancake winding, once the conductor geometry is fixed, it cannot be changed.

To understand the electrical and hydraulic circuits in the winding pack a schematic diagram is shown in the Figure 3.3. The winding pack is electrically connected in series. The hydraulic circuit is connected in parallel. To control the mass flow a control valve is present after a venturi flow meter. There are insulation breakers at each end of the winding pack in the hydraulic circuit to separate the electrical connection with the hydraulic connection. In case of quench the helium expands very fast and it cannot be escaped venturi valve. Therefore, a check valve is provided for the helium to escape.

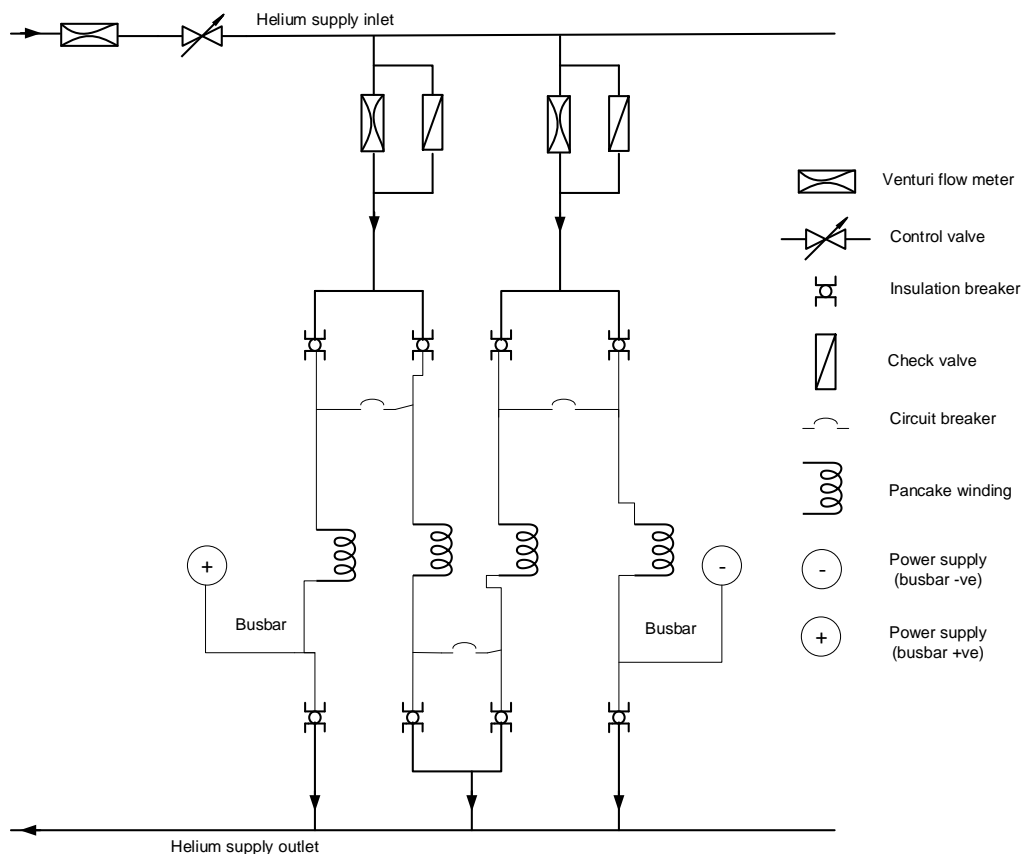


Figure 3.3: Schematic diagram representing the winding pack and bus bar.

3. Conceptual Design of a TF coil for EU DEMO

For the conceptual design a pancake winding is considered. In the pancake winding, the conductor is wound in the form of a D-shape like disks and stacked one over another. To adapt to the available space, 18 pancakes are required as shown in Figure 3.4. The dimensions of the 14 inner pancake and 2 outer pancakes are 1015 mm x 737 mm and 290 mm x 50.25 mm and the number of turns in the pancake packs is 374 and 26 respectively. The conductor length for center and side pancakes are 853 m and 741 m respectively. The total winding area is 0.77 m², which fits well into the available space of 1.10 m². There are 384 turns in total.

The thickness of ground insulation is chosen to be 10 mm. It is made of glass fibers and epoxy. Apart from the ground insulation, there are two other insulations required for electrical safety of the magnet, that is, turn insulation and pancake insulation. 1.5 mm of turn insulation is taken which consist of half overlapping Kapton-glass fiber wraps and the pancake insulation is to be 3 mm thick. For the HTS TF coil, the insulation thickness is chosen such to be consistent with the ITER design criteria [Mitc00].

After filling the winding pack and all required insulations, there is about 25 mm free space left around the winding pack. This space is filled with ground insulation material. A detailed analysis and design modification influencing the extra space are presented in Chapter 4.

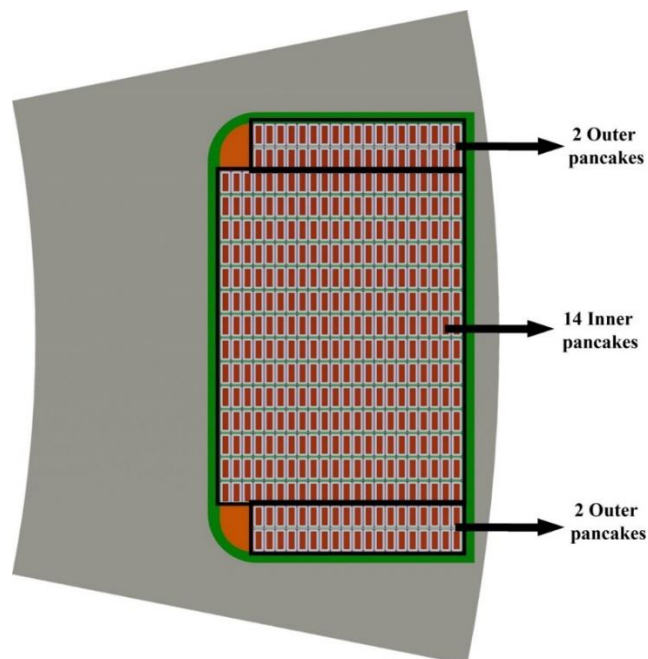


Figure 3.4: Proposed HTS winding pack cross section which has 2 outer pancakes and 14 inner pancakes with casing

3.2.4. Electromagnetic Field Calculation

Since the magnet parameters have been defined above, it is mandatory to check whether the magnetic field at plasma axis is equal to the required magnetic field from the PROCESS code. The peak magnetic field is also calculated which is necessary for defining the operating point of the conductor. For electromagnetic simulation, the pre-processor TOKEF [Mane84] and the code EFFI [Sack75] have been used. Most of the codes for calculating the magnetic field of a general, three-dimensional current distribution use formulations based on a filamentary approximation. The finite size of the conductor cross section is then approximated by a set of distributed filaments. While this method gives good results for field points outside the conductor, the singularities associated with it can lead to serious errors in the vicinity of the conductor. This makes it difficult to calculate magnetic forces accurately. In addition, large amount of data are often required to specify all of the filaments that are needed. To avoid these problems, EFFI uses a formula derived from the Bio-Savart law for a volume current distribution.

The following form of the Bio-Savart law is used for solving the volume integration as shown in the Figure 3.5.

$$\vec{B}(p) = \left(\frac{\mu_0}{4\pi} \right) \iiint_S \vec{J} \frac{d\vec{l} \times (\vec{r}_2 - \vec{r}_1)}{|\vec{r}_2 - \vec{r}_1|^3} dS \quad \left[\frac{Vs}{m} \right] \quad (3.1)$$

Similarly, the volume integration equation for the magnetic vector potential is as follows:

$$\vec{A}(p) = \left(\frac{\mu_0}{4\pi} \right) \iiint_S \frac{\vec{J} dl}{|\vec{r}_2 - \vec{r}_1|} dS \quad \left[\frac{Vs}{m} \right] \quad (3.2)$$

Where

r_1 = Source position vector

r_2 = Field point position vector

p = Field point

dl = Vector differential element in the direction of the current flow

dS = Differential area element perpendicular to the current flow.

J = Current density

μ_0 = Permeability of free space.

3. Conceptual Design of a TF coil for EU DEMO

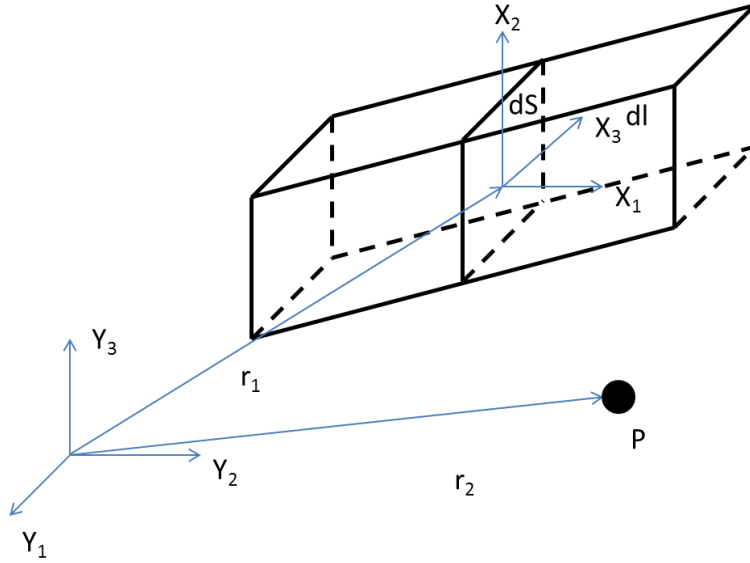


Figure 3.5: Variables for the general coil element used to define equation (3.1) and (3.2)

Apart from magnetic field calculation, EFFI is also capable of calculating magnetic flux lines, Lorentz forces and inductance.

The magnetic force exerted on a coil is calculated by integrating the vector product $\mathbf{J} \times \mathbf{B}$ over the conductor volume.

$$\vec{F} = \int \int_S \vec{J} dl \times \vec{B} dS \quad (3.3)$$

The integrals in this equation must be evaluated numerically. To make the evaluation simpler, the user has to divide the length of the conductor into short segments.

To calculate the inductance of the system of coils, EFFI uses the following formula.

$$M_{ab} = (j_b S_a S_b)^{-1} \oint_{S_a} \oint_{S_b} A_b \cdot dl_a \cdot dS_a \quad (3.4)$$

Where M_{ab} is the mutual inductance between coil a and coil b, J_b is the current density in coil b, S_a and S_b the respective coil cross-sectional areas, and A_b is the vector potential due to coil b.

3.2.5. Result of Electromagnetic Analysis

To compute the magnetic field at the plasma axis, all sixteen TF coils above have been modeled using the coil current given in Table 3.1 and the shape used in Figure

3.2. Identifying the Parameters from the PROCESS Code

3.1. The magnetic field at the plasma axis which is 9 m from the machine axis was calculated to be 6.83 T which is in good agreement with the output of the PROCESS system code (see Table 3.1 and Figure 3.6).

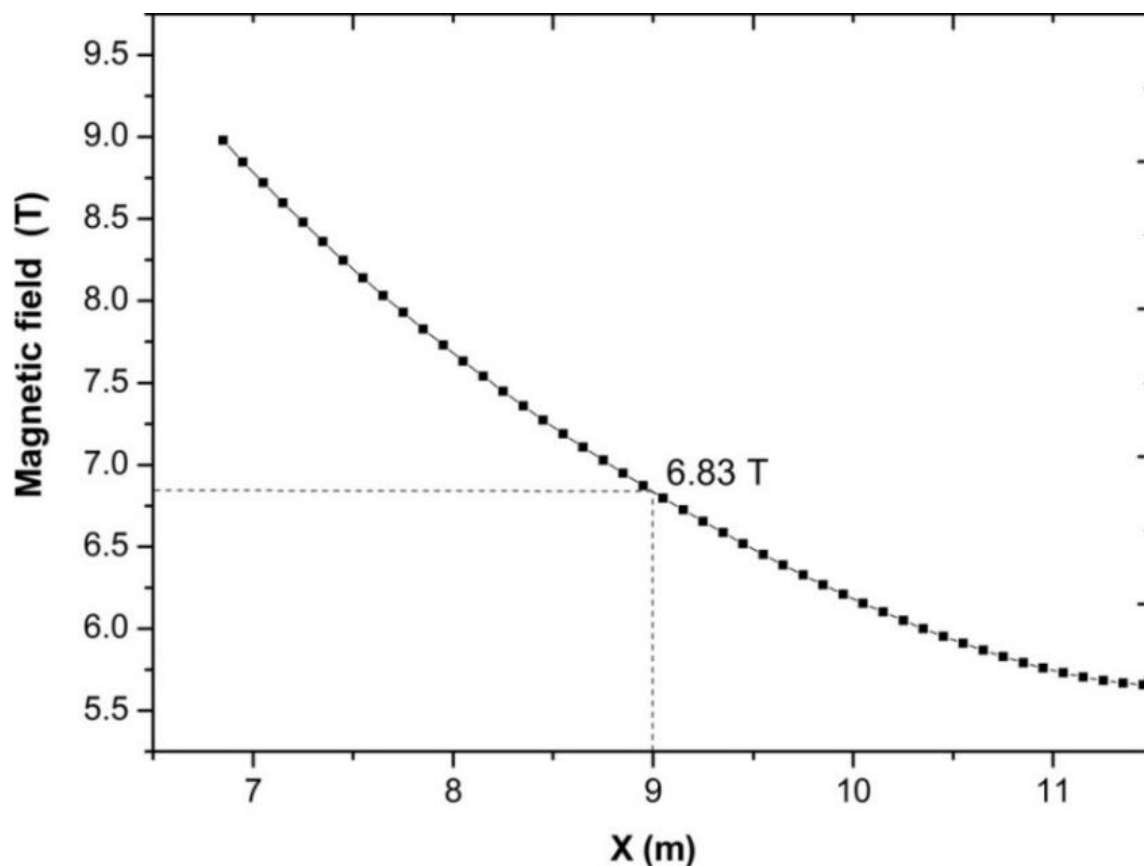


Figure 3.6: Magnetic field plotted along the center of torus. X is the radial dimension along the torus.

To determine the peak magnetic field, a cut section of the mid plane of the inner straight leg has been considered which has the highest magnetic field. The peak magnetic field is calculated in the inner edge of the winding close to the plasma wall and found to be 13.27 T as shown in Figure 3.7.

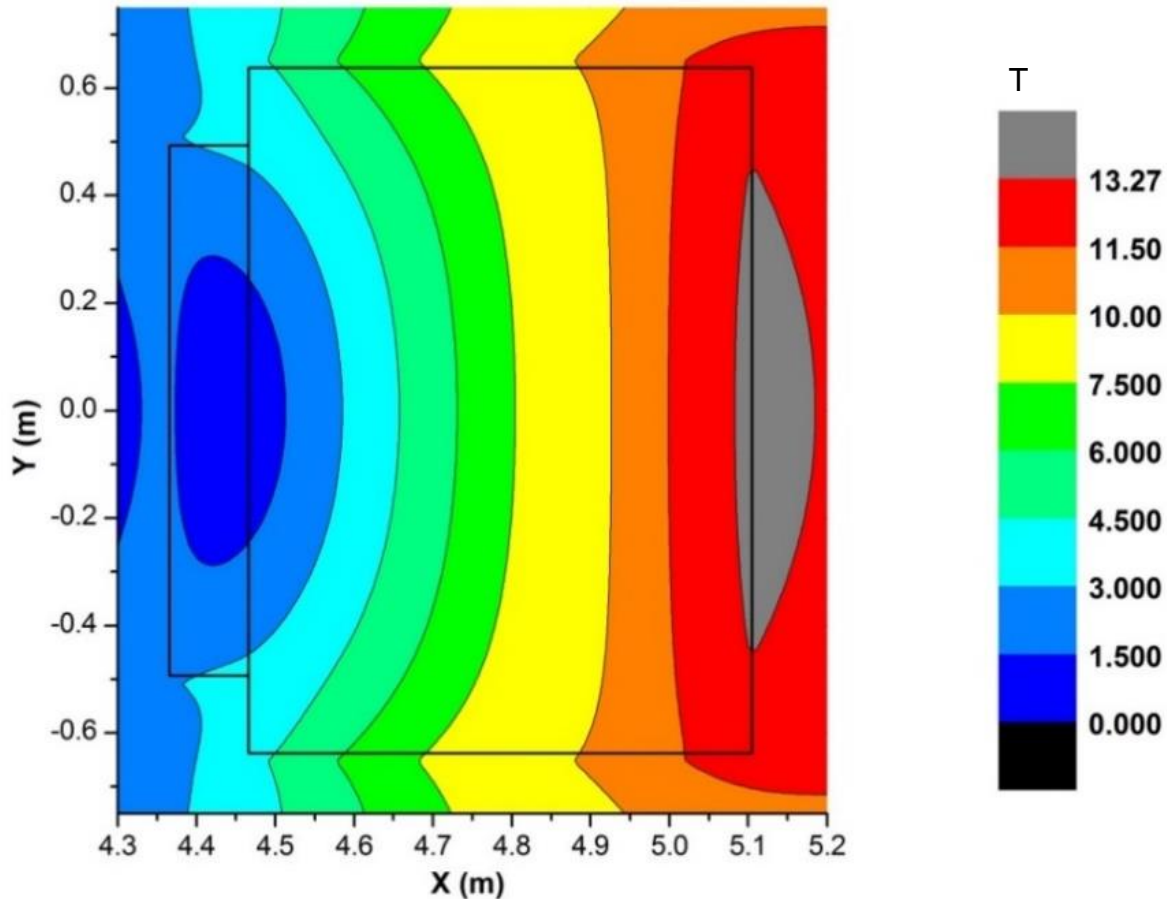


Figure 3.7: Magnetic field plotted at winding pack cross section of the inner leg of TF coil. X is radial dimension and y is axial dimension.

After computing the peak magnetic field, the inductances of all coils were calculated using EFFI. The inductance of the TF coil is needed to compute the coil discharge voltage. In the TF coil it is not sufficient to just calculate the self-inductance of the coil because all other coils are magnetically coupled as well. Therefore, to find the inductance, first, the total inductance of all the 16 coils i.e. self-inductance and the mutual inductances between coils were calculated to 7.28 H per coil.

3.2.6. Conductor Operating Point

To find the conductor operating point, the current density as a function of the magnetic field of the HTS conductor has been calculated for the amount of the superconductor as shown in

Table 3.2. The calculation has been plotted on REBCO tape data taken from [Haze10] and the results of the calculation are shown in Figure 3.7. For EU DEMO TF coil, the operating temperature of the conductor has been assumed to be below 14 K, because at peak magnetic field (13.27 T) and the operating conductor current (50 kA)

3.2. Identifying the Parameters from the PROCESS Code

meets temperature contour at approximately 14 K. The operating current of 50 kA (indicated as star symbol in Figure 3.8) results in an operating to critical current ratio of 0.7.

To evaluate the resulting temperature margin, the critical current vs temperature at 13.27 T has been taken from Figure 3.8 and shown in Figure 3.9. From this plot, the HTS conductor temperature margin is estimated to be 11.9 K.

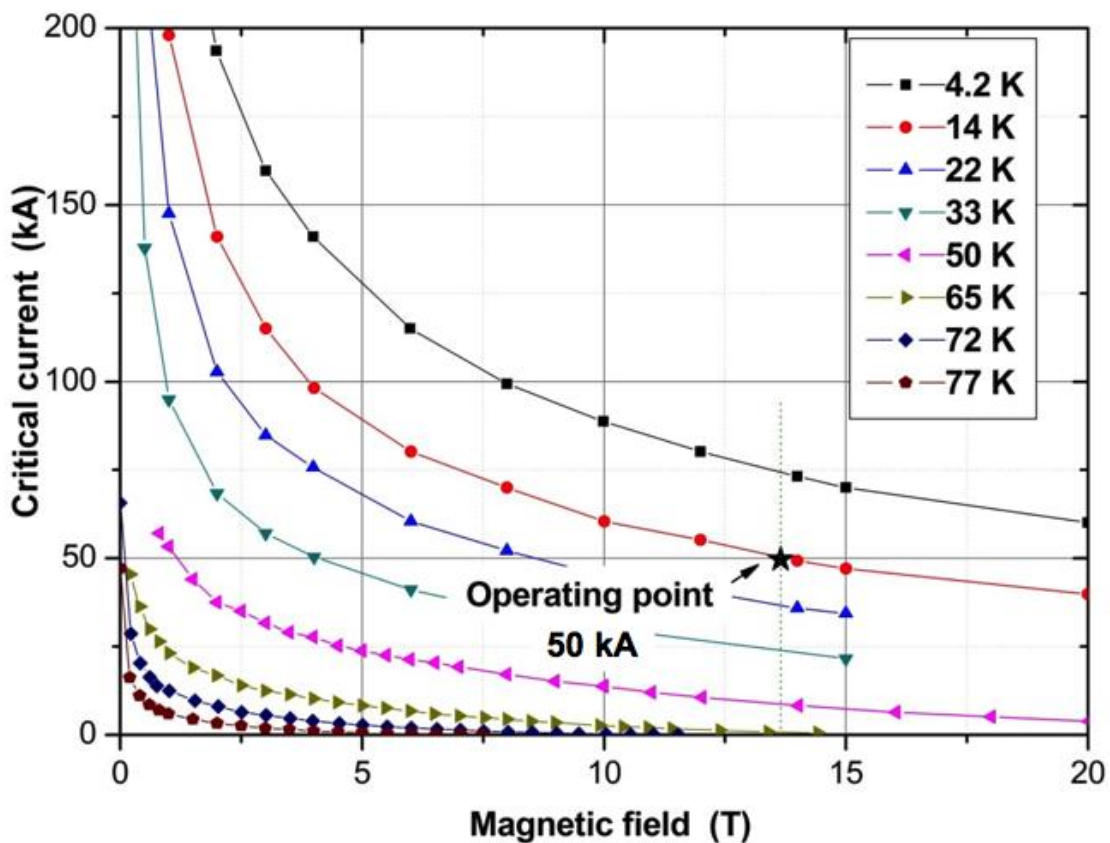


Figure 3.8: Magnetic field vs critical current at different temperatures. The operation point is indicated as black star

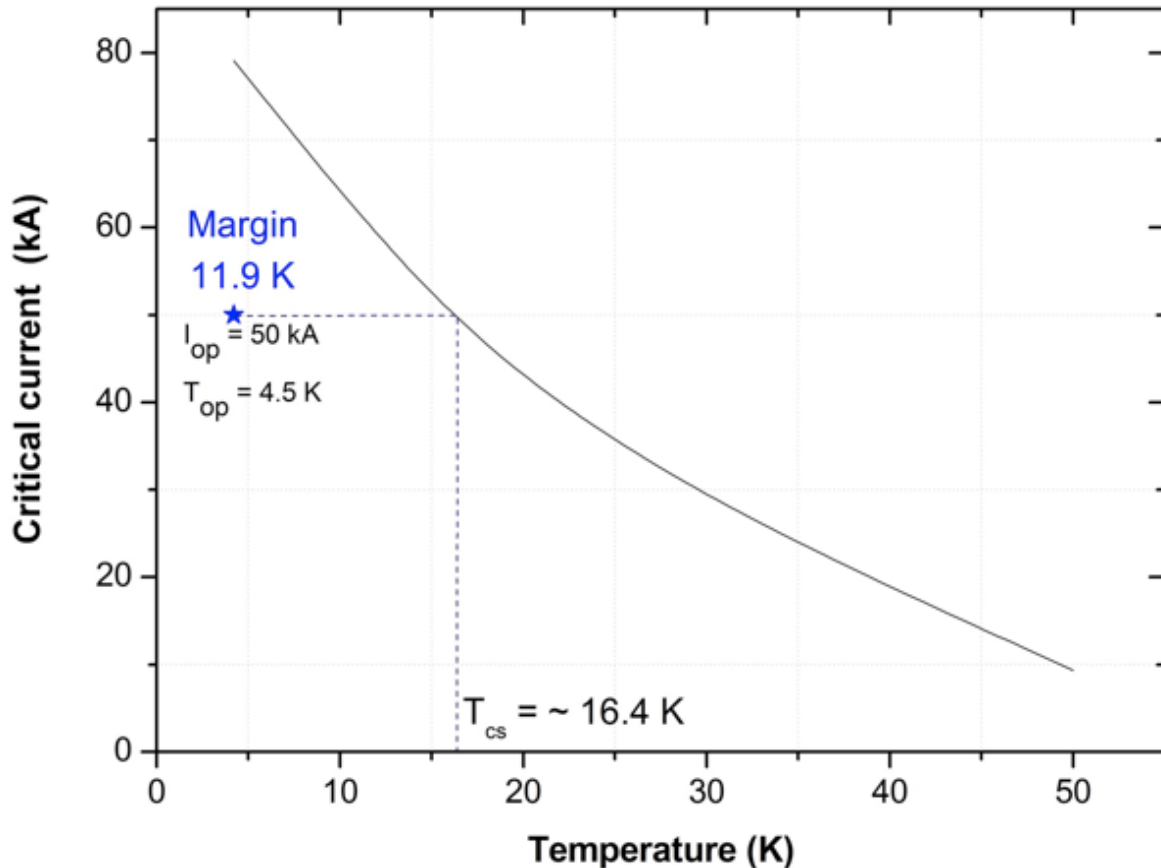


Figure 3.9: Critical current vs temperature at 13.5 T magnetic field. The operation condition is indicated as asterisk.

3.2.7. Hotspot Calculation

One important failure which has to be considered in the design of a superconducting magnet is the case of a transition of the superconducting to normal conducting phase. As the electrical resistance of the superconductor material in normal conducting mode is high, it is necessary to introduce copper as an electrical by-pass for the transport current, thus generating joule heating. To avoid excessive temperature rise, the magnet has to be discharged by introducing an external resistance parallel to the magnet. The discharge time constant τ_D determines the maximum temperature T_{max} in the magnet during the discharge. To limit T_{max} to an allowable value, which is given by the ITER hotspot criteria [Mitc09] τ_D has to be limited. The criterion limits the maximum allowable adiabatic hotspot temperature to 150 K, taking into account all materials in the conductor, i.e., superconductor, copper, helium, stainless steel jacket, and insulation.

Equation ((3.5) shows the so-called zero-dimensional adiabatic hot spot model. In this model heat conduction is neglected.

3.2. Identifying the Parameters from the PROCESS Code

$$\tau = \frac{1}{I^2} \int \frac{\rho C_p}{R} \partial T \quad (3.5)$$

Where,

ρ = density of the material

$C_p(T)$ = heat capacity of the material at constant pressure

T = temperature

τ = time

IR = Joule heating

A quench is detected only when the voltage across the terminal reaches 100 mV. Once the voltage reaches 100 mV, 1 s is required for the quench detector to decide whether there is a quench or not and 1 more second to initiate the discharge circuit to drain the current from the TF coil with an exponential time constant τ_D . In case of the HTS conductor specified in

Table 3.2 a time delay of 7 s found. The adiabatic hotspot calculations were performed for various τ_D . In Figure 3.10 the hotspot temperature has been plotted against τ_D . The result is that the magnet will reach 150 K for $\tau_D = 30.5$ s. Thus, a discharge time constant of $\tau_D = 30$ s is chosen. From this, the discharge voltage V_D for one coil is calculated using Equation (3.6) and the inductance per coil of 7.28 H. The result is $V_D = 12.2$ kV

$$V_D = \frac{L \cdot I_{op}}{\tau_D} \quad (3.6)$$

Where,

V_D = Discharge voltage

L = Inductance per coil (which is simulated using EFFI code)

I_{op} = Operating current

τ_D = Discharge time constant

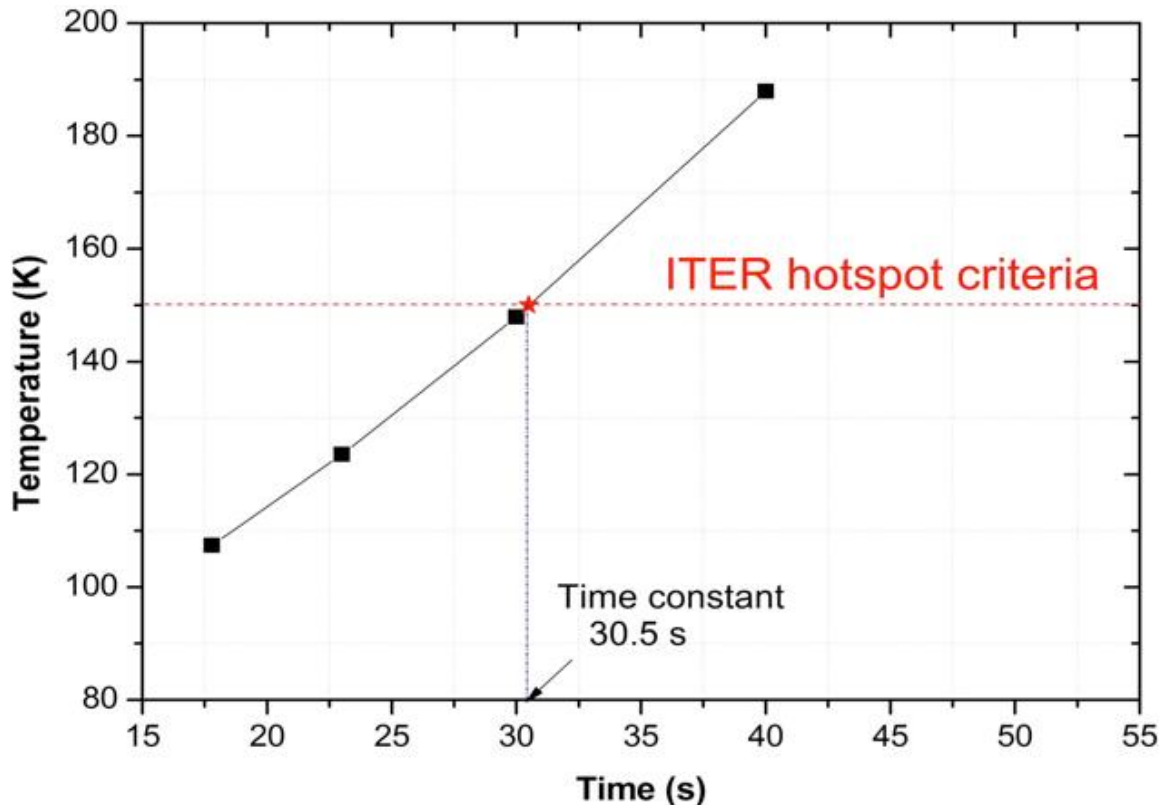


Figure 3.10: Time vs adiabatic hotspot temperature. The operation condition is indicated as asterisk.

3.3. Electromagnetic Analysis Conclusion

In this chapter, the shape of the TF coil is shown and the electromagnetic calculations are derived.

Based on the current analysis, it can be said that:

A HTS winding pack principally fits in the given winding pack area and can produce the required magnetic field at plasma axis for the EU DEMO. With the design proposed herein, the peak magnetic field at the superconductor is 13.27 T. The use of HTS increases the temperature margin to more than 11.9 K. Compared to the PROCESS code, an increase of the discharge time constant from 17.78 s for a low temperature superconductor to 30 s is possible with HTS, which helps in limiting the discharge voltage. All the parameters are summarized in Table 3.3.

With these results it is demonstrated that at 4.5 K the actual available HTS material can be used to design a TF coil for EU DEMO within available winding pack space.

3.3. Electromagnetic Analysis Conclusion

Table 3.3: Summary

Parameter	Value and unit
Number of TF coil	16
Total current in one TF coil	19.2 MA
Peak field on conductor	13.27 T
Inductance per coil	7.28 H
Operation current	50 kA
Energy stored in one TF coil	9.09 GJ
Total number of conductor turns in winding pack	384
Total winding pack area used	0.77 m ²
I_{op}/I_c	0.7
Operating temperature	4.5 K
Current sharing temperature	16.4 K
Temperature margin	11.9 K
Discharge time constant	30 s
Discharge voltage	12.2 kV
Adiabatic hotspot temperature	144 K
Conductor length of inner pancake	853 m
Conductor length of outer pancake	741 m

4. Structural Analysis of the TF Magnet for EU DEMO

4.1. Structural Analysis

4.1.1. Introduction to Mechanical Analysis

The TF coil in EU DEMO carries high currents (in MA) and produces high fields, which subjects the coil to high magnetic pressure and forces. In a torus, the internal magnetic field varies with the inverse of the coil radius. This produces a net centering load on individual TF coils as shown in the Figure 4.1 [Mose75]. The non-uniform magnetic pressure leads to a change in the ideal shape from a circular torus form to a D-shape form. The shape arises by mathematically matching the local radius of curvature of the coil to the magnetic pressure and the assumption that the inner leg can be supported radially by another structure [Titu03]. The details of the mathematical model which has been used to calculate the hoop force on the winding pack will be explained in section 4.1.2.

After calculating the magnetic fields and hoop force, it is necessary to perform a structural analysis to determine the stresses in the coil casing (steel support structure) and in the winding pack. As it is of particular interest to know the performance of the winding pack rather than of the whole TF coil structure, a 2-D model of the inboard leg in the midplane (Figure 3.4) has been created. The midplane of the inboard leg was identified as the area with the highest stresses. This has been confirmed by a similar analysis for the JT-60SA TF coil system [NPDD10].

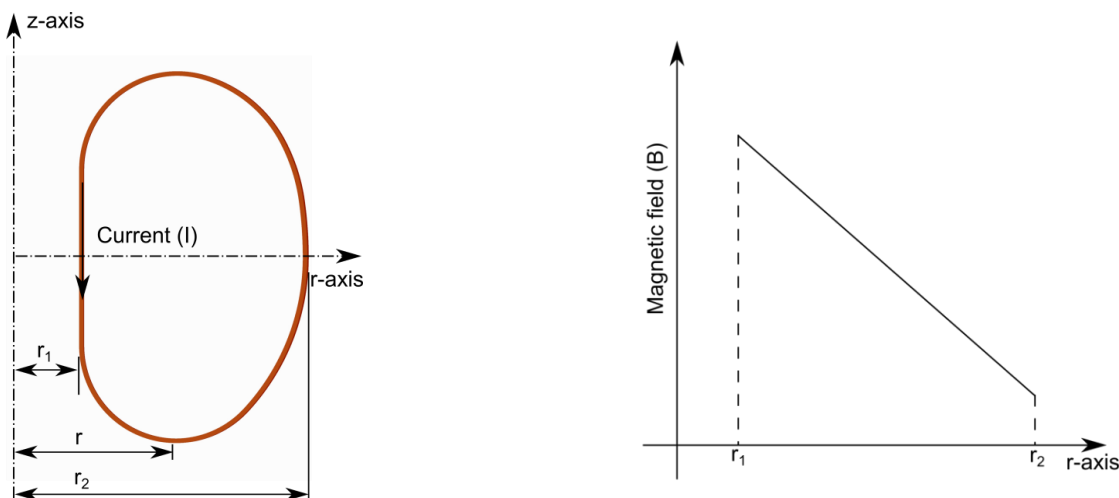


Figure 4.1: Ideal D shaped toroid and the magnetic field inside the toroid as a function of the radius.

4.1.2. Constant Tension Coil and Hoop Force

Firstly, we assume a non-circular thin sheet of a torus in which the plasma is encapsulated. This torus is made up of a number of current filaments (N), each lying in a rz plane. These current carrying filaments are assumed to be uniformly distributed around the z -axis as shown in Figure 4.2. With the minimum distance from the z -axis to the current sheet r_1 (as shown in Figure 4.1) the maximum field within the current sheet is expressed as

$$B_m = \frac{\mu_0 N I}{2\pi r_1} \quad (4.1)$$

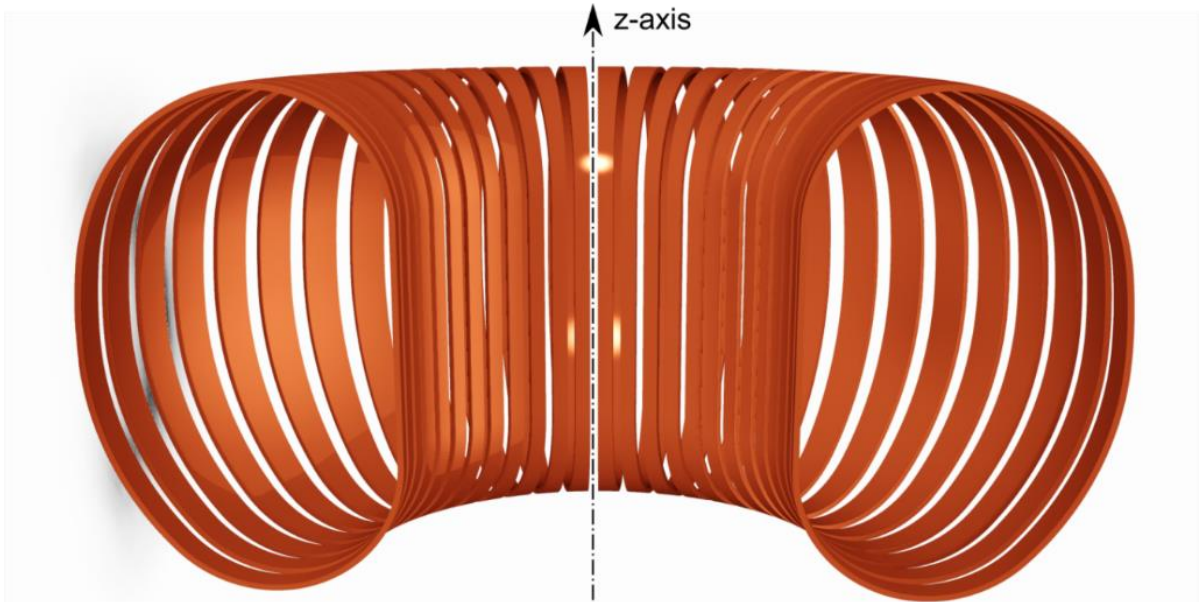


Figure 4.2: Ideal thin shell tori composed of a current sheet uniformly distributed on a surface which has non-circular cross section.

The field in the ϕ -direction inside the torus can be expressed as (4.2).

$$B = \frac{B_m r_1}{r(r)} \quad (4.2)$$

Figure 4.3 illustrates a segment of the torus in the rz -plane where it carries a current I . The magnitude of the field inside the torus at this location is B , and the radius of curvature of the torus at this location is ρ . If the conductor segment of the length $\rho d\theta$ is in equilibrium under the influence of the electromagnetic load and a simple average tension T at its ends, then the force balance results as in equation (4.3)

$$T = \frac{1}{2} I B \rho \quad (4.3)$$

4. Structural Analysis of the TF Magnet for EU DEMO

By combining equation (4.2) and (4.3) one gets

$$T = \frac{I\rho B_m r_1}{2r} \quad (4.4)$$

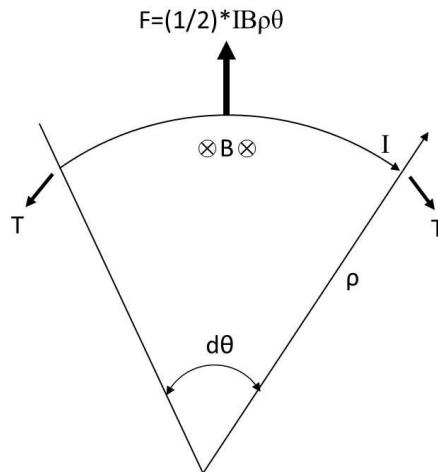


Figure 4.3: Segment of a thin-shell torus with total current I . The magnitude of the field within the torus at this location is B and the local radius of curvature is ρ .

Equation (4.4) describes how the radius of the curvature ρ must vary to maintain T constant around the entire periphery of the shell. That is,

$$\rho = kr \quad (4.5)$$

Where

$$k = \frac{2T}{IB_m r_1} = \frac{4\pi T}{\mu_0 N I^2} \quad (4.6)$$

and

N =total number of coils in the torus

I =total ampere turns per coil

The local radius of the curvature at a point on a curve lying in the rz -plane of a TF coil is derived by [FiSh71]

$$\rho = \frac{\pm \left[1 + \left(\frac{dz}{dr} \right)^2 \right]^{3/2}}{d^2 z / dr^2} \quad (4.7)$$

Combining equation (4.5) and (4.7) results in a differential equation which has a number of solutions depending on k such that each solution represents a constant tension as follows:

$$r \frac{d^2 z}{dr^2} = \frac{\pm 1}{k} \left[1 + \left(\frac{dz}{dr} \right)^2 \right]^{3/2} \quad (4.8)$$

Equation (4.8) is of second order and therefore requires two integrations. The procedure for carrying out the first integration is given by [FiSh71], who performed the second integration numerically. The resulting coil form and the suggested means of support are illustrated in Figure 4.4. This figure shows a constant tension curve whose local radius of curvature is proportional to the distance from the z -axis, as required by equation (4.5). The curve begins and ends tangential to a cylinder section which supports the net force on the coil towards the z -axis. This central support is frequently called a buckling cylinder. The extreme dimensions from machine axis are given by

$$r_1 = r_0 e^{-k} \quad (4.9)$$

$$r_2 = r_0 e^{+k} \quad (4.10)$$

and

$$k = \frac{1}{2} \log_e \left(\frac{r_2}{r_1} \right) \quad (4.11)$$

The curve segment of the coil is completely determined by specifying of k and either r_1 , r_2 or r_0 . This coil geometry is known as the Princeton-D [FiSh72].

4. Structural Analysis of the TF Magnet for EU DEMO

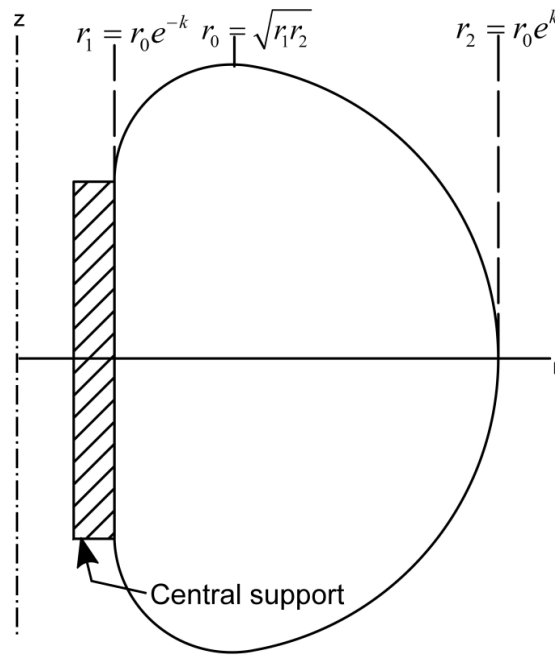


Figure 4.4: Example of an ideal constant tension toroidal coil shape.

Figure 4.5 shows an exploded view of the curved and straight segments of the D-shaped coil to illustrate the force balance. The magnetic load dF on the curved coil segment is everywhere normal to the coil, and non-uniform because of its r dependence, as shown by Equation (4.2). The shape of the curved segment is such that it is under constant tension and experiences no net load in r -direction. If the cylindrical support compensates the net centering force (F_{bc}) then the straight segment of the coil is under constant tension too.

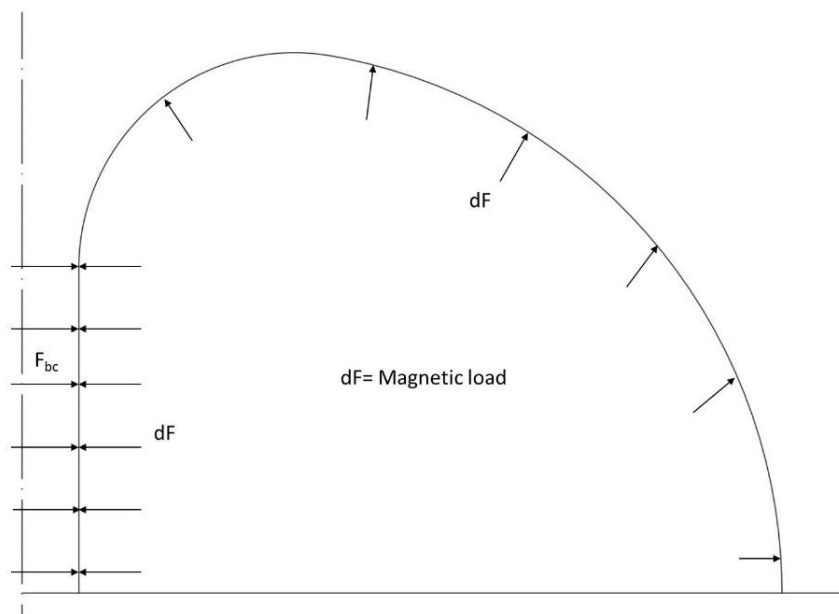


Figure 4.5: Exploded view of the straight and curved segments of the upper half of the constant tension shape.

The total force in z-direction on the top half of this coil is two times the total tension and the total force on the top half of the torus is two times number of coils times the total tension, which can be written as follows based on equation (4.1), (4.6) and (4.11):

$$NF_z = \frac{B_m^2 \pi r_1^2}{\mu_0} \log_e \left(\frac{r_2}{r_1} \right) \quad (4.12)$$

where

F_z = force per coil in z-direction

N = number of coils in the torus

Thus, F_z is the hoop force acting on the coil.

To illustrate the hoop force and stress, the TF coil system of various TOKAMAKs is considered. In Table 4.1, some actual TOKAMAK parameters are listed. By substituting these parameters in the equation (4.12) the hoop force is calculated. The hoop force is divided by the total amount of steel in the winding pack and casing to calculate total hoop stress.

Table 4.1: Comparison of hoop forces and stress for selected TOKAMAK systems

	JT-60SA	ITER	EU DEMO (July 2012)
r_1	1.2 m	2.347 m	5.103 m
r_2	5.7 m	7.915 m	13.446 m
N	18	18	16
B_m	5.6 T	11.8 T	13.27 T
F_z	23 MN	194.54 MN	694.1 MN
Steel in the casing	0.041 m ²	0.341 m ²	1.33 m ²
Steel in the winding pack	0.013 m ²	2.62E-4 m ²	0.398 m ²
Steel in the radial plates	0	0.598 m ²	0
Total hoop stress	401.5 MPa	324.88 MPa	428.53 MPa
% Hoop stress by winding pack	23.06	43.05	23.61
% hoop stress by the case	76.93	56.94	76.39

4. Structural Analysis of the TF Magnet for EU DEMO

From the table it can be seen that the hoop force increases with the size of the TF coil but the hoop stress is comparable. This is of course expected because the amount of stainless steel in the TF coil is the result of the design. For JT 60-SA and EU DEMO there are no radial plates present in the winding pack as it is the case for ITER. Therefore, the percentage hoop stress shared by the winding pack is comparable. In ITER, the radial plates contribute to support the hoop force generated by the conductor.

4.1.3. D Structural Analysis of the Inboard Leg in the Midplane

Each TF coil experiences a massive mechanical load originated by Lorentz forces in the winding pack. The Lorentz forces are calculated using the conductor current and the local magnetic field generated by the whole torus resulting in a deformation of both the coil case and the winding pack. With a 3-D electromagnetic analysis using the code EFFI [Sack75], the magnetic field was calculated and the magnetic field components F_i , $i=x,y,z$, at various (x,y) points for $z = 0$ are generated. Here the contributions from the CS and PF coils are not considered. The magnetic field components were then used to calculate the Lorentz forces within the software COMSOL [Http00]. With this software one can easily extend conventional models for one type of physics into Multiphysics models that solve coupled physical phenomena.

4.1.4. Modeling

To analyze the 2-D model, in the elastic regime two general types of the analysis are considered, plane stress and plane strain.

4.1.4.1. Plane Strain

To illustrate the plane strain and plane stress model, a simplified 3-D object is assumed whose 2-D structural analysis needs to be done. In plane strain situation, the strain within the thickness, or in z-direction, is zero. This means by definition that all the sides of the midplane (as shown in Figure 4.6) are fixed, which results in no displacement in z-direction.

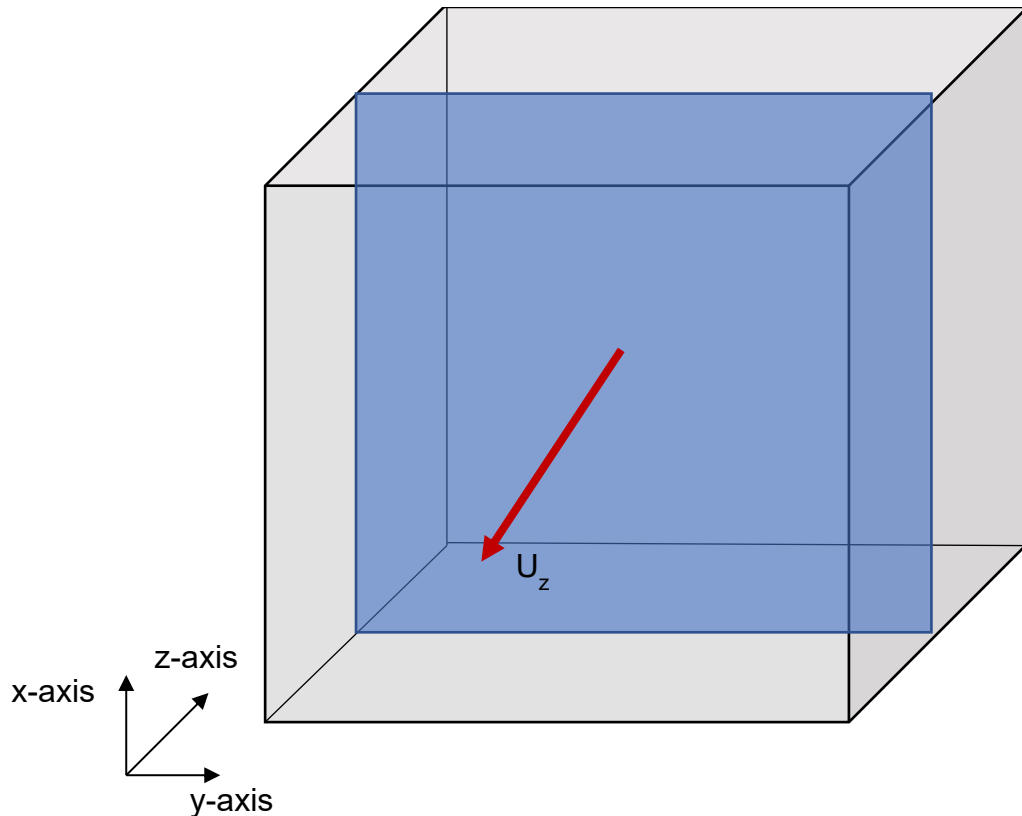


Figure 4.6: The plane strain and plane stress models. The displacement in the mid plane is denoted by U_z

4.1.4.2. Plane Stress

In case of plane stress situation, the stress within the thickness or in z-direction is zero. This means that the edges of the midplane (as shown in Figure 4.6) are free to move, this results in a displacement in z-direction.

Usually the strain model results in lower stress than that of the plane stress model. As in the magnets the conductor tends to move a bit due to the Lorentz force, the plane stress model looks more appropriate. In order to check the results on the stress both models are used in the simulations.

4.1.5. Modeling Criteria

The maximum allowable stress for SS316LN is defined in the Structural Design criteria for magnets [Jong08] and shown in equation (4.13).

$$\frac{2}{3} * \text{yield strength} \quad (4.13)$$

4. Structural Analysis of the TF Magnet for EU DEMO

The yield strength of the SS316LN is 1000 MPa, therefore the maximum allowable stress is 667 MPa. This is relevant for the coil case and for the conductor jacket.

The maximum allowable shear stress in the insulation is defined by the LHD criteria [KYUM94] and shown in Equation (4.14)

$$\frac{\sigma_N}{\sigma_0} + \frac{\tau_N^2}{\tau_0^2} = 1 \quad (3.14)$$

where

σ_N, τ_N are the normal and shear stress components respectively

σ_0, τ_0 are the tensile and shear strengths determined experimentally

The value of σ_0, τ_0 are 38 MPa and 27 MPa at 77 K [KYUM94].

4.1.6. Introduction to various models simulated in COMSOL

In study 1, the stainless steel case geometry given by the PROCESS code and is converted in the EUROfusion CAD model[Harm13]. The winding pack is filled using the generic conductor already shown in Figure 3.4. After filling the available space for the winding pack with HTS conductors and insulations, approximately 25 mm extra space is left between the ground insulation of the winding pack and the casing. This extra space is uniformly filled with the same ground insulation material. For simplicity the winding pack is rigidly connected to the coil casing (so-called bonded model) and plane-strain elements are used. In addition, the Young's modulus of the cable space, the so-called "homogenised cable space without helium", is used as shown in Table 4.2. More details about the material properties are described in section 4.1.7.

In study 2, the case geometry is modified by increasing the thickness of the stainless-steel casing facing to the plasma by 25 mm. The winding pack geometry was not changed. In addition, the sharp edge corners in the casing at the plasma facing side are smoothed out by introducing a corner radius of 34 mm (Figure 4.8).

In study 3, the Young's modulus of the cable space has been changed; the so-called "homogenised cable space with helium" is used as shown in Table 4.2. When the TF coil is energized, due to such huge Lorentz forces acting on the winding pack, the winding pack including ground insulation detaches from the casing in the inboard leg

towards the center of the machine (so-called de-bonding). This situation is taken into account by introducing a suitable boundary condition that is explained in section 4.1.8. Finally, plane-stress elements were used as they should give a more realistic approximation of the 2-dimensional mechanical behavior of the TF coil in vertical direction.

In study 4, the same boundary conditions are used as for study 3, but a conservative approach is used for the mechanical properties of the cable space. Here it is assumed that the cable space has zero Young's modulus. In reality, the stress will be between those obtained in study 3 and study 4.

In all studies the structural analysis was performed at room temperature, i.e., the cool-down of the coil has not been considered.

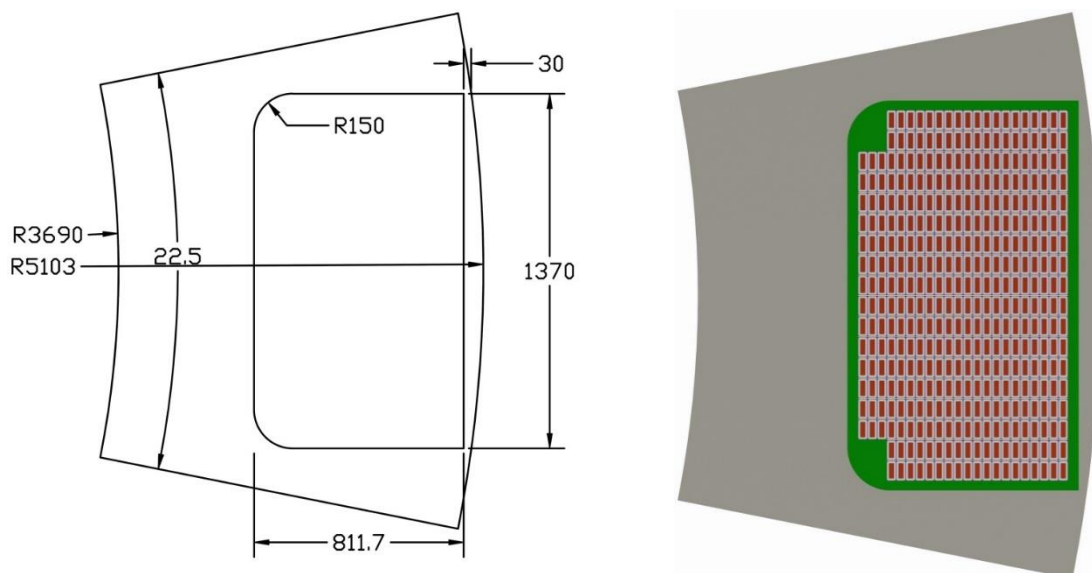


Figure 4.7: a: Cut sectional view of the TF coil in the mid-plane of the inboard straight leg with the geometrical parameters as taken from the PROCESS code. b: shows the cut sectional view of TC coil in the mid-plane of the inboard straight leg with the winding pack.

4. Structural Analysis of the TF Magnet for EU DEMO

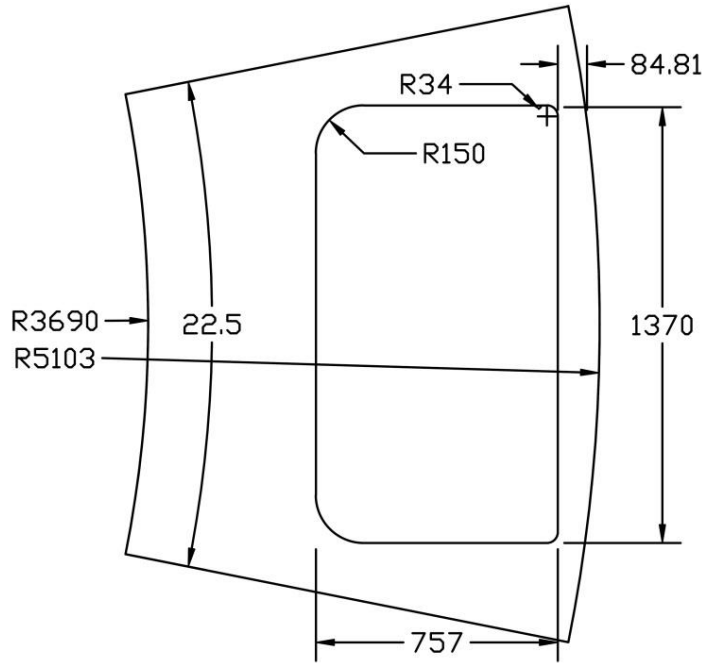


Figure 4.8: Cut sectional view of the modified TF coil in the mid-plane of the inboard straight leg.

4.1.7. Material Properties

The isotropic material properties were taken from ITER DDD and are shown in Table 4.2. For the homogenized cable space, the material property was averaged with cable components in that cable space. To calculate the weighted averages, percentages of cable components such as copper, YBCO, solder, hastelloy and helium are taken from chapter 3. The percentage of each component is multiplied with the material property (i.e young's module, poisson ratio and density) of each material with averaged over the percentage. In the studies the effect of the homogenized cable space with and without helium is used.

Table 4.2: Material properties used in simulation

	Young's Modulus	Poisson ratio	Density
Conductor jacket and casing	205 GPa	0.3	7900 kg/m ³
Turn insulation and pancake insulation	7 GPa	0.33	1816 kg/m ³
Ground insulation	12 GPa	0.33	1948 kg/m ³
Filler material	7 GPa	0.33	1816 kg/m ³
Homogenised cable space without helium	139 GPa	0.337	6700 kg/m ³
Homogenised cable space with helium	95.7 GPa	0.22	6221 kg/m ³

4.1.8. Boundary Conditions

Two boundary conditions are applied for study 1 to study 4 simulations in COMSOL to take into account all 16 TF coils.

First, a sliding condition (roller boundary condition) is used on the outer sides of the casing facing the neighbor coils, which means there is no displacement in the direction perpendicular to it. Since the inboard leg of all the TF coils are in contact in azimuthal direction, there is no displacement in toroidal direction. This is seen in Figure 4.9 with thick red lines on upper and lower sides of the stainless-steel casing. The second boundary condition is represented by the Lorentz force (F_x , F_y), which is generated by the current carrying conductor in a magnetic field. Here the current carrying cable is approximated by a homogeneous area inside the conductor jacket as shown in Figure 3.2.

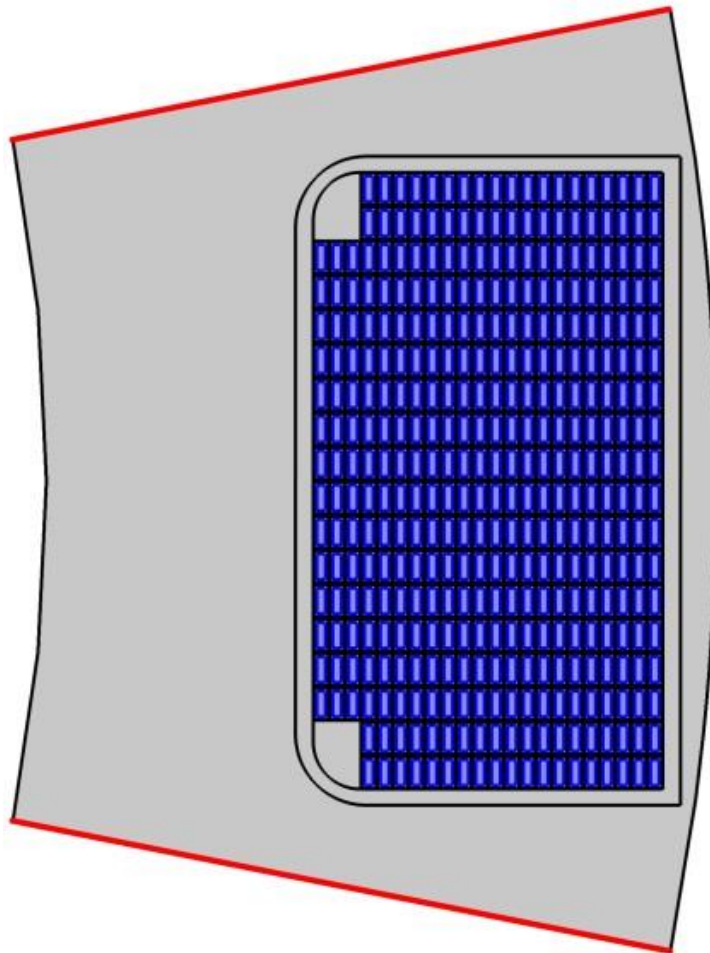


Figure 4.9: Boundary conditions applied in COMSOL (red lines denote sliding boundary condition).

4. Structural Analysis of the TF Magnet for EU DEMO

In addition to the boundary conditions described above an extra boundary condition called frictionless contact pair was introduced between the winding pack and the stainless-steel casing to simulate debonding of the winding pack from the stainless-steel casing as shown in the Figure 4.10. A frictionless contact pair essentially means that there is no fix contact between the winding pack and the stainless-steel case. To reduce the computational time only one half of the coil is modeled and a symmetric boundary condition is introduced.

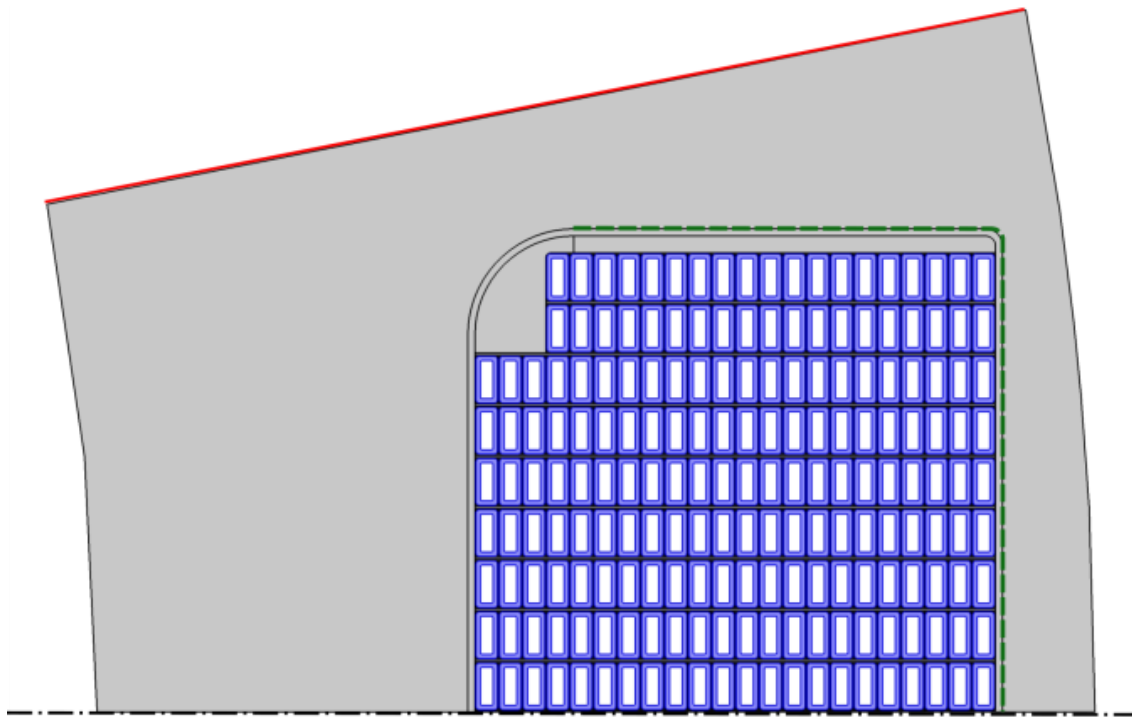


Figure 4.10: Boundary conditions applied in COMSOL (red line denotes sliding boundary condition; green dotted line denotes debonding of winging pack from case and black dash-dotted line denotes symmetry).

4.1.9. Results of the Structural Analysis

For all studies, the Von Mises stress of the casing and the conductor jacket, the displacement, the shear stress in the insulation, and the parameter of the LHD criteria are determined and compared.

4.1.9.1. Results of Study 1

The Von Mises stress in the mid-plane of the inboard leg of TF coil are shown in Figure 4.11. The peak stress is around 619 MPa, which is localized at the inner edges of the casing facing the winding pack. According to the ITER DDD [Mitc00], the permissible stress in the case is $(2/3) \times$ yield strength of SS316, which is 633MPa (yield stress of SS316 is 950 MPa).

The Lorentz forces act in the radial direction and push the inboard leg of the TF coil towards the center of the machine. Since the inboard leg of the TF coil is closely attached to that of its two neighbors, they can only move radially towards the center of the machine. In addition, the bonded model is used. Both together result in a deformation of the part of the casing of the inboard leg which faces to the plasma. The deformation and the displacement of the stainless-steel casing are shown in Figure 4.12.

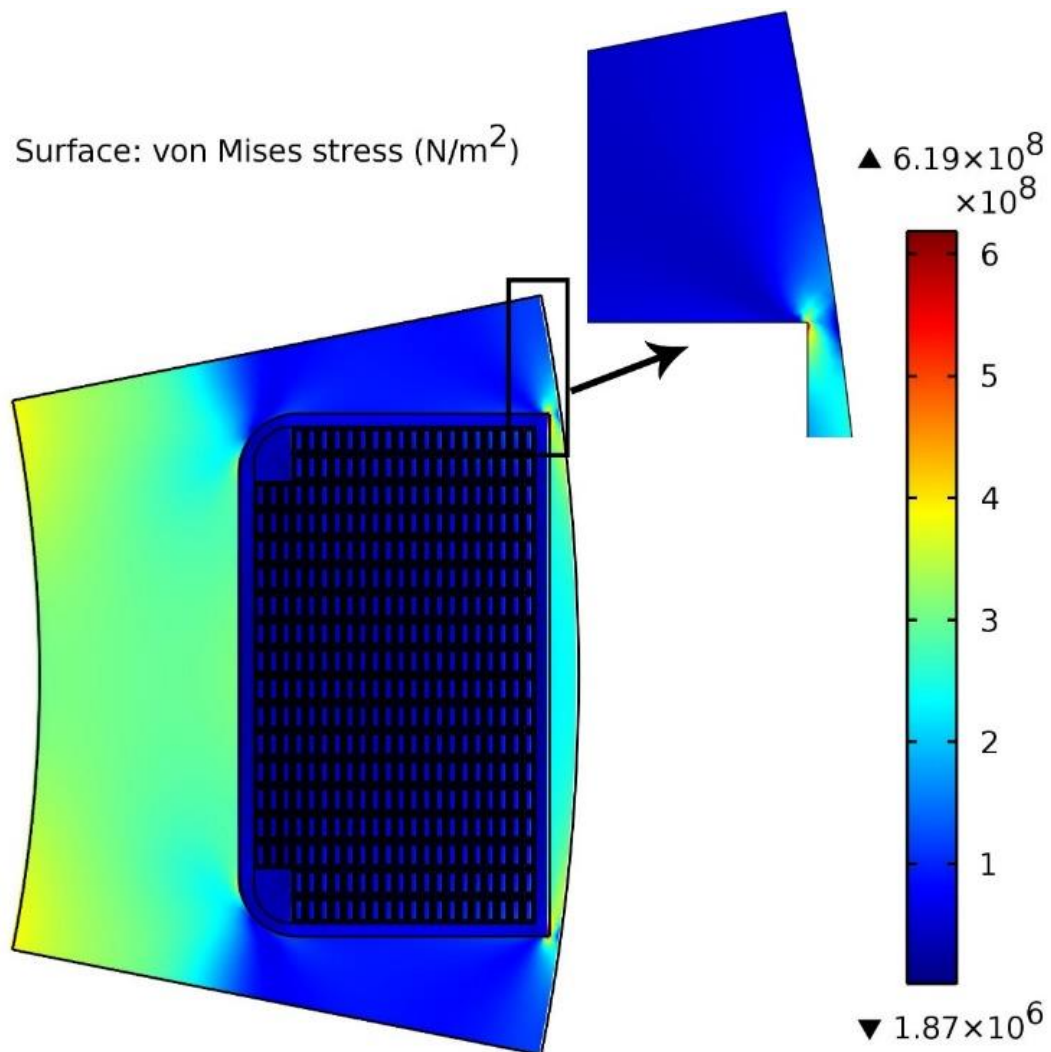


Figure 4.11: Von Mises stress (N/m²) of the casing in the mid-plane of the inboard leg of TF coil for study 1. The region where the peak stress is located is shown in a marked rectangle

4. Structural Analysis of the TF Magnet for EU DEMO

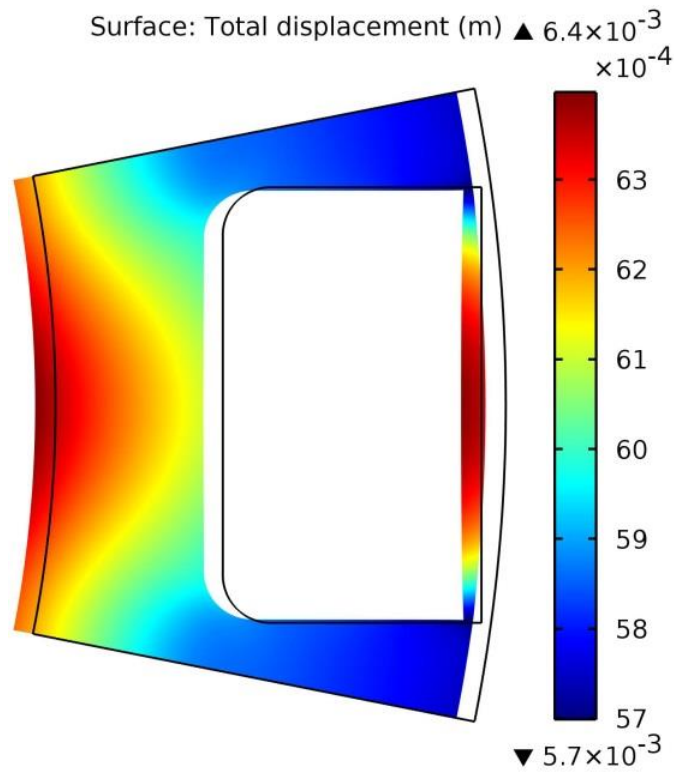


Figure 4.12: Total displacement (m) in the mid-plane of the inboard leg of TF coil along with deformation (scaled by a factor 10)

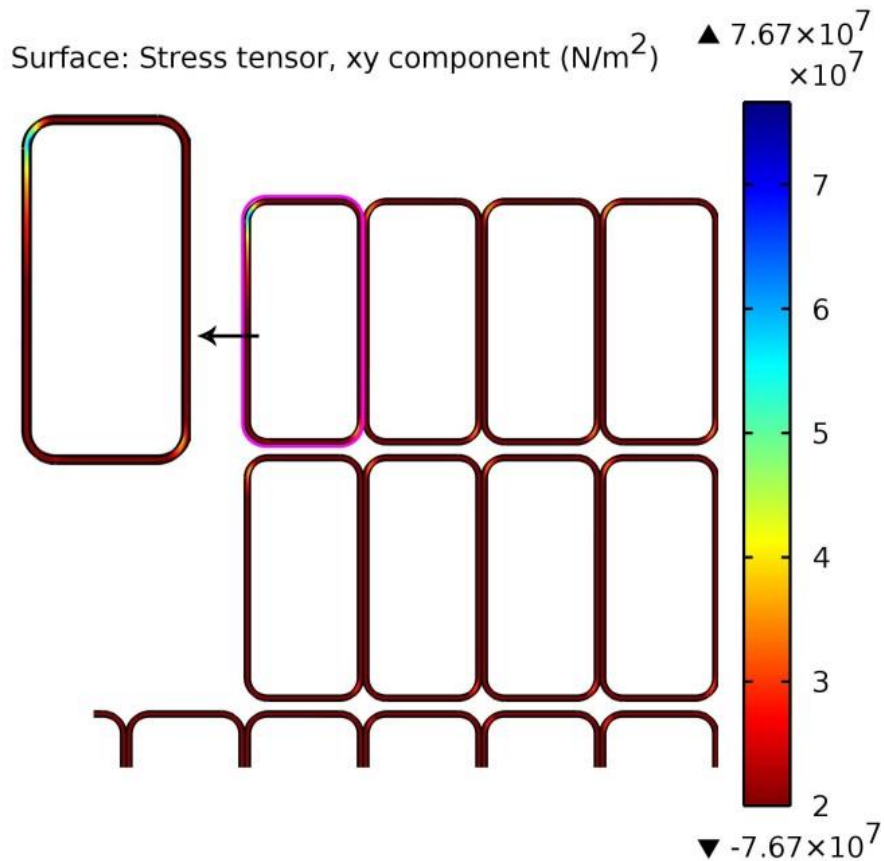


Figure 4.13: Shear stress (N/m^2) in the turn insulation of the side pancake.

The Lorentz forces in the winding pack with the resulting deformation cause shear stress in the turn insulation. This can be critical as if the shear stress is too high this will be the origin for cracks, which would lead to insulation failure. The measure for the critical shear stress in the turn insulation is called LHD criterion which is described in section 4.1.5. According to the ITER design criteria, the shear stress for static condition should be less than 85 MPa. For the present simulation, the peak shear stress is 76.7 MPa and located in the corner of the upper and lower side pancakes as shown in Figure 4.13. The LHD criteria for the shear should be less or equal to 1. As shown in Figure 4.14, the very local peak value is 5.25. The peak stress in the conductor jacket is 178 MPa, which is acceptable.

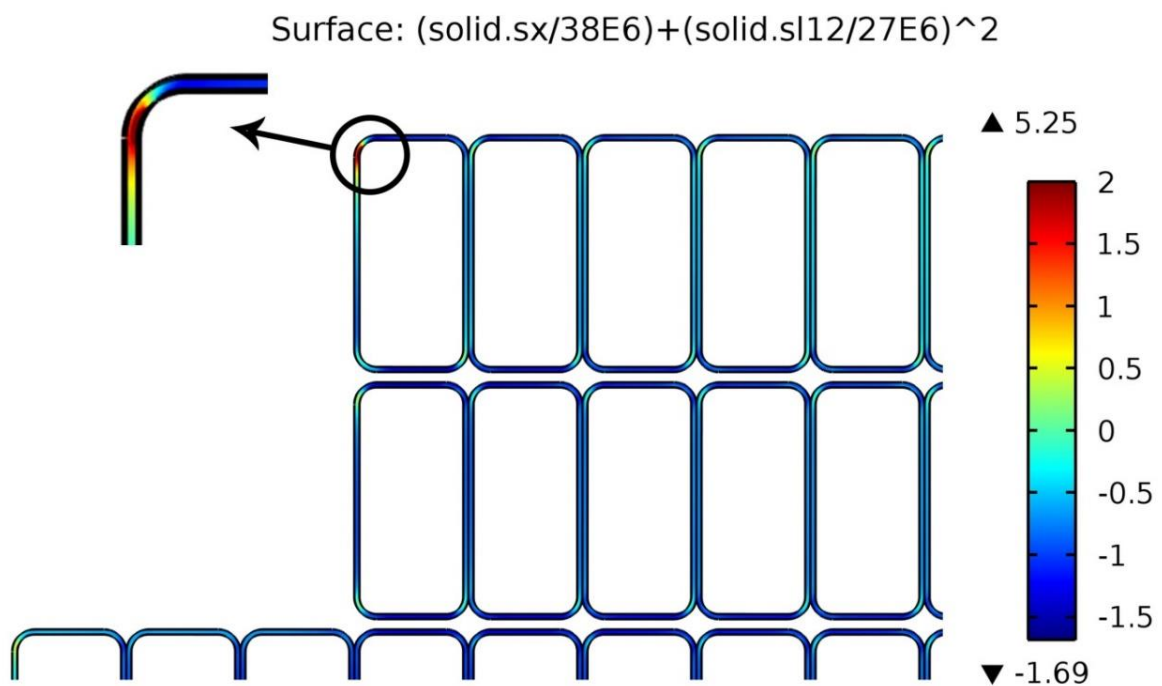


Figure 4.14: LHD shear criteria for the turn insulation of the side pancake

4.1.9.2. Results of Study 2

The challenge is to minimize the issues with all the design constraints, without changing the external dimensions of the TF coil, which would have a big impact on the whole DEMO design. Keeping all constraints in mind, it was possible to add extra steel in the casing of the inboard leg of TF coil facing to the plasma. This is possible as there is extra space of 25 mm around the winding pack available, which was filled for the study 1 with ground insulation, only. This design improvement helps to stiffen the winding pack at the plasma side. Further the inner corner of the casing space for the winding pack of the inboard leg of TF coil is rounded with $R = 34$ mm. The improved

4. Structural Analysis of the TF Magnet for EU DEMO

design is shown in Figure 4.8. The modified geometry model was imported in COMSOL and the simulation was repeated.

Due to these modifications, the peak Von Mises stress in the casing of the study 2 was reduced to 604 MPa as shown in the Figure 4.15. The displacement of the inboard leg of TF coil is decreased from 6.4 mm to 5.75 mm (as shown in the Figure 4.16). The deformation of the casing of the inboard leg of the TF coil facing to the plasma is also reduced.

The shear stress in the inboard leg of the TF coil is also decreased from 76.7 MPa (as seen in Figure 4.13) to 68.4 MPa (as shown in Figure 4.17). The peak value from the LHD criteria in the inboard leg of the TF coil is also reduced from 5.25 (as shown in Figure 4.14) to 4.75 as shown in Figure 4.18. The Von Mises stress in the conductor jacket is 157 MPa.

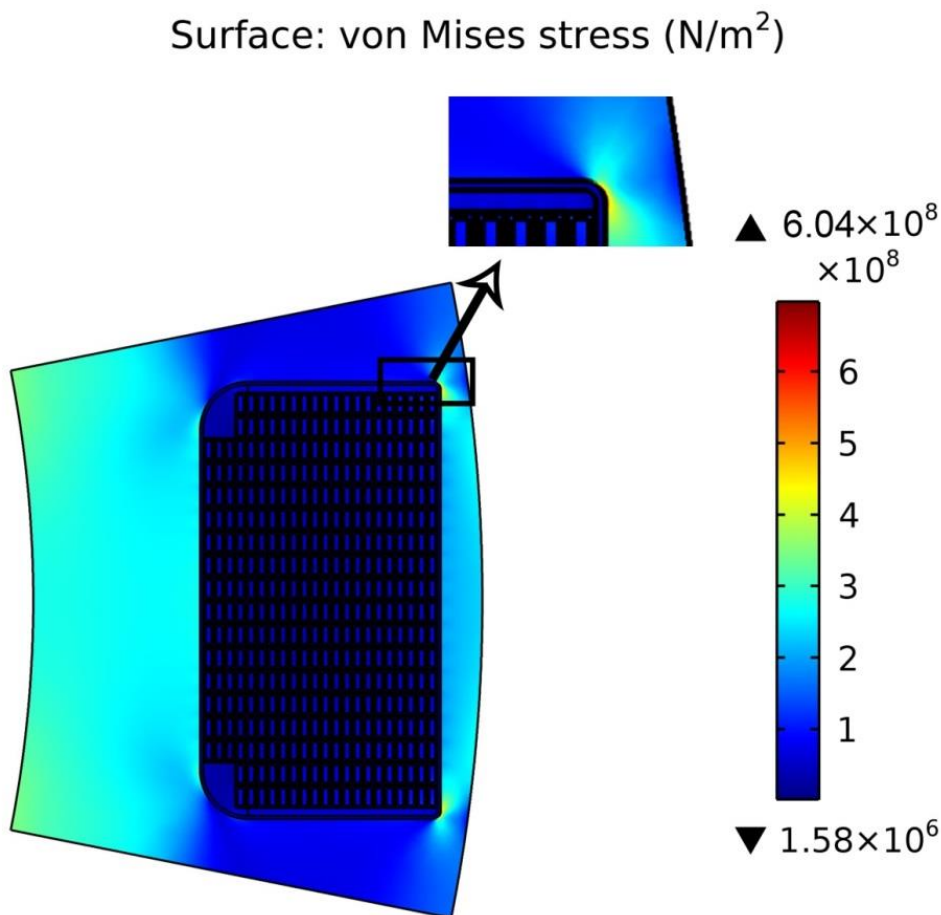


Figure 4.15: Von Mises stress (N/m²) in the mid-plane of the inboard leg of TF coil for study 2. The region where the peak stress is located is shown in a marked rectangle

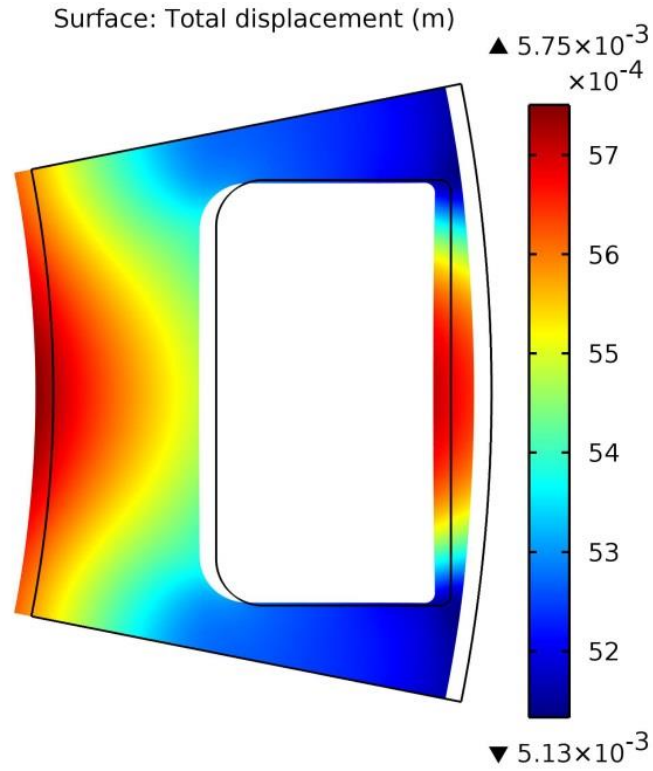


Figure 4.16: Total displacement (m) of the mid-plane of the inboard leg of TF coil along with deformation (scaled to 10 times) for modified geometry.

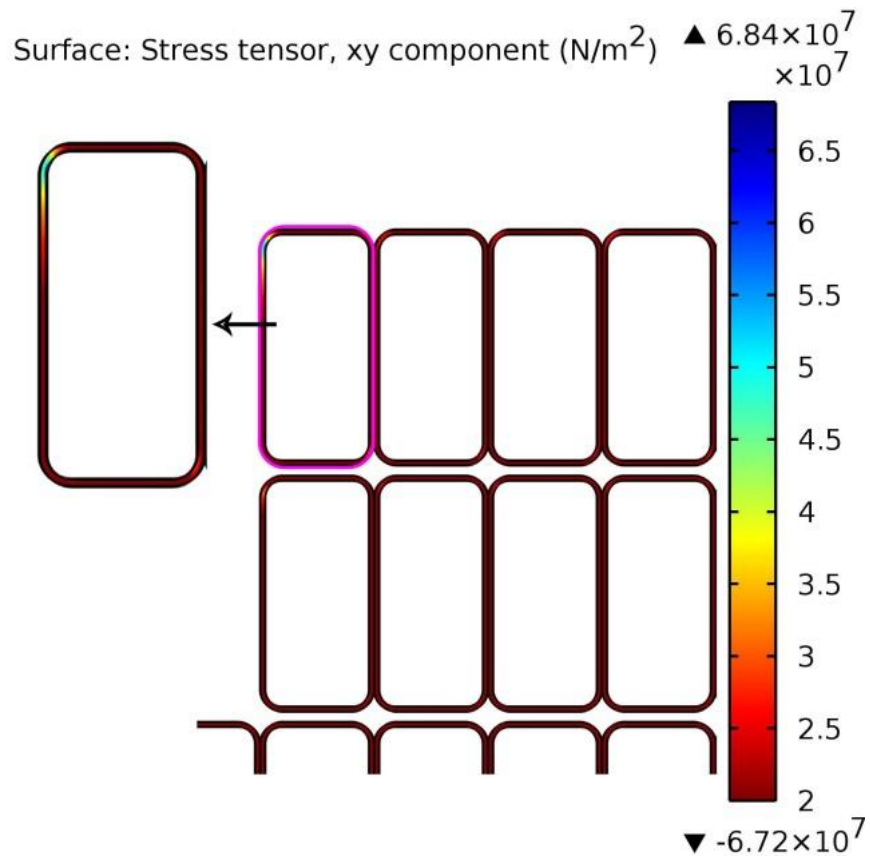


Figure 4.17: Shear stress (N/m^2) in the side pancake turn insulation of the mid-plane of the inboard leg of TF coil for modified geometry.

4. Structural Analysis of the TF Magnet for EU DEMO

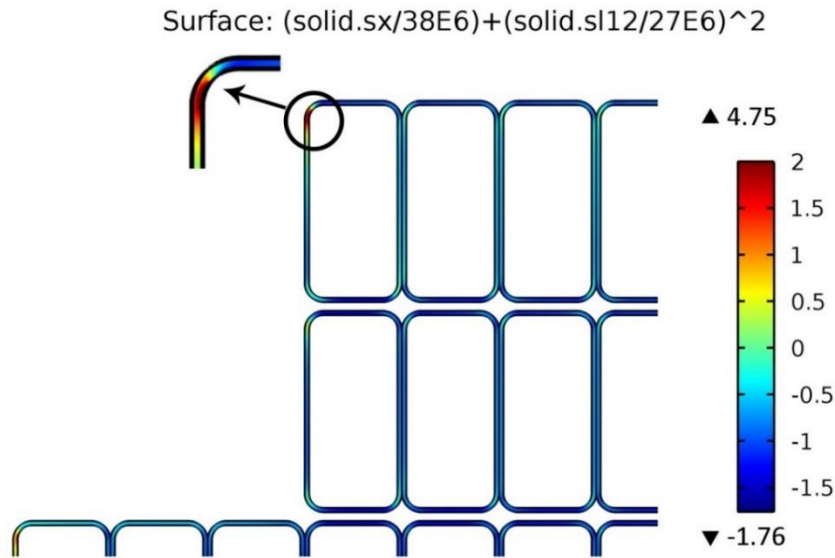


Figure 4.18: LHD shear criteria for the turn insulation of the side pancake

4.1.9.3. Results of Study 3 (Debonding Model)

In study 3, as discussed in the section 4.1.6, the debonding of the winding pack in the plasma end of the mid-plane of the inboard leg of the TF coil has been introduced whose results can be seen in Figure 4.19. Unlike in study 1 and 2 the peak Von Mises stress concentration is not localized at the inner edges of the case but is better distributed across the case of the TF coil. This is because the winding pack is not rigidly bonded to the casing.

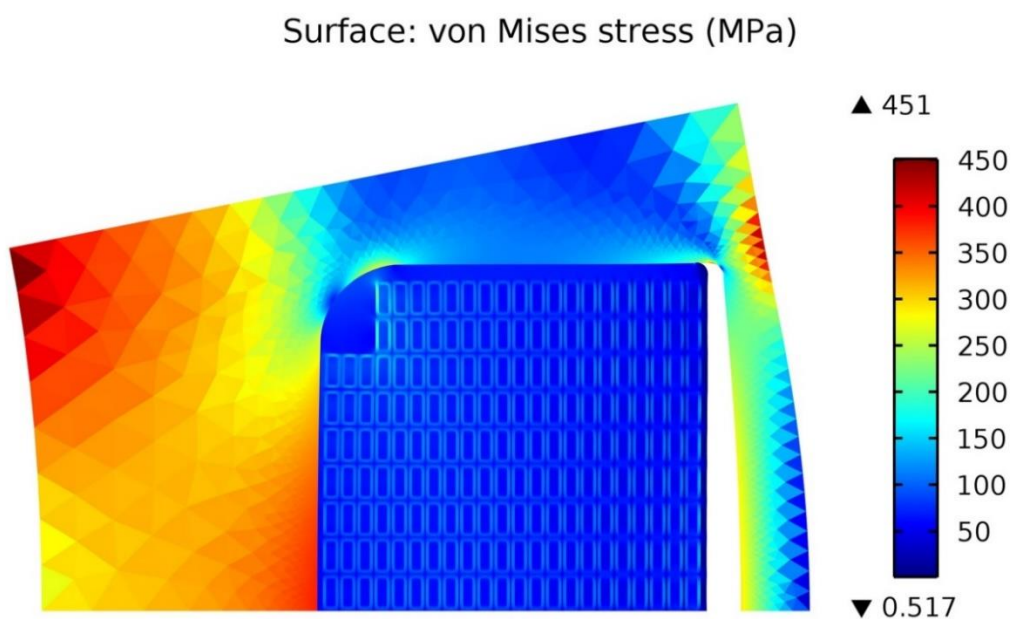


Figure 4.19: Von Mises stress (N/m^2) in the mid-plane of the inboard leg of TF coil for study 3 and debonding of the winding pack from the case (scaled to 10 times).

Due to the debonding of the winding pack from the plasma end of the casing, the Lorentz force in the winding pack adds up in the inner side of the inboard leg. Therefore, the displacement of the TF coil case is 6.55 mm as it can be seen in Figure 4.20 which is greater than study 1 and study 2.

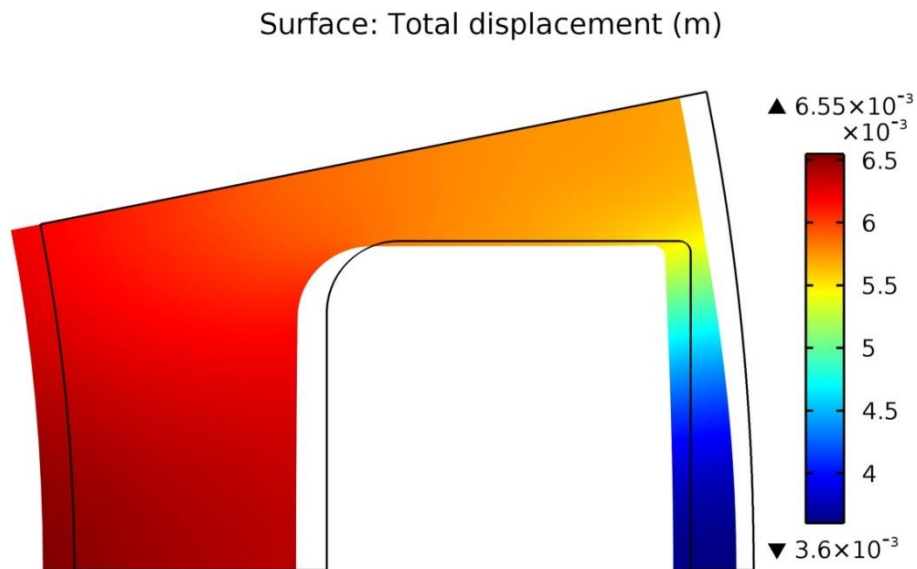


Figure 4.20: Total displacement (m) of the mid-plane of the inboard leg of TF coil along with deformation (scaled to 10 times) for study 3.

The shear stress in the turn insulation is shown in Figure 4.21 and a maximum value of 68.9 MPa is found which is close to the values for study 2.

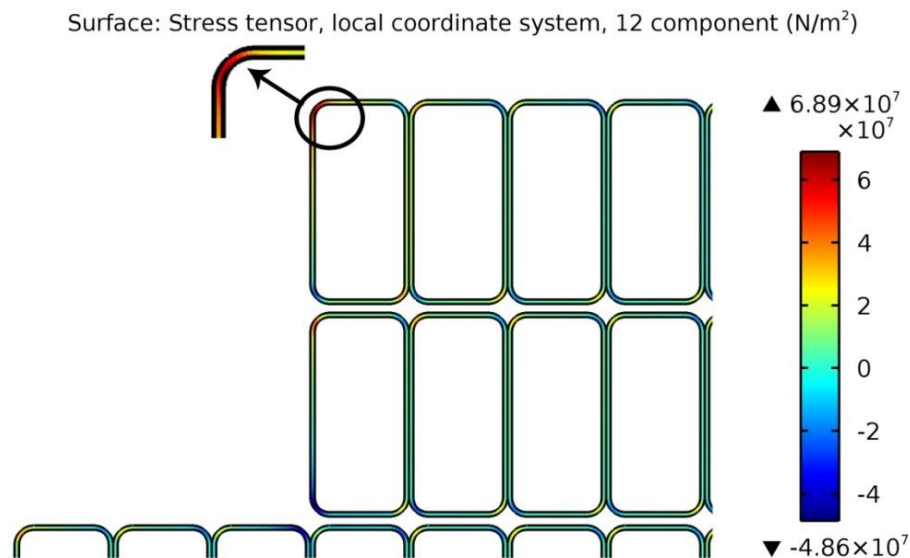


Figure 4.21: Shear stress (N/m²) in the side pancake turn insulation of the mid-plane of the inboard leg of TF coil for study 3.

4. Structural Analysis of the TF Magnet for EU DEMO

If looking to the LHD criteria for study 3, a maximum value of 3.68 is found as shown in Figure 4.22. This is less than for study 1 and study 2 because the normal stress component is reduced due to the debonding of the winding pack. The Von Mises stress in jacket is 227 MPa.

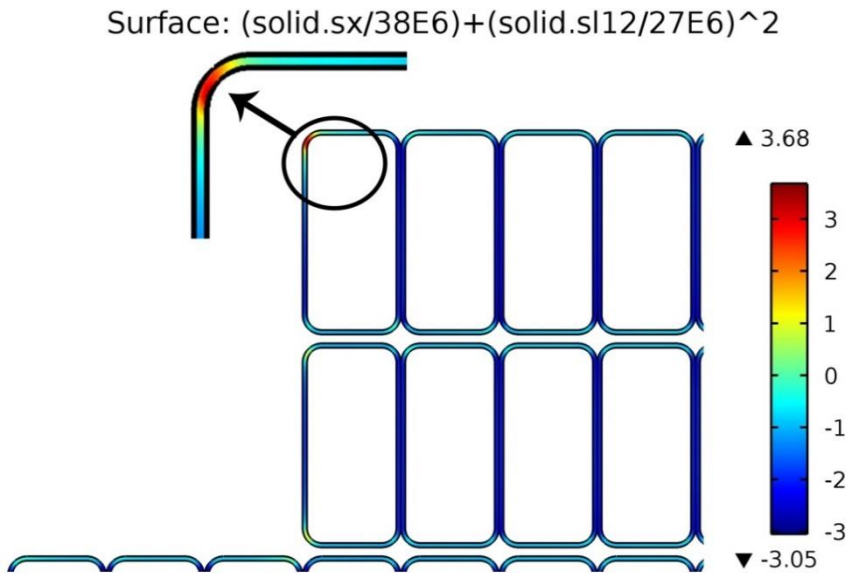


Figure 4.22: LHD shear criteria for the turn insulation of the side pancake for study 3.

4.1.9.4. Results of Study 4

In study 4, the simulation has been performed using ideal elastic properties. This led to exaggerated Von Mises stresses of up to 2760 MPa in the inner corner of the jacket caused by the much lower stiffness of the conductor where the stress can only be transferred via the jacket and not via the cable space. Figure 4.23 shows the Von Mises stress in both the casing and the winding pack.

Thus the simulation was repeated with ideal elastic-plastic properties of stainless steel in the region of the highest stresses (study 4B) [HGFV16]. With this approach the resultant Von Mises stresses were found to be ≈ 1000 MPa. This number still exceeds the allowable stress defined by the design criteria. Figure 4.24 shows in addition the enlarged view of the highly stressed jacket region. From these results it is expected that local plastic deformation will occur to relax peak stresses in the jacket. The high stress region is very local.

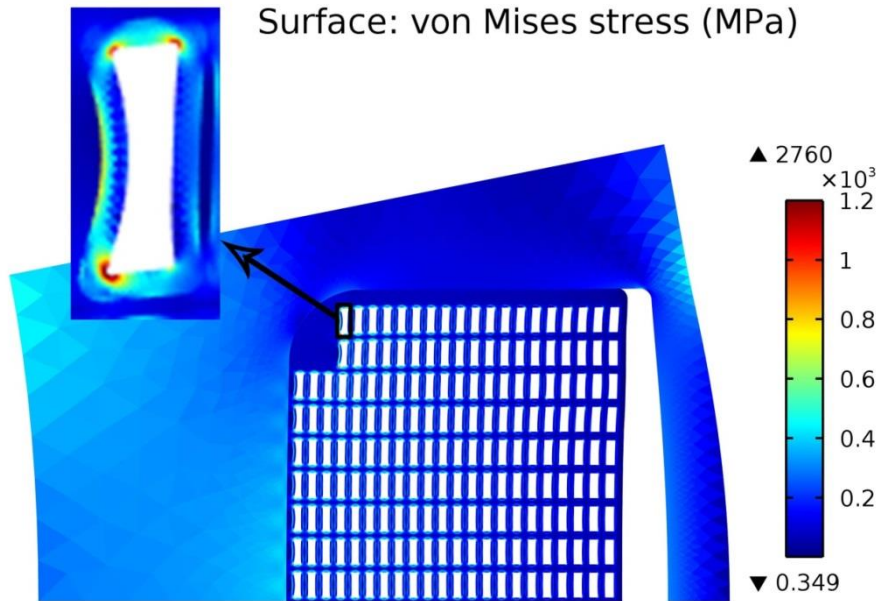
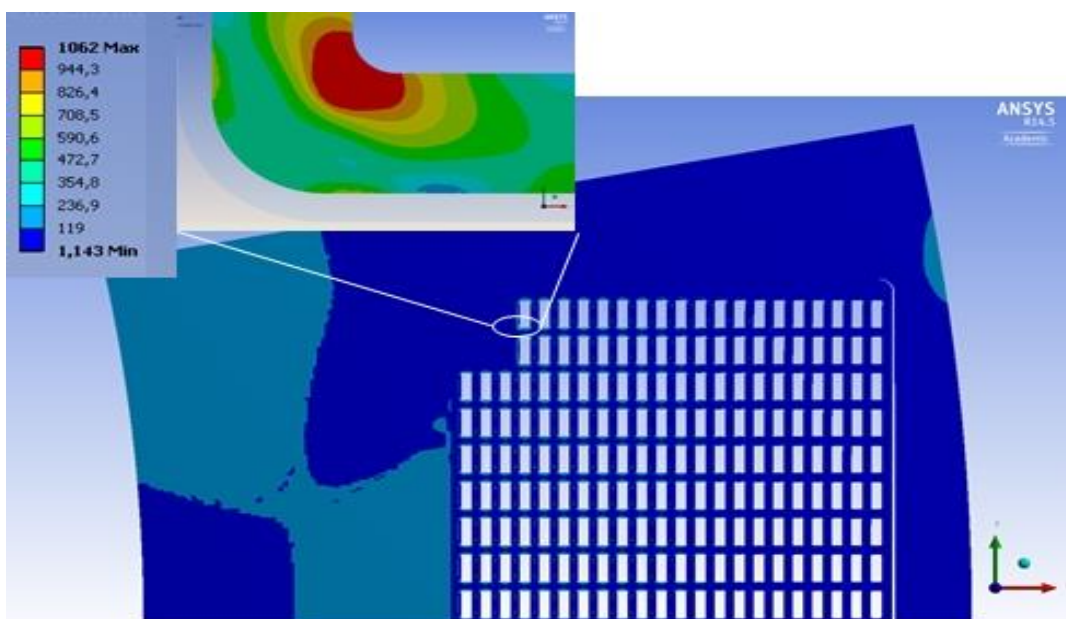


Figure 4.23: Von Mises stress (N/m²) for both the casing and the winding pack in the mid-plane of the inboard leg of TF coil for study 4. The region where the peak stress is located is shown in a marked rectangle

The maximum displacement of the case due to the Lorentz force is 6.67 mm and can be seen in the Figure 4.25. Since the winding pack is debonded, the displacement of the nose is significant than the other end. There is no significant change in the shear stress (as shown in Figure 4.26) and in the LHD criteria (as shown in Figure 4.27) in the insulation. The various studies used for structural analysis are compared in Table 4.3.



4. Structural Analysis of the TF Magnet for EU DEMO

Figure 4.24: Von Mises stress in both the casing and the winding pack for the ideal elastic model. The zoomed picture shows the maximum stress in the jacket area calculated with the ideal elastic-plastic model.

Surface: Total displacement (mm)

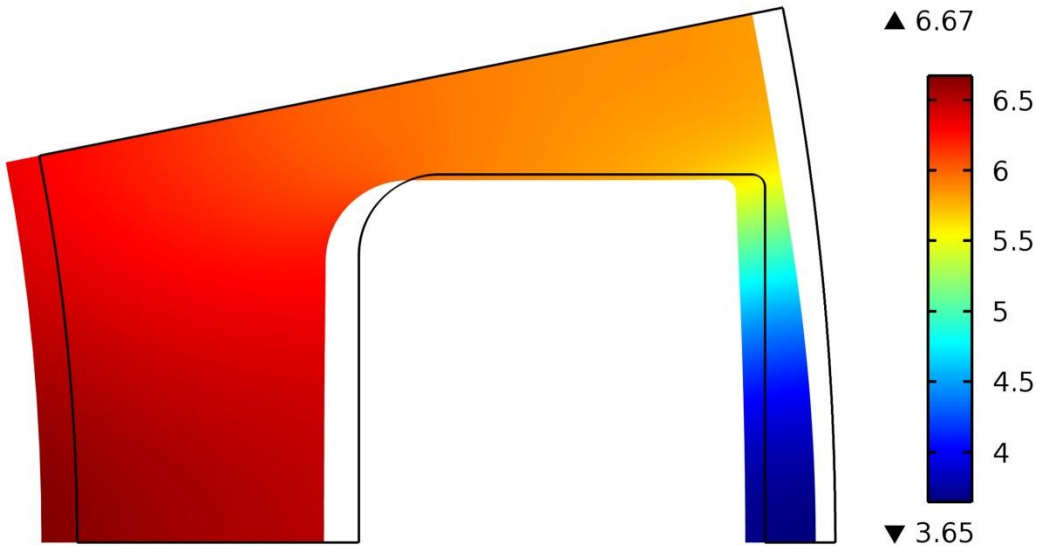


Figure 4.25: Total displacement (m) of the mid-plane of the inboard leg of TF coil along with deformation (scaled to 10 times) for study 4.

Surface: Stress tensor, xy component (N/m²)

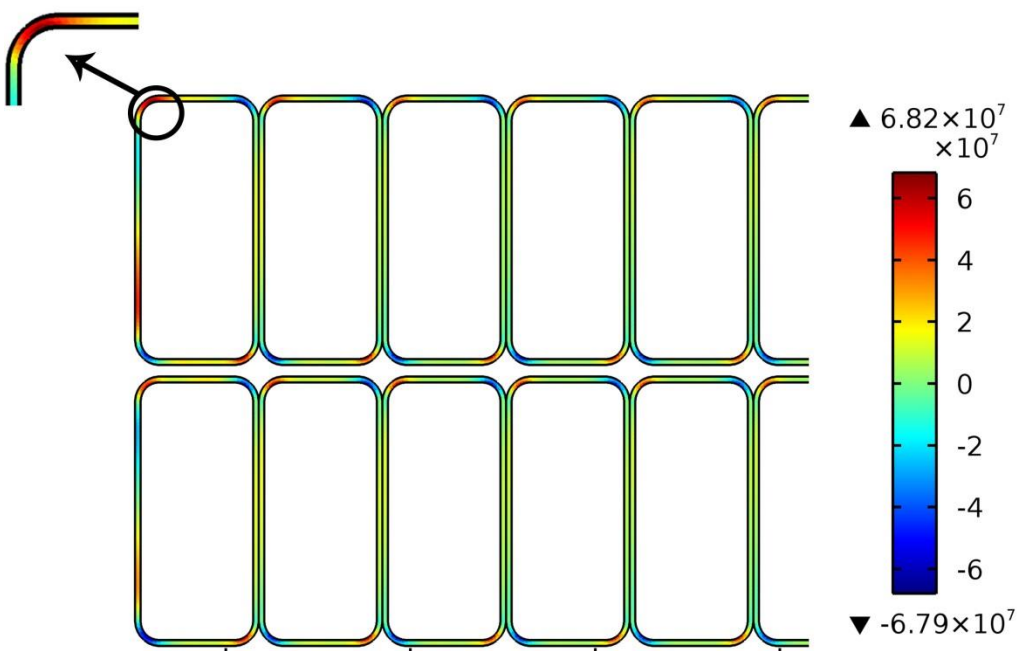


Figure 4.26: Shear stress (N/m²) in the side pancake turn insulation of the mid-plane of tinboard leg of TF coil for modified geometry.

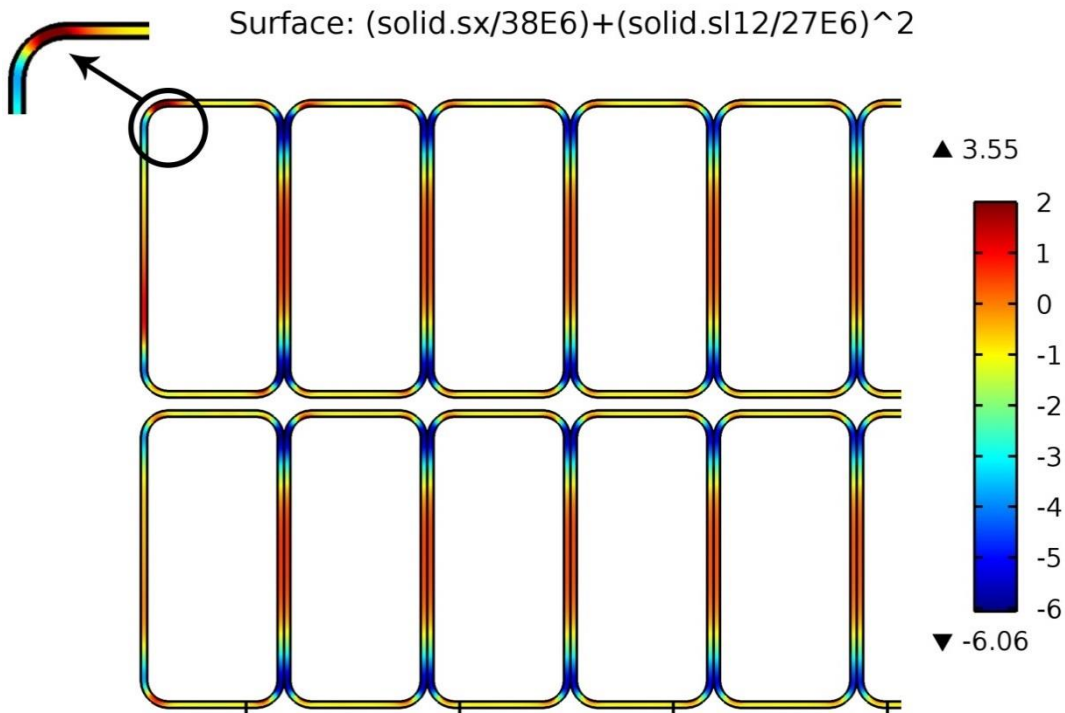


Figure 4.27: LHD shear criteria for the turn insulation of the side pancake for study 4.

Table 4.3: Comparison of various studies used for structural analysis.

	Study 1	Study 2	Study 3	Study 4	Study 4B
Von Mises stress in the case (MPa)	619	609	451	459	
Von Mises stress in the jacket (MPa)	178	157	227	2760	≈1000
Displacement (mm)	6.4	5.75	6.55	6.67	
Shear stress in the turn insulation (MPa)	76.7	68.4	68.9	68.2	
LHD criteria	5.25	4.75	3.68	3.55	

4.2. Structural Calculation Conclusion

Using the casing geometry as given by PROCESS code of July 2012, a 2-D structural analysis was performed and different model assumptions were made and compared. In study 1 and study 2, the plasma facing side of the casing shows high stresses due to the bonding of the winding pack. In reality the winding pack will detach from the case due to high Lorentz force, as investigated in study 3 and study 4. The maximum allowable stress in SS316 is 633 MPa and the Von Mises stress in the study 3 and study 4 are below the maximum value.

4. Structural Analysis of the TF Magnet for EU DEMO

In study 1, study 2 and study 3, the stress in conductor jacket is low which is due to the usage of the homogenized cable material properties. If the Young's modulus of the cable is set to zero as done in study 4, there are enormous stresses observed in the jacket. At present, there are no material properties of the cable available. But it can be concluded that in reality the Von Mises stress lies somewhere in between the results obtained in study 3 and study 4.

The shear stresses in the turn insulation and also the maximum value of the so-called LHD design criteria are high for study 1. To reduce the shear stress in the turn insulation, the design was modified. There is no significant change in the shear stresses in study 2, study 3 and study 4. But from the values obtained for the LHD criteria, it can be seen that they are getting closer to 1, because the direction of normal stress tensor changes due to the modified case as well as debonding of the winding pack.

In the future the structural analysis has to be repeated using the actual cable properties. The radius of the rounded corner of the jacket can be modified as well to reduce the local stresses inside the jacket which may help to push the LHD criteria value below 1.

5. Thermal Hydraulic Modeling of the HTS Conductor

5.1. Introduction to the Conductor Quench Modeling

The TF HTS conductor will be internally cooled with supercritical helium flowing through the conductor [Dres02b]. Cooling the conductor internally has its advantages such as i) very high cooled surface that can be obtained by subdividing the conductor into many individual strands and subdividing into strands also provides the ability to rapidly remove heat input from the conductor [YHKK82]. The source of the heat input or perturbation comes from flux jumps, mechanical events [Bott88], electromagnetic transients[Bott88], conductor joints [Wils87], AC losses [BoMi88], non-perfect thermal shielding of the 4 K environment and nuclear heat [Bott88]. The perturbation time spectrum for the events listed above range from 0.001 ms to 10000 ms. Depending on the balance between heat deposition and heat removal, the conductor will either stay in superconducting state or it will lose superconductivity and there will be a sudden temperature rise due to joule heating. In case of loss of superconductivity, the heat is conducted not only through heat conduction but also through the expulsion of warm helium. A schematic view of possible perturbations and effects of these perturbation is summarized in Figure 5.1.

For a internally cooled conductor, the behavior of the coolant during a quench can be modeled using the following simplified set of mass, momentum and energy conservation equations for the helium density ρ_{he} , velocity v_{he} and temperature T_{he} [Arp72].

$$\begin{aligned}
 \frac{\partial \rho_{he}}{\partial t} + \frac{\partial v_{he} \rho_{he}}{\partial x} &= 0 \\
 \frac{\partial p_{he}}{\partial x} &= -2 \frac{f_{he}}{D_{he}} \rho_{he} |v_{he}| v_{he} \\
 \rho_{he} C_{he} \frac{\partial T_{he}}{\partial t} + \rho_{he} v_{he} C_{he} \frac{\partial T_{he}}{\partial x} &= 2 \frac{f_{he}}{D_{he}} \rho_{he} |v_{he}| v_{he}^2 + \frac{\rho_w h}{A_{he}} (T_{co} - T_{he})
 \end{aligned} \tag{5.1}$$

5. Thermal Hydraulic Modeling of the HTS Conductor

where p_{he} is the pressure, C_{he} is the heat capacity of helium, D_{he} is the hydraulic diameter and f_{he} is the friction factor of the flow. The above relation holds when friction dominates the momentum balance, which is usually the case in coils cooled by long pipes. Depending on the heating rate, heat transfer and flow characteristics, heating induced flow can be significant and participate to the quench propagation.

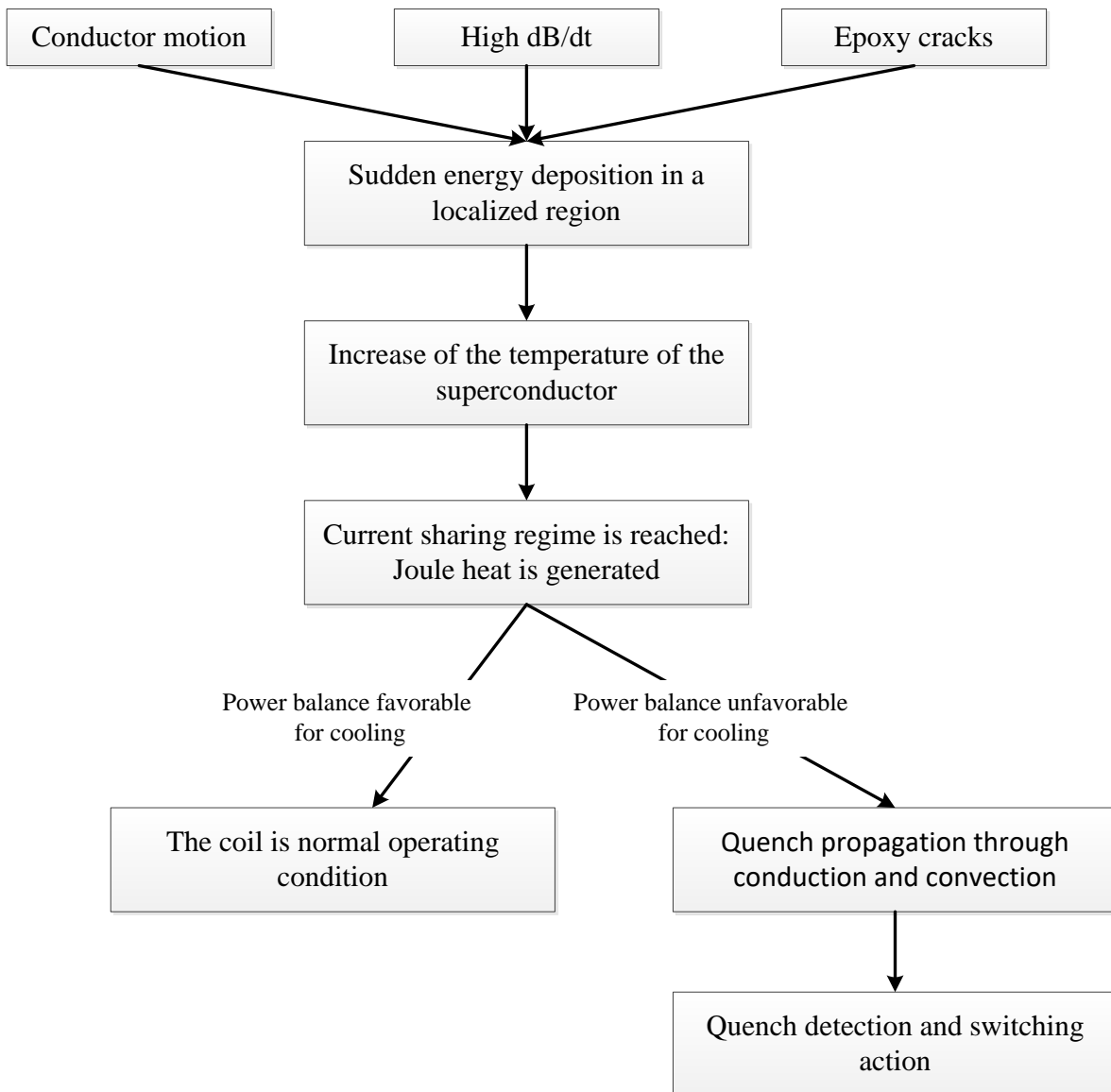


Figure 5.1: The event tree for the evolution of an initial thermal disturbance in a superconducting cable.

5.2. Hydraulic Analysis

5.2.1. Friction Factor Co-relation

The selection of the friction factor for the hydraulic model is a prerequisite for determining the pressure drop and temperature rise in the conductor pancakes. The

relationship can be given by modifying momentum equation (as shown in equation (5.1)) of a single-phase fluid flow (as shown in equation (5.2)).

$$\frac{\partial p_{he}}{\partial x} = -2 \frac{f_{he}}{D_{he}} \frac{|\dot{m}_{he}| \dot{m}_{he}}{\rho_{he} A^2} \quad (5.2)$$

where A is the cross-sectional area.

To calculate the pressure drop, the above equation needs to be integrated over the length of the conductor (L).

$$\Delta p_{he} = -2 \frac{f_{he}}{D_{he}} \frac{\dot{m}_{he}^2}{\rho_{he} A^2} L \quad (5.3)$$

The hydraulic diameter D_{he} can be written as

$$D_{he} = \frac{4A}{w_p} \quad (5.4)$$

where w_p is called wetted perimeter. It is the area where the supercritical helium is touching the conductor.

By substituting equation (5.4) in (5.3) we get

$$\Delta p_{he} = -2 \frac{f_{he} L w_p}{D_{he}} \frac{\dot{m}_{he}^2}{A^3} \quad (5.5)$$

From the equation (5.5), the relation between mass flow \dot{m} and pressure drop Δp determines the maximum heat that can be extracted. In addition, it affects the efficiency of the cryogenic system through the pumping work necessary to circulate the coolant [LeBa11]. In general, it is always desirable to have the lowest possible pressure drop for a given mass flow, or, conversely, to be able to circulate the highest possible mass flow for a given pressure drop. In a forced-flow cooled system, a high mass flow has various benefits:

- the amount of heat that can be removed from the system in steady state under a given temperature increase is directly proportional to the mass flow.

5. Thermal Hydraulic Modeling of the HTS Conductor

- the local heat transfer coefficient increases with increasing mass flow. A large heat transfer is beneficial to the stability of the superconductor;
- for a given mass flow, a reduced pressure drops results in a smaller temperature change due to Joule–Thomson expansion of the helium from the inlet to the outlet of the cooling pipe;

Nowadays, the LTS conductors used for fusion magnets are of CICC type and use a large number of wires of small diameter (approximately 0.8 mm) bundled in a multi-stage cable, resulting in high friction in the bundle region [LeBa11]. High friction is not only because of the friction factor co-relation but due to smaller hydraulic diameter in the bundle region. In the past decades many co-relations of such cable were discussed and most of the co-relations were function of Reynolds number or specific to specific conductor's hydraulic diameter. A co-relation was specified in Katheder's [Kath94] where he used not only Reynold number but also void fraction. The void fraction is the ratio of area of helium to the cable space. The co-relation is valid for the Reynold number ranging from 20 to 40000. The Katheder co-relation is accepted for most of the CICC type cables. As the strands in the HTS conductor concept [WFBS15] have a much larger diameter (approximately 6 to 9 mm) and the cable has much larger channels for cooling, the CICC friction factor is not a proper candidate. In the analysis presented in the following the friction factor of the EURATOM LCT conductor has been used [BKSV98] as this conductor has a similar geometry. Figure 5.2 and Figure 5.3 shows different conductors, the EURATOM LCT conductor and the ITER TF conductor. A comparison of the friction factor co-relation for CICC type LTS conductor and the EURATOM LCT conductor is shown in Figure 5.4. In a later stage the friction factor of a specific HTS conductor has to be determined.

$$f_{LCT} = \begin{cases} 47.65 * Re^{-0.885} & Re < 1500 \\ 1.093 * Re^{-0.338} & 1500 < Re < 2 * 10^5 \\ 0.0377 & Re > 2 * 10^5 \end{cases} \quad (5.6)$$

with f_{LCT} equal to friction factor for EURATOM LCT coil and Re equal to Reynolds number.

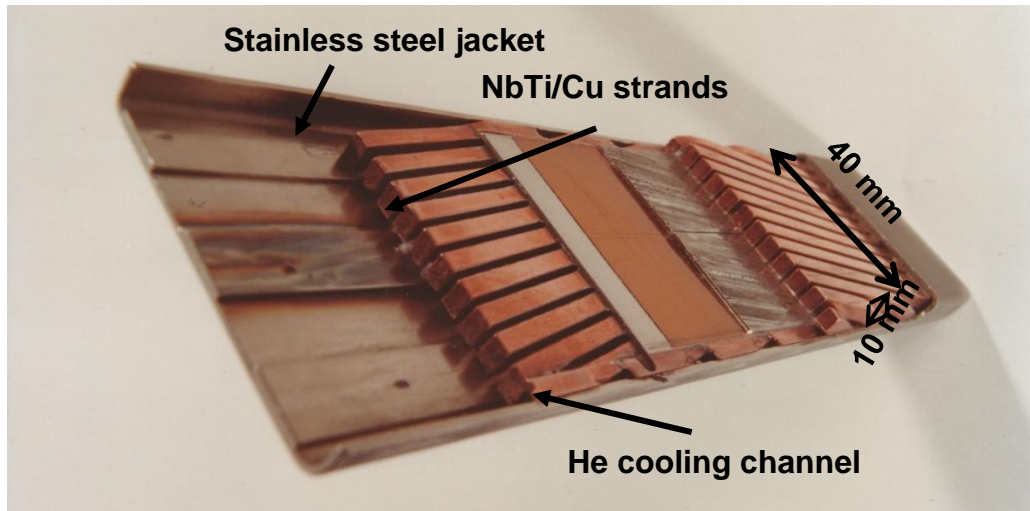


Figure 5.2: The figure shows EURATOM LCT Coil conductor. Picture is from Kernforschungszentrum Karlsruhe

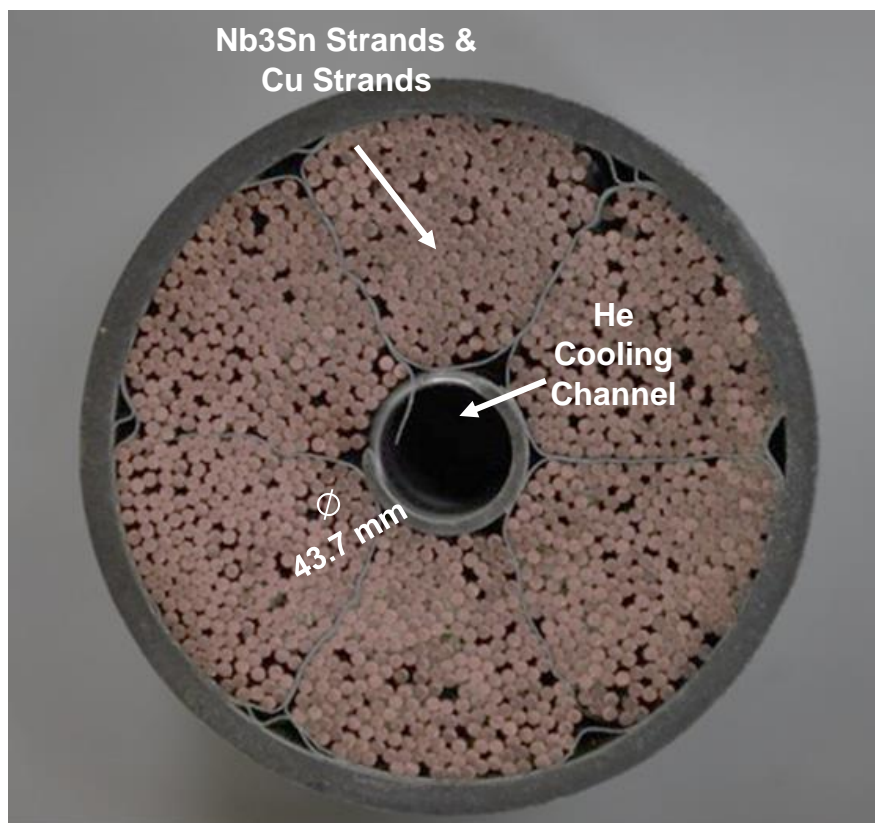


Figure 5.3: ITER TF coil conductor. Reference: ITER Newlines #141, 23 July 2010

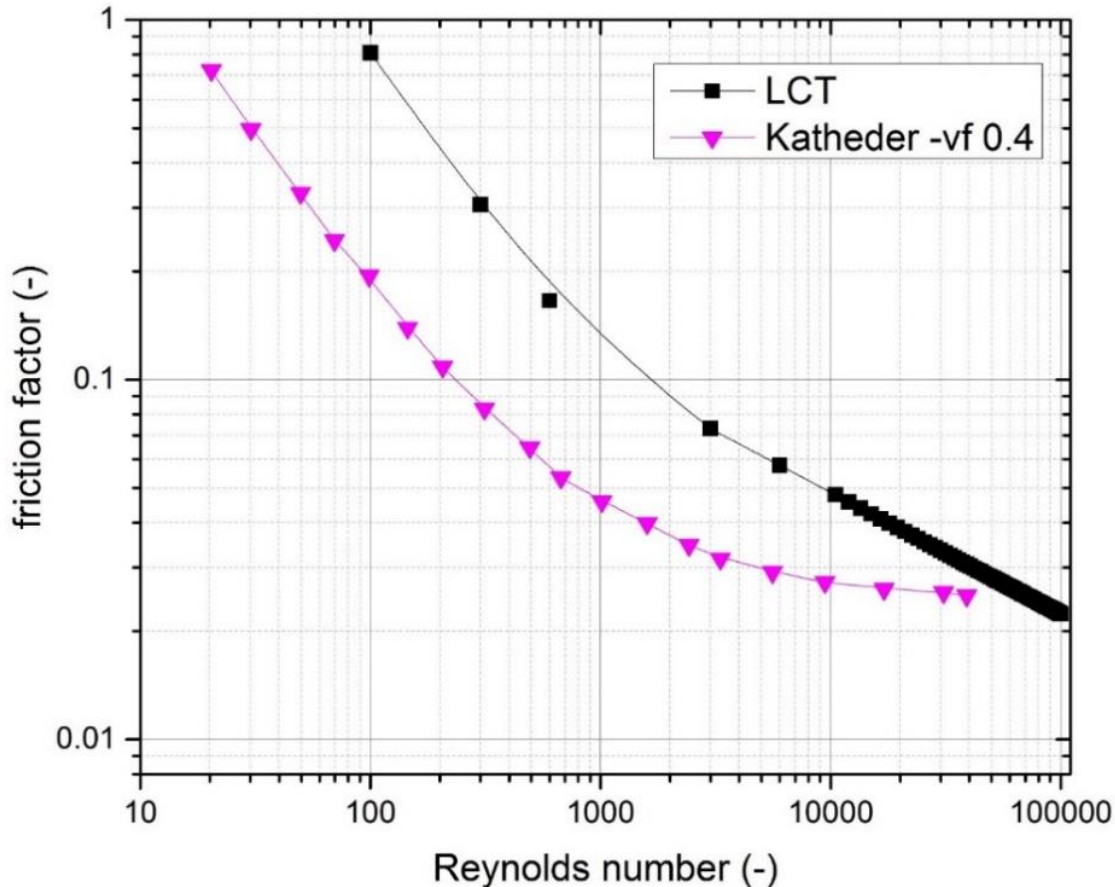


Figure 5.4: Friction factor of the helium flow in a CICC, from the various correlations. The correlation of Katheder has been evaluated for a cable void fraction of 40%.

5.2.2. Heat Load Imposed on the Conductor

Beside friction losses two other sources of heat load have to be considered.

- Steady state heat load by conduction Q_{cond} from the coil casing as the casing is in general at a higher temperature than the winding pack.
- Heat deposition from neutrons generated in the plasma Q_{nucl} : the amount of heat decreases exponentially in radial direction and varies also in azimuthal direction around the plasma (as shown in Figure 5.5) [Boni14].

The TF coil case cooling will remove most of this neutron heat load with supercritical helium flowing through channels in the case wall. However, some amount of heating will conduct through the coil ground wrap insulation and into the helium-cooled conductors. This heat load has the adverse effect of a direct impact on the stability and safety margin of the superconductor [MyPR95].

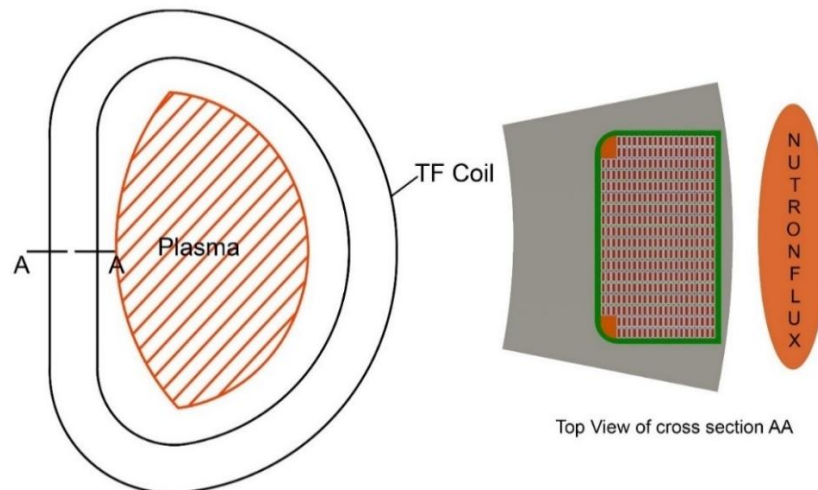


Figure 5.5: left side: figure represent the schematic representation of plasma and TF coil. right side: figure represents the cross section of AA with TF coil case winding pack and neutron flux due to plasma

5.2.3. Hydraulic Analysis Results

The HTS TF coil winding pack consists of 14 inner pancakes and 2 outer pancakes on both sides, whose conductor length is 858 m and 741 m respectively. The TF coil conductor is cooled by forced flow supercritical helium at 4.5 K and 6 bar, as in ITER.

For the simulation, an average heat load Q_{cond} of 0.006 W/m is assumed which counts for heat conduction through the coil casing. This value is estimated from experiences of various coil tests [BKSV98].

The nuclear heat load Q_{nucl} is added along the 1st turn by taking 200 W per coil and dividing it by the number of pancakes, i.e., 18, resulting in 0.2849 W/m. Although the exponential decrease of the heat load is not considered the collection of Q_{nucl} in the 1st turn is a conservative approach as it overestimates the temperature increase there.

Table 5.1 collects all the parameters relevant for the hydraulic analysis.

Table 5.1: Collection of parameters used in the hydraulic analysis

Parameter	Unit	Value
Conductor length	M	39
Helium cross section	m ²	272.209E-6
Wetted perimeter	M	305E-3
Helium inlet temperature	K	4.5
Helium inlet pressure	Bar	6
Heat load $Q_{\text{cond}}/ Q_{\text{nucl}}$	W/m	0.006 along the whole conductor 0.291 along the 1 st turn

5. Thermal Hydraulic Modeling of the HTS Conductor

For given mass flow rates and different nuclear heat loads, the temperature and pressure profiles along the conductor are calculated as a function of helium mass flow rate for different heat loads Q_{nucl} by solving energy and momentum conservation equations as shown in equation (5.1) and implemented in the HE-SS code [Bott87].

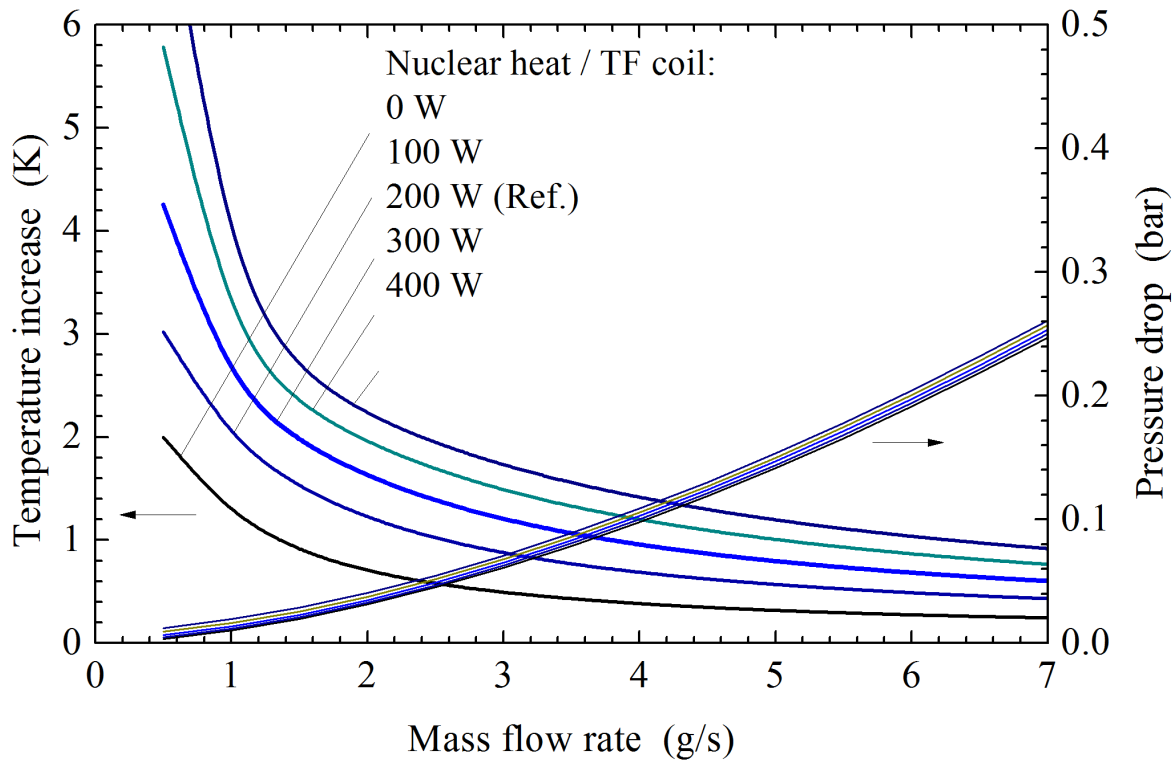


Figure 5.6: Temperature increase and pressure drop of the inner pancake conductor for different nuclear heat loads Q_{nucl} . 200 W/coil is the reference [Boni14].

Figure 5.6 shows the temperature increase and pressure drop of the inner pancake for different nuclear heat deposition with 200 W per coil as reference [Boni14]. It can be seen that for increasing mass flow rates, the temperature rise decreases whereas the pressure drop increases, as expected. Unlike LTS conductors where the temperature margin is very low (for ITER less than 1 K), the HTS conductor can be operated with a much lower mass flow rate due to its much higher temperature margin. A lower mass flow rate is linked to a lower pressure drop and results in a much lower pumping power for the cryogenic system. A second advantage of the high temperature margin is the possibility of accepting higher heat loads than for LTS. As an example, with LTS with a temperature margin of 1 K and a heat load of 200 W per coil, a mass flow rate much higher than 4 g/s in the inner winding would be necessary. Using HTS, a nuclear heat load of 400 W per coil is acceptable even with a mass flow rate below 2 g/s which results in a temperature increase of 2.4 K.

5.3. Quench Analysis

The initiation and propagation of a quench is governed by classical balance and circuit equations that can be written most conveniently in the form of a coupled system of partial and ordinary differential equations [BoZi92a]. Although the geometry in superconducting magnets is three dimensional, a reduction to one dimension is chosen with the conductor length as dimension. This is a common way to visualize the quench propagation and already provides a very good basis to establish simplified scaling laws. The length of conductor is about hundreds of meters and the conductor cross section is in millimeter. Because the geometries of the conductor are so different 1-D analysis is chosen. Additionally, due to the different thermal properties along and perpendicular to the conductor, the quench propagation along the conductor is dominant. The 1-D analysis leads to conservative results regarding temperature rise and pressure development as quench propagation through neighbor conductors is neglected.

5.3.4. Model and Boundary Conditions

For modeling the quench, the conductor is simplified in three parts,

- The tapes consist of REBCO, Hastelloy and copper and are combined as one component.
- The second component is the jacket.
- The third component is the helium.

The thermal coupling between the different components is considered. The tapes and the jacket are coupled with the helium by heat transfer with the wetted perimeter as parameter. A thermal resistance between the tapes and the jacket is also considered. Figure 5.7 illustrates the couplings.

The temperature of the conductor T_{co} is obtained from a heat diffusion equation:

$$A\bar{C}\frac{\partial T_{co}}{\partial t} - \frac{\partial}{\partial x}\left(A\bar{k}\frac{\partial T_{co}}{\partial x}\right) = A\dot{q}_{Joule}^m + p_w h(T_{he} - T_{co}) + \sum_{\substack{j=1 \\ j \neq i}}^N \frac{T_j - T_i}{H_{ij}} \quad (5.7)$$

with averaged heat capacity C and thermal conductivity k of the composite conductor,

$$\bar{C} = \sum_i f_i \rho_i c_i \quad (5.8)$$

$$\bar{k} = \sum_i f_i k_i$$

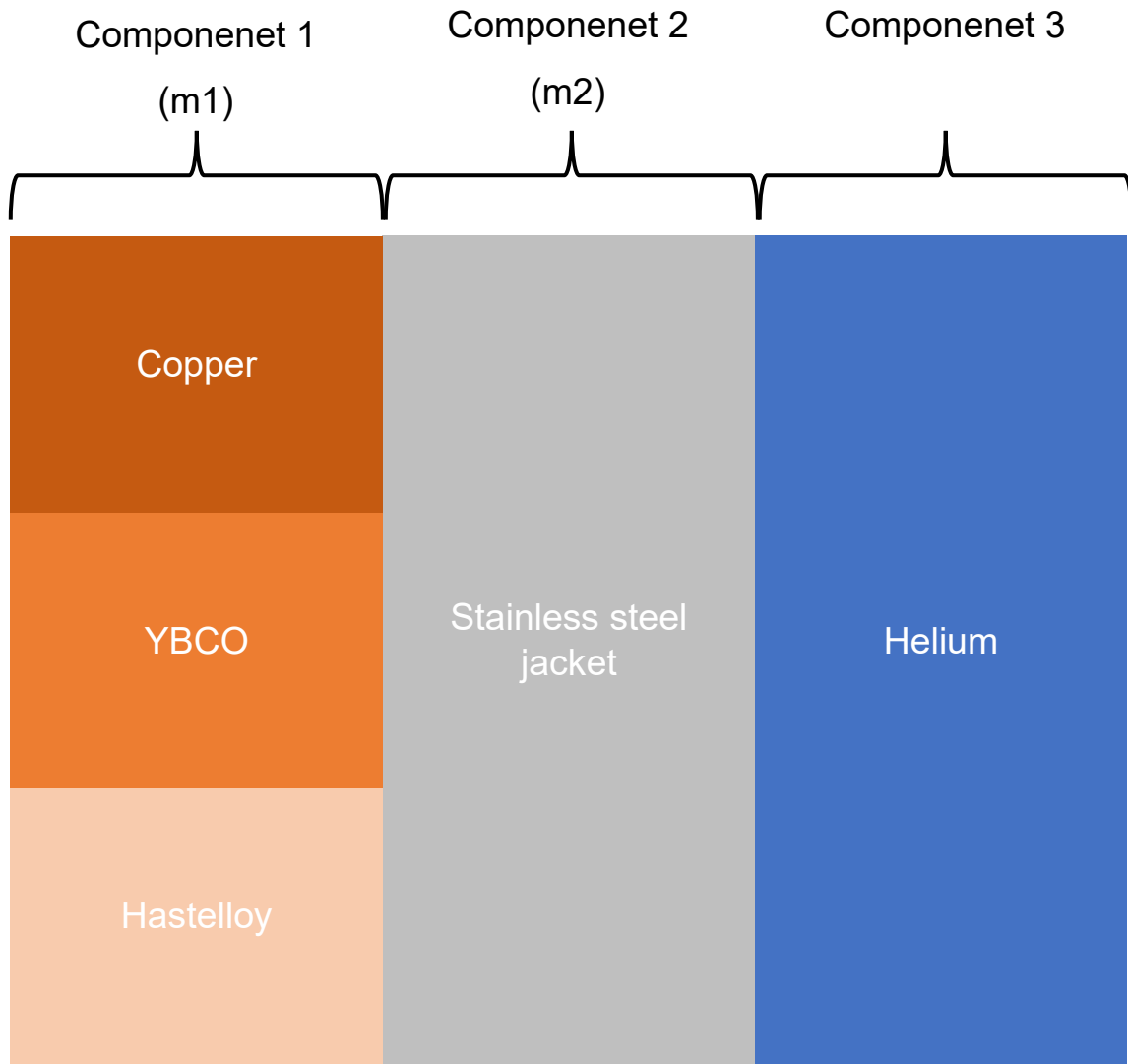


Figure 5.7: Thermal link between Helium, conductor and jacket for 1D analysis.

In equation (5.9), the thermal resistance among two thermal components H_{ij} to model thermal coupling within a cable is considered. The corresponding values can be estimated in the case of soldered cables, where the thermal coupling takes place through thermal conduction. Such an estimate is not possible in the case when the thermal coupling takes place through contact surfaces, such as in multi-strand Rutherford or bundled cables. Lacking experimental measurements of thermal resistances, estimates can be obtained assuming that the electrical and thermal contact resistances are correlated through the Wiedeman-Franz-Lorenz law [WiWo97]:

$$H_{ij} = \frac{R_{ij}}{L_0 T} \quad (5.9)$$

where

H_{ij} is the thermal contact resistance, R_{ij} is the interstrand resistance per unit length, L_0 is the Lorenz number ($2.45 \cdot 10^{-8}$ [$\Omega W/K^2$]) and T is the average temperature of the two components.

5.3.4.1. Joule Heating and Current Sharing

A special attention in superconducting composites must be given to the joule heat generation term.

$$\dot{q}_{Joule} = \dot{q}_{Joule}(T, B, I) \quad (5.10)$$

where the temperature T and the field B are functions of position and time while the current I transported by the conductor is only a function of time through the solution of the circuital equation explained later on. The term joule heat arises when the superconducting material is not able to carry the whole operating current I_{op} , which exceeds the limit in the current density specified by the $J_c(B, T)$ surface. A resistance will then develop and joule heat dissipation will appear. For computing the joule heat term, the presence of a parallel shunt through the copper must be taken into account: whenever the current density in the superconductor exceeds the limiting value, the superconductor develops a resistance and this causes the resistive split of the current I_{op} between the copper and the superconductor. In reality the resistance developed in the superconductor is a complex function of temperature, magnetic field and current, but is in any case much greater than that of copper. This results in the complete transfer of the current to the copper exceeding the maximum value that the superconductor can carry at a given T and B .

$$I_{Cu} = I_{op} - I_c(B, T) \quad (5.11)$$

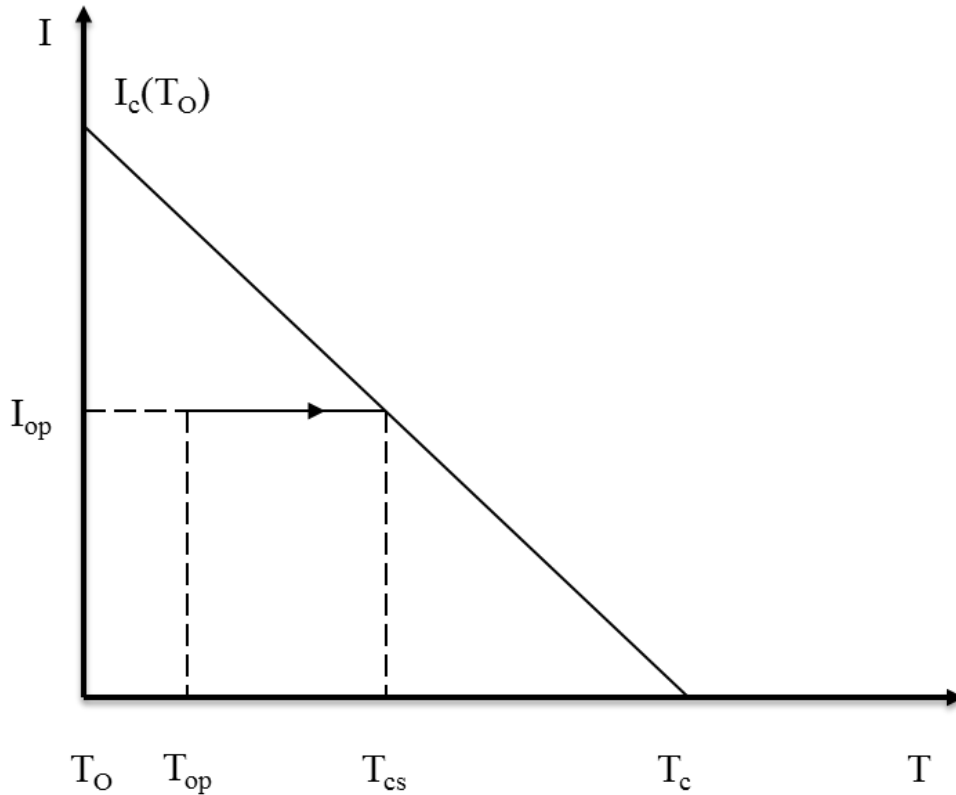


Figure 5.8: Effect of the temperature increase on the critical current and on the operating position: the current in the superconductor remains constant at the I_{op} value as long as the temperature is below T_{cs} , then decreases along the I_c curve. At T_c the current carried by the superconductor is zero, and all the current I_{op} flows in the shunting copper.

Let us consider the magnetic field as constant B_0 and examine the $I_c(B, T)$ curve. The operating temperature is T_{op} and the operating current I_{op} . If we keep the operating current constant and increase the temperature, we will reach the critical line at the temperature T_{cs} given approximately by the relation

$$T_{cs} = T_c - \frac{I_{op}}{I_c(B_0, T_0)} (T_c - T_0) \quad (5.12)$$

where the temperature T_0 is a reference point and the hypothesis of linear dependence of J_c on T has been made (as shown in the Figure 5.8).

At the temperature T_{cs} the superconductor is carrying a current which is equal to the maximum allowed I_c . Because any further increase in T results in a decrease of I_c , if the temperature of the superconductor is raised over T_{cs} the current exceeding I_c will be transferred to the neighboring copper, due to the normal resistivity of the superconducting material is higher than that of copper. In this regime the total current

I_{op} will be “shared” between superconductor and copper. This is the reason for the naming of the T_{cs} as current sharing temperature. As the critical temperature T_c is reached, no current will flow in the superconductor, and the whole current I_{op} will flow in the copper. The temperature regime between T_{cs} and T_c is the so called current sharing regime.

5.3.4.2. Heat Transfer Correlations

A key to the proper simulation of the quench in the cable is the knowledge of the heat transfer between the cable and helium. The correlations take a very different form and nature depending on the helium condition (eg. liquid helium, supercritical helium and superfluid helium), the flow regime and the heat exchange geometry. At present this is the most general approach as it relies on experimental data. The correlation models for the heat transfer coefficient have typical data fitting accuracy in the range of some 10 %, and predictive capability within a factor 2 [Bott99].

The definition of the heat transfer coefficient (h) (as shown in equation (5.16)) is used in the simulation is the heat flux per unit length along the flow direction x . Depending on the particular geometry or condition, other variables and parameters will be needed (such as Reynolds number, Prandtl number and Nusselt number) for the heat transfer coefficient.

The Reynolds number can be written as:

$$\text{Re} = \frac{\rho v D_h}{\nu} \quad (5.13)$$

where ρ is the helium density, v is the helium velocity and ν is the helium dynamic viscosity.

The Prandtl number can be written as:

$$\text{Pr} = \frac{\nu C_p}{K} \quad (5.14)$$

where C_p is the helium specific heat and K is its thermal conductivity.

The Nusselt number can be written as:

5. Thermal Hydraulic Modeling of the HTS Conductor

$$Nu = \frac{hD_h}{K} \quad (5.15)$$

Where h is the heat transfer coefficient and D_h is the hydraulic diameter.

For the turbulent forced flow of supercritical helium, a steady state heat transfer correlation can be approximated by the Dittus–Boelter form, as shown by Yaskin [YJYG77] and Giarratano [GiAS71]. A best fit of the available data is obtained with the following expression, which includes a correction for large temperature gradients at the wetted surface:

$$h_{DB} = 0.0259 \frac{K}{D_h} Re^{0.8} Pr^{0.4} \left(\frac{T_{he}}{T_s} \right)^{0.716} \quad (5.16)$$

where T_{he} is the helium temperature and T_s is the heated surface temperature.

The heat transfer is usually of the order of $1000 \text{ W}\cdot\text{m}^{-2}\cdot\text{K}^{-1}$. From the above equation it can be said that a large temperature difference between the heated surface and the helium causes an appreciable decrease of the heat transfer coefficient.

As for the transients typically less than 1 ms, strong variations of the heat transfer are observed. Experiments conducted on short samples to measure the transient heat transfer were conducted by Giarratano [GiSt83] and Bloem [Blo86]. The results of the experiments showed an initial peak below 1 ms. The peak decreased inversely to the square root of time in approximately 100 ms. This phenomenon could be explained as the diffusion of heat in the thermal boundary layer. The heat transfer could be computed by considering the analytical solution of diffusion due to a heat flux step at the surface is given in equation (5.17) [Blo86].

$$h_{BLQ} = \frac{1}{2} \sqrt{\frac{\pi K \rho_{he} c_{he}}{t}} \quad (5.17)$$

where ρ_{he} is the density of helium and c_{he} is the specific heat of helium. The above expression is shown to fit the experimental data between times 1 ms till the steady state is fully developed. Initially the equation (5.17) would predict a high heat transfer coefficient which is consistent with the analytical calculation.

For the TF coils maximum heat is deposited between 10 and 100 ms. To simulate the quench a heat pulse of 100 ms was used. Therefore, the transient heat transfer equation is not used for the current simulation.

5.3.5. Material Properties

A major problem faced by any HTS magnet is quench detection due to the slow quench propagation. To analyze the complex phenomena, the CryoSoft code THEA [BoRB00] ,[Cryo13][Cryo13] is used to perform a 1-D thermohydraulic analysis.

Before using THEA the material properties of REBCO and Hastelloy have to be identified. The critical surface of REBCO is parametrized by fitting equation (5.18) [WBMM00] to the data presented in [Haze11]. The results are shown in the Figure 5.9 and the fit parameters are given in

Table 5.2. Other parameters for REBCO like thermal conductivity, specific heat, electrical resistance are taken from CRYOCOMP software [Noti00] whereas the material properties of Hastelloy were taken from [LuCZ08].

$$J_c(B, T) = \frac{A}{B} B_{irr}(T)^\beta \left(\frac{B}{B_{irr}(T)} \right)^p \left(1 - \frac{B}{B_{irr}(T)} \right)^q \quad (5.18)$$

$$B_{irr}(T) = B_{irr0} \left(1 - \frac{T}{T_{c0}} \right)^\alpha$$

Table 5.2: Fit parameters for the critical surface of REBCO

Parameter	Value	Units
T_{c0}	90	K
B_{irr0} (Parallel to c plane)	132.5	T
A	1.82962E8	$\text{Nm}^{-3}\text{T}^{-\beta}$
P	0.5875	
Q	1.7	
A	1.54121	
B	1.96679	

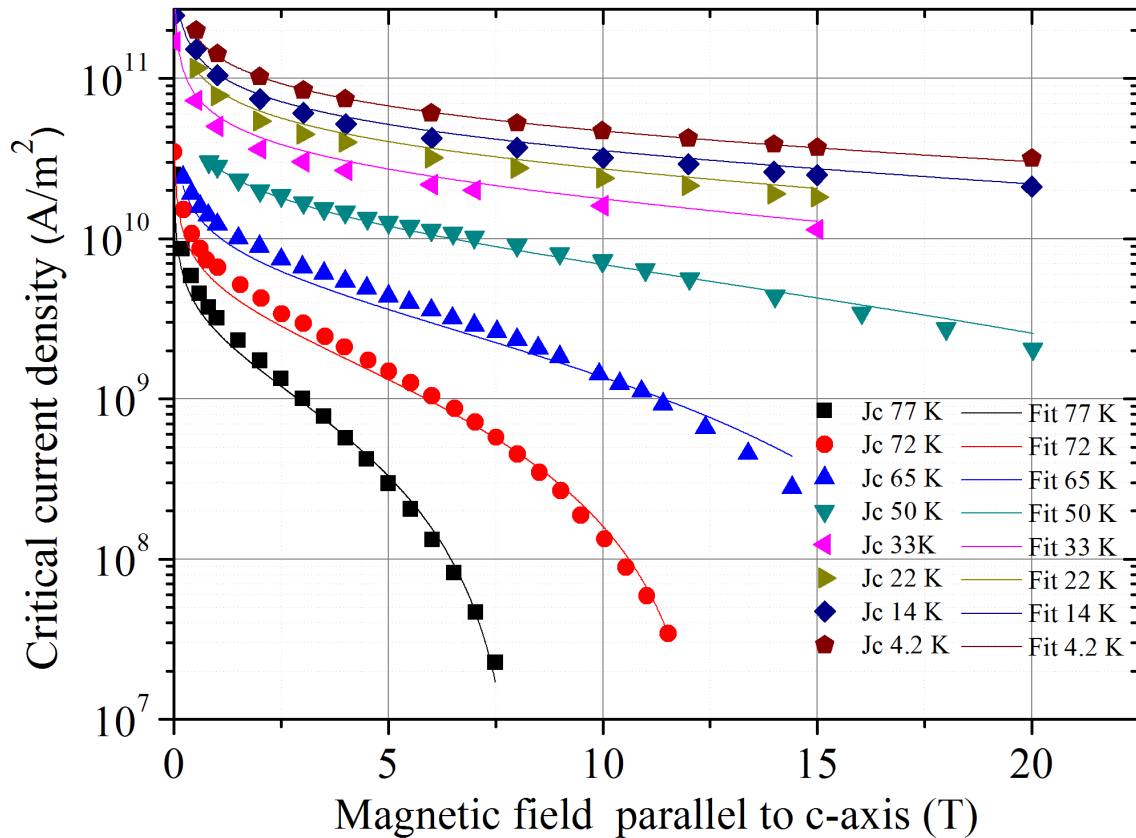


Figure 5.9: Critical current density data of *REBCO* as a function of magnetic field parallel to c-axis and fitting function.

5.3.6. Quench Analysis Results

The quench behavior of the HTS cable is exemplarily studied by modelling a 39 m long conductor, corresponding to the length of the innermost turn, carrying 50 kA in a constant magnetic field of 13.55 T using a homogenized conductor model. A constant n -value of 15 has been used. In this model all tapes are merged together forming one homogenized block of *REBCO*+copper+Hastelloy (m1) embedded in a stainless-steel jacket (m2). This model takes into account the fact that the Hastelloy substrate and the *REBCO* layer are very close together resulting in an almost equal temperature. The supercritical helium at 4.5 K flows in the conductor and exchanges heat with (m1) and (m2). The Dittus-Boelter correlation as implemented in THEA is used for determining the heat transfer coefficient. Constant mesh option is used with a mesh size of 10 cm. A heat pulse of 704 J just large enough to initiate a quench was deposited in the center of the conductor over a length of one meter for 100 ms.

Table 5.3: Parameters used in the THEA input.

Parameter	Unit	Value
Thermal components		
Conductor length	m	39
Area of REBCO	m ²	1.826E-6
Area of copper	m ²	555E-6
Area of Hastelloy	m ²	91.3E-6
Area of steel	m ²	1056.25E-6
Hydraulic parameters		
Helium cross section	m ²	272.209E-6
Hydraulic diameter	m	5.3903E-03
Helium inlet temperature	K	4.5
Helium inlet pressure	ar	6
Heat load $Q_{\text{cond}}/ Q_{\text{nucl}}$	W/m	0.006 along the whole conductor 0.291 along the 1 st turn

The voltage rise of the REBCO+copper+Hastelloy block is shown in Figure 5.10. As quench detection limits a value of 100 mV [Jkna08] and in addition a value of 400 mV was chosen, as this value is proposed in [CDNL12]. As visible in Figure 5.10 these values were reached after 24.24 s and 30.08 s. The voltage rise time is considerably longer than in case of LTS because of the extremely high critical temperature T_c which is 70 K even at 13.5 T leading to a very large heat capacity of the solid material. Adding 2 s for quench detection and initiation of the coil discharge results in delay time constants of $t_{\text{del},1} = 26.24$ s and $t_{\text{del},2} = 32.08$ s respectively. After this time an exponential current decrease is used with a time constant of $t_D = 30$ s. 30 s were chosen to limit the discharge voltage to about 11 kV [GBBF14]. This is much larger than the time constant estimated in the PROCESS code. But it should be mentioned that recently the discharge time constant was also increased to 30 s to limit the eddy currents flowing in the vacuum vessel.

5. Thermal Hydraulic Modeling of the HTS Conductor

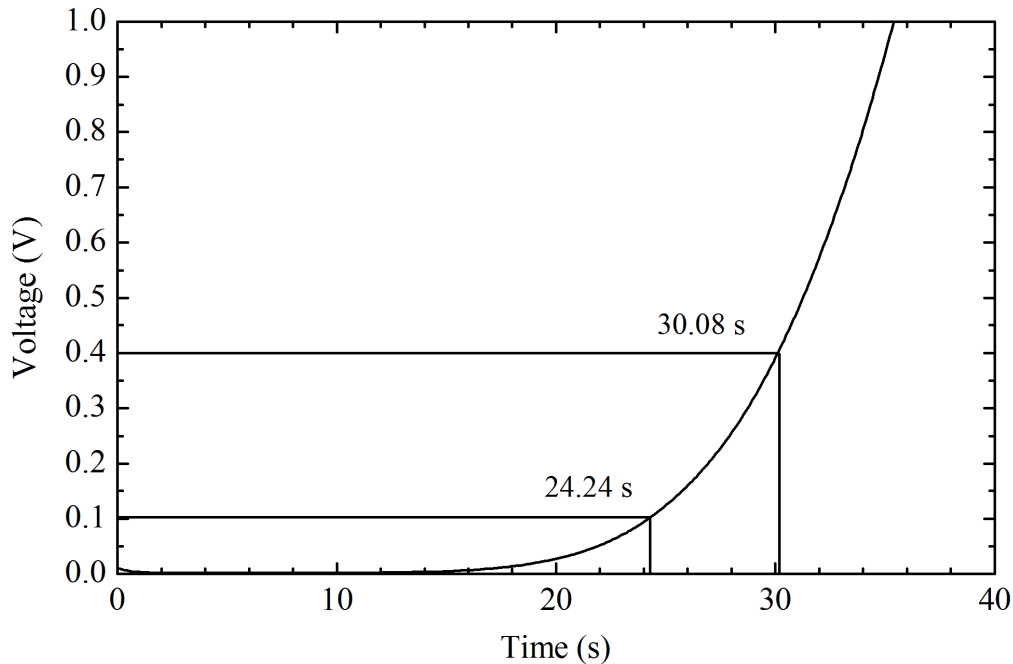


Figure 5.10 : Development of resistive voltage of the HTS conductor as a function of time.

Figure 5.11 and Figure 5.12 shows the temperature evolution for both t_{del} separately. For $t_{del,1}$ the maximum temperature is lower than the ITER design criteria of $T_{max} = 150$ K. For the longer $t_{del,2}$ which results from the unusual high quench detection voltage of 400 mV, the calculation shows a quite high conductor temperature close to 230 K. These calculation shows that quench detection and discharge of such a HTS-TF coil is feasible but should use a QD voltage level in the order of 100 mV.

To quench the conductor a 1 m long heater was assumed in the center of the conductor. A heating power of 7.04 kW/m is needed for a period of 0.1 seconds. The evolution of the normal zone length in the conductor can be seen in Figure 5.13. A blue rectangle in the Figure 5.13 shows the zoomed version of the evolution of normal zone length in the first 10 seconds. From the zoomed plot it can be seen that initially the normal zone length decreases and looks like that the conductor recovers. But after 10 seconds the helium near quench heats up and propagates the quench. The slow quench propagation is due to the high heat capacity of the HTS conductor. This is a fundamental difference to the LTS conductor where the normal zone propagation [WaKi00] is faster due to low heat capacity and lower T_c when compared to HTS.

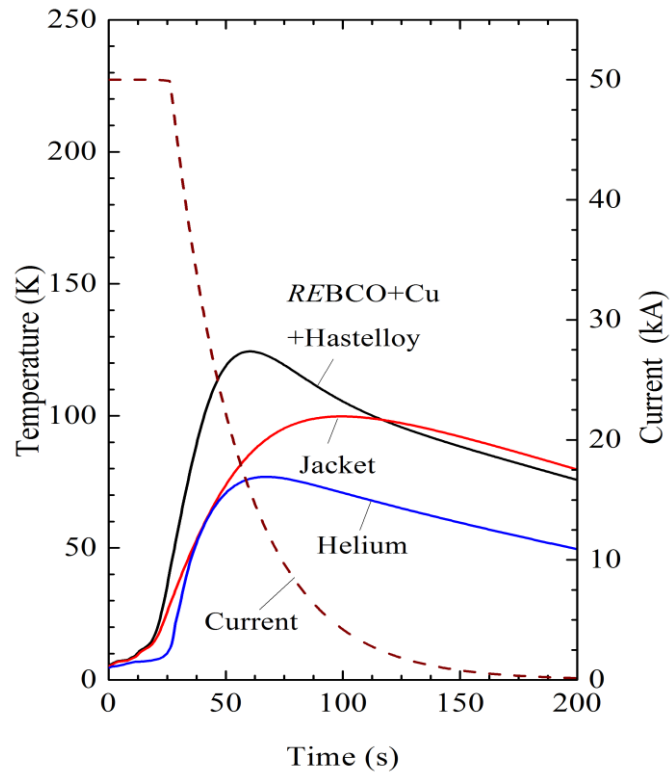


Figure 5.11: Conductor, jacket and helium temperature evolution during quench of 39 m long HTS conductor for the delay time $t_{del,1}$.

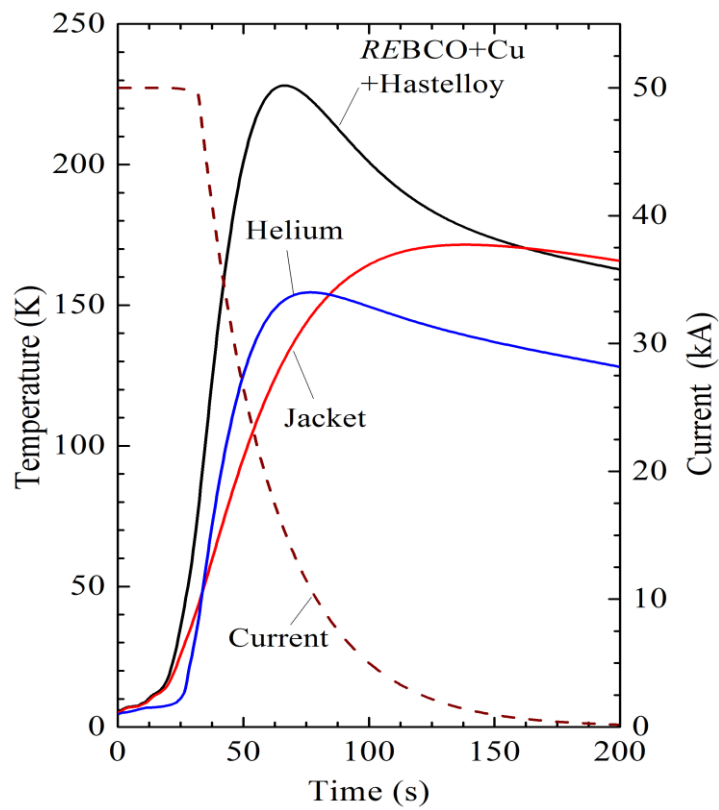


Figure 5.12: Conductor, jacket and helium temperature evolution during quench of 39 m long HTS conductor for the delay time $t_{del,2}$ (right).

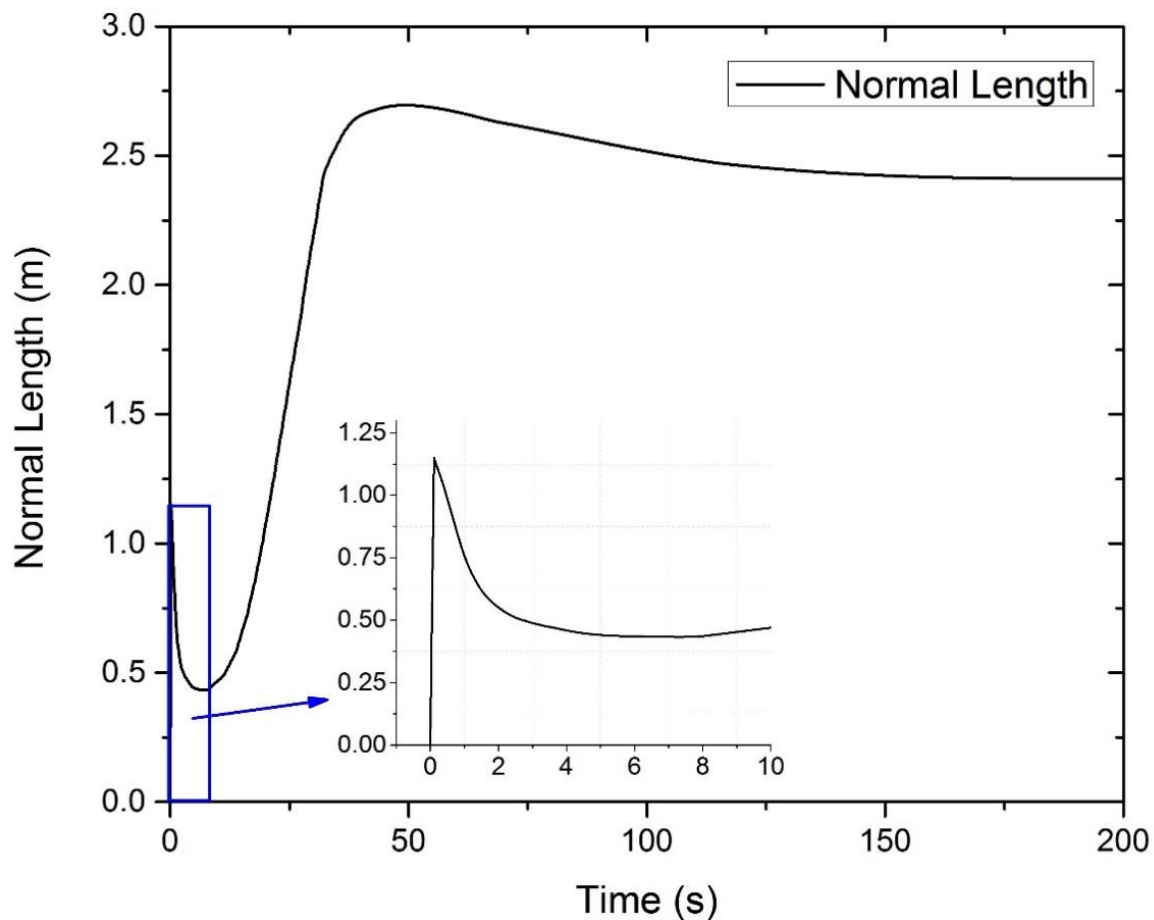


Figure 5.13: Evolution of the normal zone length with respect to time. The figure also shows a zoomed section of normal zone length for the first 10 seconds.

In Figure 5.14, the distribution of the helium mass flow along the conductor at various time steps is plotted. From the figure it can be seen that due to the heat pulse initially there is an effect of helium back flow caused by the local pressure rise at the heated region. This also improves the local heat transfer coefficient and reduces the normal length due to high heat capacity of supercritical helium. From the figure it is also seen that the hot helium front moves forward. Therefore, the maximum temperature is shifted from the center of the heat pulse towards the conductor end.

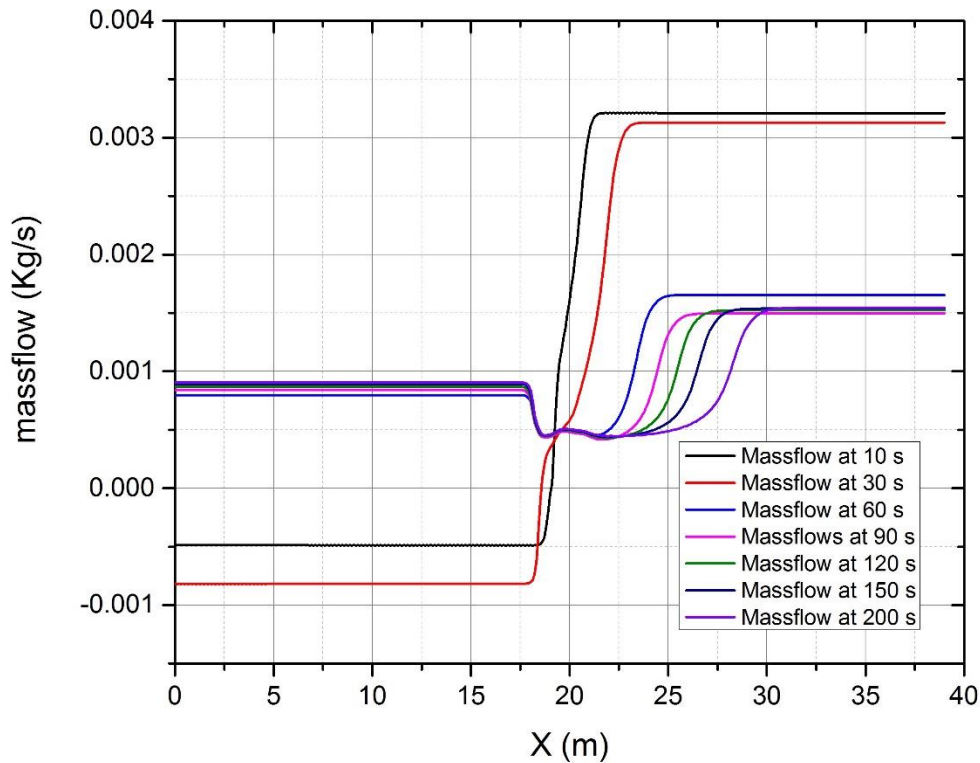


Figure 5.14: Evolution of the massflow with respect to time.

5.4. Summary on Conductor Modelling

The TF coil is subjected to heat loads from plasma. To remove the heat load the conductor is cooled by flowing supercritical helium through the conductor. During the forced flow, the important parameters are the heat produced due to the frictional losses, mass flow and pressure drop. The selection of the friction factor co-relation is one key parameter. For the conductor design the friction factor co-relation used from EURATOM LCT coil was chosen because it is the closer to the current HTS conductor design than a CICC friction factor. From the relationship between the mass flow, temperature raise, and the pressure drop it can be said that the TF coil can operate at lower mass flows with higher temperature increase because it has higher temperature margin. Unlike in the case of LTS conductors the temperature margin is in the order of 1-2 K, therefore the mass flow must be increased to reduce the temperature increase.

A first attempt of a quench analysis of the innermost turn of the inner pancake leads to an extremely slow voltage rise where 100 mV is reached after more than 24 s. The slow raise in voltage is for the fact that high temperature superconductor has very high T_c even at a magnetic field of 13.5 T. Using a discharge time constant of 30 s (which corresponds to a feasible discharge voltage of ~ 11 kV), a maximum temperature of 125 K is obtained and the ITER hot spot criterion is fulfilled. From the normal length zone,

5. Thermal Hydraulic Modeling of the HTS Conductor

it can be seen that due to high heat capacity the propagation of normal zone length is very slow. The length of the quenched area is very small, which could result in burning of conductor locally if not detected properly.

6. Summary and Conclusion

A conceptual design of EU DEMO TF coil is evolved with the input from the PROCESS Code whereas the conductor geometry of the coil is defined using an iterative process. The electromagnetic analysis is performed to assess the peak magnetic field and determine the conductor performance. The parameters identified for the design of the TF coil from the PROCESS code are; number of coils, total current, toroidal field at plasma axis, available winding pack area and overall steel cross section. It is ensured that the inner leg of the D-shaped coil is straight, the tangents of the successive arcs match and the sum of all angles for each the upper and lower half of the coil is 180° . The criteria for HTS conductor are based on its ability to sustain quench current and propagate quench, possess sufficient superconductor area to provide adequate operating margin, optimum area for helium flow and ensure effective cooling with minimum pressure drop. Once the conductor geometry is finalized, a TF coil can be wound using layer or pancake winding.

The electromagnetic analysis undertaken, and calculations derived, ensure that the HTS winding pack fits in the given winding pack area and is able to produce the required magnetic field at plasma axis for the EU DEMO. The stress of the casing and the conductor jacket, the displacement, the shear stress in the insulation, and the parameter of the LHD criteria are determined and compared.

After choosing the conductor proportions and the geometry for a TF coil, either a layer or pancake winding may be selected. The proposed pancake has a total winding area for the eighteen pancakes used is 0.77 m^2 and it fits finely into the available space of 1.10 m^2 as shown in Figure 3.3. The electrical circuit in the winding pack is connected in series while the hydraulic circuit is connected in parallel.

For the defined magnet parameters involving TF coils, it is mandatory to check whether the magnetic field at plasma axis is equal to the required magnetic field from the PROCESS code. The peak magnetic field is also calculated for defining the operating point of the conductor and for electromagnetic simulation, the pre-processor TOKEF [Mane84] and the code EFFI [Sack75] have been used. For electromagnetic analysis, sixteen TF coils have been modeled using the coil current given in Table 6.1 and the shape used in Figure 3.1.

The electromagnetic field calculations using EFFI enable to check the magnetic field for defining the operating point of the conductor and the inductances of the coils. The current density of the HTS conductor is calculated for finding the conductor operating point (Table 6.1). The hotspot calculation is made to study the temperature rise to ensure that the transition of the superconducting to normal conducting phase is avoided. The ITER hotspot criteria limits the maximum allowable adiabatic hotspot temperature to 150 K, taking into account all materials in the conductor, i.e., superconductor, copper, helium, stainless steel jacket, and insulation.

The results of the electromagnetic analysis stipulate that the HTS winding pack fits into the given winding pack area, produces the required magnetic field at plasma axis and available HTS material can be used to design a TF coil for EU DEMO. The stress of the casing as also the conductor jacket, the displacement, the shear stress in the insulation, the parameter of the LHD criteria are determined and compared. Structural analysis or a thermo hydraulic analysis is then performed to analyze the performance of the winding pack. A 2-D model of the inboard leg that is identified as the area with the highest stresses, constant tension coil and hoop stress are calculated assuming current carrying filaments are uniformly distributed around the z-axis (Figure 4.2). The comparison of hoop forces and stress for selected TOKAMAK systems are tabulated in Table 6.1.

Using the code EFFI [Sack75], a 3-D electromagnetic analysis is carried out, to calculate the magnetic field and generate the magnetic field components. To analyze the 2-D model, two general types of the analysis are considered, plane stress and plane strain. In order to conduct the studies, various models simulated in COMSOL are deliberated and two boundary conditions viz. roller boundary condition and that represented by the Lorentz force, are applied from study 1 to study 4 to take into account all 16 TF coils.

The results of study 1 indicate that the peak stress in the conductor jacket is 178 MPa, which is acceptable. Von Mises stress for study 2 in conductor jacket is 157 MPa. In study 3, the debonding of the winding pack in the plasma end of the mid-plane of the inboard leg of the TF coil is introduced and the Von Mises stress in jacket is 227 MPa. In study 4, the simulation is done using ideal elastic properties and the results of the all the studies are presented and compared in Table 4.3. The 2-D structural analysis using the casing geometry as given by the PROCESS code is performed by evaluating the constant tension coil and the hoop stress and it is found to be within acceptable limits.

The modelling criteria of the HTS conductor depends on the plasma heating rate, heat transfer from the heat source to the conductor, helium flow characteristics and friction factor for the hydraulic model. A comprehensive hydraulic analysis has been performed to determine these four parameters. These parameters are then used to compute the pressure drop and temperature rise in the conductor. During quench, the conductor took 24 seconds to reach 100 mV (quench detection voltage). Despite slow raise the conductor temperature raised is below 150 K (satisfying ITER criteria).

The TF coil case cooling design tends to intercept most of this heat load. However, some amount of heating will conduct through the coil ground wrap insulation. This heat load has the adverse effect of a direct impact on the stability and safety margins of the superconductor. The study concludes that using HTS, a nuclear heat load of 400 W/coil is no problem even with a mass flow rate below 2 g/s.

Table 6.1: summary of the results

Parameter	Value and unit
Number of TF coil	16
Total current in one TF coil	19.2 MA
Peak field on conductor	13.27 T
Inductance per coil	7.28 H
Operation current	50 kA
Energy stored in one TF coil	9.09 GJ
Total number of conductor turns in winding pack	384
Total winding pack area used	0.77 m ²
I_{op}/I_c	0.7
Operating temperature	4.5 K
Current sharing temperature	16.4 K
Temperature margin	11.9 K
Discharge time constant	30 s
Discharge voltage	12.2 kV
F_z	694.1 MN
Steel in the casing	1.33
Steel in the winding pack	0.398 m ²
Total hoop stress	428.53 MPa
% Hoop stress by winding pack	23.61
% hoop stress by the case	76.39
Area of REBCO	1.826E-6 m ²
Area of copper	555E-6 m ²
Area of Hastelloy	91.3E-6 m ²
Area of steel	1056.25E-6 m ²
Nuclear heat	400 W/coil

6. Summary and Conclusion

Supercritical helium mass flow	2 g/s
Conductor length of inner pancake	853 m
Conductor length of outer pancake	741 m
Helium cross section	272.209E-6 m ²
Hydraulic diameter	5.3903E-03 m
Helium inlet temperature	4.5 K
Helium inlet pressure	6 bar
Heat load $Q_{\text{cond}}/ Q_{\text{nucl}}$	0.006 along the whole conductor 0.291 along the 1 st turn W/m

Bibliography

- [Afp06] AFP, NEW SCIENTIST TECH AND: *Green light for nuclear fusion project*. URL <https://www.newscientist.com/article/dn10633-green-light-for-nuclear-fusion-project/>
- [Amel15] AMELICHEV, VADIM: *SuperOx 2G-HTS wire: production, applications and outlook*. URL https://elenia.tu-bs.de/fileadmin/content/sls/8sls/SLS_Mi_7_Amelichev.pdf
- [Arp72] ARP, V: Forced Flow, Single-Phase Helium Cooling Systems. In: TIMMERHAUS, K. D. (Hrsg.): *Advances in Cryogenic Engineering: A Collection of Invited Papers and Contributed Papers Presented at National Technical Meetings During 1970 and 1971*. Boston, MA : Springer US, 1972 — ISBN 978-1-4684-7826-6, S. 342–351
- [ArPi08a] ARIOLA, MARCO ; PIRONTI, ALFREDO: *Magnetic Control of Tokamak Plasmas* : Springer, 2008 — ISBN 9781848003231
- [ArPi08b] ARIOLA, MARCO ; PIRONTI, ALFREDO: *Magnetic Control of Tokamak Plasmas*, 2008
- [Bals00] BALSHAW, N H: *Comparison table of „Conventional“ Tokamaks*. URL <http://home.clara.net/balshaw/tokamak/table-of-tokamaks.pdf>
- [Bart13] BARTH, CHRISTIAN: *High Temperature Superconductor Cable Concepts for Fusion Magnets*, KIT Scientific Publishing, 2013
- [Baye16] BAYER, CHRISTOPH M: *Characterization of High Temperature Superconductor Cables for Magnet Toroidal Field Coils of the DEMO Fusion Power Plant* : KIT Scientific Publishing, 2016 — ISBN 9783731506058
- [BCCC87] BOURNE, L. C. ; COHEN, MARVIN L. ; CREAGER, WILLIAM N. ; CROMMIE, MICHAEL F. ; STACY, ANGELICA M. ; ZETTL, A.: Onset of superconductivity in Y-Ba-Cu-O at 100 K. In: *Physics Letters A* Bd. 120 (1987), Nr. 9, S. 494–496 — ISBN 0375-9601
- [BeMü86] BEDNORZ, J G ; MÜLLER, K A: Possible highTc superconductivity in the Ba-La-Cu-O system. In: *Zeitschrift für Physik B Condensed Matter* Bd. 64 (1986), Nr. 2, S. 189–193
- [BFMN18] BRUZZONE, PIERLUIGI ; FIETZ, WALTER H. ; MINERVINI, JOSEPH V. ; NOVIKOV, MIKHAIL ; YANAGI, NAGATO ; ZHAI, YUHU ; ZHENG, JINXING: High temperature superconductors for fusion magnets. In: *Nuclear Fusion* Bd. 58 (2018), Nr. 10, S. 103001
- [BKSV98] BEARD, D S ; KLOSE, W ; SHIMAMOTO, S ; VECSEY, G: The IEA Large Coil Task Development of Superconducting Toroidal Field Magnets for Fusion Power. In: *Fusion Engineering and Design* Bd. 7 (1998), S. 1–230
- [Bloer86] BLOEM, W.B.: Transient heat transfer to a forced flow of supercritical helium at 4.2 K. In: *Cryogenics* Bd. 26, Elsevier (1986), Nr. 5, S. 300–308
- [BoMi88] BOTTURA, LUCA ; MINERVINI, JOSEPH V.: Detailed distribution of AC losses in the NET TF coil during normal operation. In: *ASC Conference*. San Francisco, 1988
- [Boni14] BONIFETTO, R; LACROIX, B; LEWANDOWSKA, B; SAVOLDI-RICHARD, L; SEDLAK, K; VALLCORBA, R; ZANINO, R: Proposal of scaling laws for thermal-hydraulic analyses in burn conditions. In: *memo MCD 2.2 D01 v.4* (2014)
- [Booz02] BOOZER, ALLEN H.: What is a stellarator? In: *Physics of Plasmas* Bd. 5 (2002), Nr. 5, S. 1647–1655
- [BoRB00] BOTTURA, L. ; ROSSO, C. ; BRESCHI, M.: A general model for thermal, hydraulic and electric analysis of superconducting cables. In: *Cryogenics* Bd. 40

- (2000), Nr. 8–10, S. 617–626
- [Bott87] BOTTURA, L.: HE-SS: a computer program for steady state analysis of helium cooled conductors. In: *internal report NET/IN/87-62* (1987)
- [Bott88] BOTTURA, LUCA: Transient thermal analysis of force-cooled conductor. In: *12th ICEC Conference*. Southanotin, 1988, S. 182–186
- [Bott99] BOTTURA, LUCA: Heat transfer correlations. In: *CryoSoft Internal Note* (1999)
- [BoZi92a] BOTTURA, L. ; ZIENKIEWICZ, O. C.: Quench analysis of large superconducting magnets. Part I: model description. In: *Cryogenics* Bd. 32 (1992), Nr. 7, S. 659–667
- [BoZi92b] BOTTURA, L ; ZIENKIEWICZ, O C: Quench Analysis of Large Superconducting Magnets .2. Model Validation and Application. In: *Cryogenics* Bd. 32 (1992), Nr. 8, S. 719–728 — ISBN 0011-2275
- [BrSt02] BRAAMS, C M ; STOTT, P E: Nuclear Fusion: half a century of magnetic confinement research. In: *Plasma Physics and Controlled Fusion* Bd. 44, IOP Publishing (2002), Nr. 8, S. 1767
- [Bruz06] BRUZZONE, PIERLUIGI: 30 Years of conductors for fusion: A summary and perspectives. In: *IEEE Transactions on Applied Superconductivity* Bd. 16 (2006), Nr. 2, S. 839–844
- [CDNL12] COATANEA, M. ; DUCHATEAU, J. L. ; NICOLLET, S. ; LACROIX, B. ; TOPIN, F.: Investigations about quench detection in the ITER TF coil system. In: *IEEE Transactions on Applied Superconductivity* Bd. 22 (2012), Nr. 3, S. 3–6
- [CFBL17a] CIATTAGLIA, S ; FEDERICI, G ; BARUCCA, L ; LAMPASI, A ; MINUCCI, S ; MOSCATO, I: The European DEMO fusion reactor: Design status and challenges from balance of plant point of view. In: *2017 IEEE International Conference on Environment and Electrical Engineering and 2017 IEEE Industrial and Commercial Power Systems Europe (EEEIC / I&CPS Europe), 2017* — ISBN VO -, S. 1–6
- [CFBL17b] CIATTAGLIA, SERGIO ; FEDERICI, GIANFRANCO ; BARUCCA, LUCIANA ; LAMPASI, ALESSANDRO ; MINUCCI, SIMONE ; MOSCATO, IVO: The European DEMO fusion reactor: Design status and challenges from balance of plant point of view. In: *Conference Proceedings - 2017 17th IEEE International Conference on Environment and Electrical Engineering and 2017 1st IEEE Industrial and Commercial Power Systems Europe, EEEIC / I and CPS Europe 2017* (2017), Nr. 633053 — ISBN 9781538639160
- [Ches67] CHESTER, P F: Superconducting magnets. In: *Reports on Progress in Physics* Bd. 30 (1967), Nr. 2, S. 561–614
- [Cond00] *Conductus @ Superconducting Wire Technology Advantages*. URL http://www.suptech.com/Benefits_and_Performance_Advantage_Oct_21.pdf
- [Corc00] *CORC cable CICC for fusion magnet*. URL <http://advancedconductor.com/wp-content/uploads/2018/05/CICC-768x124.jpg>
- [Cryo13] CRYOSOFT: *Thea-Thermal, Hydraulic and Electric Analysis of Superconducting Cables. Users' Guide ver. 2.2*, 2013
- [Cvan09] C VAN DER LAAN, D: *YBa2Cu3O7- δ coated conductor cabling for low ac-loss and high-field magnet applications*. Bd. 22, 2009
- [Demo00] demo1_jul12_build_coils_2KYJLN_v1_0_2KYWWJ_v1_0
- [Dres02a] DRESNER, LAWRENCE: *Stability of Superconductors* : Springer US, 2002 — ISBN 978-0-306-45030-3
- [Dres02b] DRESNER, LAWRENCE: *Stability of Superconductors* : Springer US, 2002
- [Dres95] DRESNER, LAWRENCE: *Stability of superconductors* : Plenum Press, 1995 — ISBN 9780306470646

- [FBCC09] FLESHLER, STEVEN ; BUCZEK, D ; CARTER, B ; CEDRONE, P ; DEMORANVILLE, KENNETH ; GANNON, J ; INCH, J ; LI, XIAOPING ; U. A.: *Scale-up of 2G wire manufacturing at American Superconductor Corporation*. Bd. 469, 2009
- [FiSh71] FILE, J ; SHEFFIELD, G V: Large superconducting magnet design for fusion reactors. In: *IEEE Transactions on Nuclear Science* Bd. 18 (1971), Nr. 4, S. 277–282
- [FiSh72] FILE, J ; SHEFFIELD, G V: A Large Superconducting Magnet for Fusion Research. In: *4th International Conference on Magnet Technology, 1972*, S. 240–243
- [FKWB14] FEDERICI, G. ; KEMP, R. ; WARD, D. ; BACHMANN, C. ; FRANKE, T. ; GONZALEZ, S. ; LOWRY, C. ; GADOMSKA, M. ; U. A.: Overview of EU DEMO design and R&D activities. In: *Fusion Engineering and Design* Bd. 89, Elsevier B.V. (2014), Nr. 7–8, S. 882–889
- [FoSa04] FORD, P.J. ; SAUNDERS, G.A.: *The Rise of the SUPERCONDUCTORS*, 2004 — ISBN 9780748407729
- [FoSu04] FOSSHEIM, KRISTIAN ; SUDBOE, ASLE: *Superconductivity: Physics and Applications*, 2004 — ISBN 9780470844526
- [GBBF14] GADE, P V ; BARTH, C ; BAYER, C ; FIETZ, W H ; FRANZA, F ; HELLER, R ; HESCH, K ; WEISS, K: Conceptual Design of a Toroidal Field Coil for a Fusion Power Plant Using High Temperature Superconductors. In: *IEEE Transactions on Applied Superconductivity* Bd. 24 (2014), Nr. 3
- [GhMe17] GHORANNEVISS, MAHMOOD ; MESHKANI, SAKINEH: *Plasma Science and Technology for Emerging Economies*, 2017 — ISBN 9789811042171
- [GiAS71] GIARRATANO, P.J. ; ARP, V.D. ; SMITH, R.V.: Forced convection heat transfer to supercritical helium. In: *Cryogenics* Bd. 11, Elsevier (1971), Nr. 5, S. 385–393
- [GiSt83] GIARRATANO, P J ; STEWARD, W G: Transient Forced Convection Heat Transfer to Helium During a Step in Heat Flux. In: *Journal of Heat Transfer* Bd. 105, ASME (1983), Nr. 2, S. 350–357. — 10.1115/1.3245585
- [GMPG04] GONZÁLEZ, J. C. ; MESTRES, N. ; PUIG, T. ; GÁZQUEZ, J. ; SANDIUMENGE, F. ; OBRADORS, X. ; USOSKIN, A. ; JOOSS, CH ; U. A.: Biaxial texture analysis of YBa₂Cu₃O₇-coated conductors by micro-Raman spectroscopy. In: *Physical Review B - Condensed Matter and Materials Physics* Bd. 70 (2004), Nr. 9, S. 1–8
- [Harm13] HARMAN, JON: EFDA Power Plant Physics & Technology WP13 Reference DEMO CAD Model Specification 2MACBZ_v1_1 (2013)
- [Haze10] HAZELTON, D: Recent Developments in 2G HTS Coil Technology. In: *Applied superconductivity conference, August 1 - 6, 2010*, 2010
- [Haze11] HAZELTON, DREW W: Application of SuperPower 2G HTS Wire to High Field Devices Demands on conductor for high field applications. In: *International Conference on Magnet Technology - 22, 12-16 September, 2011*, 2011
- [HGFV16] HELLER, R ; GADE, P V ; FIETZ, W H ; VOGEL, T ; WEISS, K -: Conceptual Design Improvement of a Toroidal Field Coil for EU DEMO Using High-Temperature Superconductors. In: *IEEE Transactions on Applied Superconductivity* Bd. 26 (2016), Nr. 4, S. 1–5
- [Hoen80] HOENIG, M O: Internally cooled cabled superconductors. In: *Cryogenics* Bd. 20 (1980), Nr. 8, S. 427–434
- [Http00] <http://www.comsol.com/release/4.4>
- [IOFT93] IJIMA, Y ; ONABE, K ; FUTAKI, N ; TANABE, N ; SADAKATA, N ; KOHNO, O ; IKENO, Y: In-plane texturing control of Y-Ba-Cu-O thin films on polycrystalline substrates by ion-beam-modified intermediate buffer layers. In: *IEEE Transactions on Applied Superconductivity* Bd. 3 (1993), Nr. 1, S. 1510–1515

- [Iter00a] ITER: *What is ITER?* URL <https://www.iter.org/proj/inafewlines#6>
- [Iter00b] ITER BELGIUM: *ITER Reactor*. URL http://www.iterbelgium.be/files/upload/ITER_reactor.jpg
- [IwHM77] IWASA, Y ; HOENIG, M. ; MONTGOMERY, D.: Cryostability of a small superconducting coil wound with cabled hollow conductor. In: *IEEE Transactions on Magnetics* Bd. 13 (1977), Nr. 1, S. 678–681
- [Jkna08] J. KNASTER, D. BESSETTE, A. DEVRED, R. GALLIX, L. SCIBILE, N. MITCHELL, F. RODRÍGUEZ-MATEOS, E. ZAPRETILINA: The Instrumentation on the TF Coils of ITER. In: *Fusion Science and Technology* Bd. 56 (2008), Nr. 2, S. 685–689
- [Jong08] JONG, C: Magnet structural design criteria part 1: Main structural components and welds (2008)
- [Kath94] KATHEDER, H: Optimum thermohydraulic operation regime for cable in conduit superconductors (CICS). In: *Cryogenics* Bd. 34 (1994), S. 595–598
- [Keil85] KEILHACKER, M.: The asdex divertor tokamak. In: *Nuclear Fusion* Bd. 25 (1985), Nr. 9, S. 1045–1054
- [KKKW11] KOVARI, M ; KEMP, R ; KNIGHT, P ; WARD, D: The PROCESS fusion reactor systems code - summary (2011)
- [KKLK14] KOVARI, M ; KEMP, R ; LUX, H ; KNIGHT, P ; MORRIS, J ; WARD, D J: “PROCESS”: A systems code for fusion power plants—Part 1: Physics. In: *Fusion Engineering and Design* Bd. 89 (2014), Nr. 12, S. 3054–3069
- [Knig13] KNIGHT, P J: A User Guide to the PROCESS Systems Code (2013)
- [KrKa13] KRISHNAN, AJITH ; KALLUVILA, JINSHAH: *Magnetohydrodynamic Power Generation*. Bd. 3, 2013
- [KYUM94] KITAMURA, K. ; YAMAMOTO, T. ; UCHIDA, T. ; MORIYAMA, H. ; NISHIMURA, A. ; MOTOJIMA, O. ; YAMAMOTO, J.: Cryogenic shear fracture tests of interlaminar organic insulation for h. forced-flow superconducting coil. In: *IEEE Transactions on Magnetics* Bd. 30 (1994), Nr. 4, S. 1879–1882
- [LeBa11] LEWANDOWSKA, MONIKA ; BAGNASCO, MAURIZIO: Modified friction factor correlation for CICC’s based on a porous media analogy. In: *Cryogenics* Bd. 51, Elsevier Ltd (2011), Nr. 9, S. 541–545
- [LeKL06] LEE, HYUNG-WOO ; KIM, KI-CHAN ; LEE, JU: Review of maglev train technologies. In: *IEEE Transactions on Magnetics* Bd. 42 (2006), Nr. 7, S. 1917–1925
- [LuCZ08] LU, J ; CHOI, E S ; ZHOU, H D: Physical properties of Hastelloy® C-276™ at cryogenic temperatures. In: *Journal of Applied Physics* Bd. 103 (2008), Nr. 6
- [Magn00] *Magnetisch eingeschlossene Fusionsplasmen*. URL <https://www.dpg-physik.de/dpg/gliederung/fv/p/info/magnet.html?print=true&>
- [MaJa68] MADDOCK, B.J. ; JAMES, G.B.: Protection and stabilisation of large superconducting coils. In: *Proceedings of the Institution of Electrical Engineers* Bd. 115 (1968), Nr. 4, S. 543
- [Mane84] MANES, B: TOKEF: A Tokamak Input Generator for EFFI Bd. KfK 3854 (1984)
- [McSt12] MCCracken, GARRY M ; STOTT, PETER ; 2ND (Hrsg.): *Fusion: The Energy of the Universe* : Elsevier, 2012 — ISBN 9780123846563
- [MiSF08] MIRI, A M ; S, FINK ; FIETZ, W H: *Transient Behaviour of Superconducting Magnet Systems of Fusion Reactor ITER during Safety Discharge*. Bd. 2008, 2008
- [Mitc00] MITCHELL, N: ITER Design Description Document, DDD 11, TF coils and structures, 2MVZNX, ITER IDM server
- [Mitc09] MITCHELL, N: Design Description Document : DDD 11 Magnets; Section 2.2 Structural Analysis (2009), Nr. September

- [Mond16] MONDONICO, CARMINE SENATORE AND CHRISTIAN BARTH AND MARCO BONURA AND MILOSLAV KULICH AND GIORGIO: Field and temperature scaling of the critical current density in commercial REBCO coated conductors. In: *Superconductor Science and Technology* Bd. 29 (2016), Nr. 1, S. 14002
- [Moon14] MOON, SEUNG HYUN: *HTS Development and Industrialization at SuNAM*. URL https://indico.cern.ch/event/308828/contributions/1680708/attachments/589810/811813/20140521_SuNAM_at_WAMH_DESY_vf.pdf
- [Mose75] MOSES, R.W., YOUNG, W.C. (FUSION TECHNOLOGY INSTITUTE. UNIVERSITY OF WISCONSIN): Analytic Expressions for Magnetic Forces on. In: *Sixth Symposim on Engineering Problems of Fusion Research* (1975), Nr. November, S. 18–21
- [MyPR95] MYATT, R. LEONARD ; PILLSBURY, R. D. ; RADOYINSKY, A. L.: Thermal Analysis of the TPX TF Coil Case for Eddy Current and Neutron Heating. In: *IEEE Transactions on Applied Superconductivity* Bd. 5 (1995), Nr. 2, S. 925–928
- [NiMo10] NIELSEN, K E ; MOLINAS, M: Superconducting Magnetic Energy Storage (SMES) in power systems with renewable energy sources. In: *2010 IEEE International Symposium on Industrial Electronics*, 2010 — ISBN 2163-5137 VO - , S. 2487–2492
- [NoGo15] NOE, MATHIAS ; GOLDACKER, WILFRIED: Introduction in HTS Technology. In: *Principle of technical implementation for power systems and transport*. Ottobrunn, Germany, 2015
- [Noti00] *No Title*. . — <http://www.eckelsengineering.com/>
- [NPDD10] NANNINI, M ; PORTAFAIX, C ; DECOOL, P ; DOLGETTA, N ; ZANI, L ; BARABASCHI, P: Mechanical Analysis of the JT-60SA TF Coils. In: *IEEE Transactions on Applied Superconductivity* Bd. 20 (2010), Nr. 3, S. 521–524
- [NZBS15] NAKASAKI, RYUSUKE ; ZHANG, YIFEI ; BROWNSEY, PAUL ; SUNDARAM, AARTHI: *Continuous Improvements in Performance and Quality of 2G HTS Wires Produced by IBAD-MOCVD for Coil Applications*. URL http://www.superpower-inc.com/system/files/2015_1018+MT24+4OrBA_03_0.pdf
- [OnOg16] ONGENA, JEF ; OGAWA, YUICHI: Nuclear fusion: Status report and future prospects. In: *Energy Policy* Bd. 96 (2016), S. 770–778
- [Prag05] PRAGER, S: *Magnetic Confinement Fusion Science Status and Challenges*. URL https://fire.pppl.gov/aaas05_prager_mfe.pdf
- [Rao91] RAO, C.N.R: *Chemistry of High Temperature Superconductors* : WORLD SCIENTIFIC, 1991 — ISBN 978-981-02-0805-9
- [Robe08] ROBERT, ARNOUX: *Which was the first „tokamak“ — or was it „tokomag“?* URL <https://www.iter.org/newsline/55/1194>
- [Roeb12] ROEBEL, LUDWIG: Electrical conductor.
- [RoRh78] ROSE-INNES, ALISTAIR C. ; RHODERICK, EMLYN H.: Introduction to Superconductivity. In: RHODERICK, E. H. B. T. (Hrsg.) , Pergamon (1978) — ISBN 9780080216515
- [Sack75] SACKETT, S. J: Calculation of electromagnetic fields and forces in coil systems of arbitrary geometry. In: *6th IEEE Symp. on Eng. Probl. of Fusion Res., San Diego*, 1975
- [Sana00a] SANABRIA, CHARLIE: *ITER CS conductor*. URL https://nationalmaglab.org/images/magnet_development/asc/image_gallery/nb3sn/2d_gallery/iter_fusion_cs_conductor.jpg
- [Sana00b] SANABRIA, CHARLIE: *ITER TF conductor*. URL https://nationalmaglab.org/images/magnet_development/asc/image_gallery/nb3sn/2d_gallery/iter_fusion_tf_conductor.jpg
- [Schm00] SCHMUESER, PETER: *Superconductivity*. URL

- <http://www.desy.de/~pschmues/Superconductivity.pdf>
- [Schw92] SCHWARTZ, J.: A Novel superconducting toroidal field magnet concept using advanced materials. In: *Journal of Fusion Energy* Bd. 11 (1992), Nr. 1, S. 19–37
- [ScSc93] SCHOLLE, E A ; SCHWARTZ, J: MPZ stability under time-dependent, spatially varying heat loads. In: *IEEE Transactions on Applied Superconductivity* Bd. 3 (1993), Nr. 1, S. 421–424
- [Seeb98] SEEBER, B: *Handbook of Applied Superconductivity, Volume 2* : CRC Press, 1998 — ISBN 9781420050271
- [Selv11] SELVAMANICKAM, V: Second-generation HTS Wire for Wind Energy Applications. In: *Symposium on Superconducting Devices for Wind Energy* (2011)
- [Shaf01] SHAFRANOV, VITALII D: The initial period in the history of nuclear fusion research at the Kurchatov Institute. In: *Physics-Uspekhi* Bd. 44 (2001), Nr. 8, S. 835–843
- [ShSp04] SHIMOMURA, Y. ; SPEARS, W.: Review of the ITER Project. In: *IEEE Transactions on Applied Superconductivity* Bd. 14 (2004), Nr. 2, S. 1369–1375
- [Smir09] SMIRNOV, V P: Tokamak foundation in USSR/Russia 1950–1990. In: *Nuclear Fusion* Bd. 50, IOP Publishing (2009), Nr. 1, S. 14003
- [StZa65] STEKLY, Z J J ; ZAR, J L: Stable Superconducting Coils. In: *IEEE Transactions on Nuclear Science* Bd. 12 (1965), Nr. 3, S. 367–372
- [Taká97] TAKÁCS, S.: AC losses in superconducting cables and their expected values in magnetic systems. In: *Superconductor Science and Technology* Bd. 10 (1997), Nr. 10, S. 733–748
- [TCBM11] TAKAYASU, M ; CHIESA, L ; BROMBERG, L ; MINERVINI, J V: Cabling Method for High Current Conductors Made of HTS Tapes. In: *IEEE Transactions on Applied Superconductivity* Bd. 21 (2011), Nr. 3, S. 2340–2344
- [ThTa82] THOME, RICHARD J. ; TARRH, JOHN M.: *Mhd and Fusion Magnets: Field and Force Design Concepts* : John Wiley & Sons, 1982 — ISBN 9780471093176
- [Titu03] TITUS, PETER H: Structural Design of High Field Tokamaks (2003), S. 1–15
- [WaKi00] WANG, QIULIANG ; KIM, KEEMAN: Numerical Model for Thermal Hydraulic Analysis In Bd. 14 (2000), Nr. 9, S. 985–996
- [Walk00] WALKER, THOMAS: *Der Kern der Plasma-Anlage besteht aus dem Plasmagefäß und 70 supraleitenden Spulen. Die komplette Elektrotechnik wurde mit der Wscad-Suite geplant.* URL <https://www.all-electronics.de/ecad-fuer-wendelstein-7-x/>
- [WaNM87] WATANABE, KAZUO ; NOTO, KOSHICHI ; MUTO, YOSHIO: Overview of Superconducting Materials Researches held in HFLSM at Tohoku University. In: *Science reports of the Research Institutes, Tohoku University. Ser. A, Physics, chemistry and metallurgy* Bd. 33 (1987), Nr. 2, S. 393–414
- [WBMM00] WESCHE, R ; BRUZZONE, P ; MARCH, S ; MARINUCCI, C ; UGLIETTI, D: Thermal stability and quench. In: *HTS4Fusion*. Karlsruhe
- [WeCa11] WESSON, J ; CAMPBELL, D J: *Tokamaks, International Series of Monographs on Physics* : OUP Oxford, 2011 — ISBN 9780199592234
- [WFBS15] WOLF, MICHAEL J. ; FIETZ, WALTER H. ; BAYER, C. ; SCHLACHTER, SONJA I. ; HELLER, R. ; WEISS, K.-P.: HTS CroCo - a stacked HTS conductor optimized for high currents and long length production. In: *IEEE Transactions on Applied Superconductivity* (2015)
- [Wils08] WILSON, MARTIN N.: NbTi superconductors with low ac loss: A review. In: *Cryogenics* Bd. 48 (2008), Nr. 7–8, S. 381–395 — ISBN 0011-2275
- [Wils87] WILSON, M N: *Superconducting Magnets* : Oxford press, 1987 — ISBN 9780198548102

- [WiWo97] WILSON, M.N. ; WOLF, R.: Calculation of minimum quench energies in Rutherford cables. In: *IEEE Transactions on Applied Superconductivity* Bd. 7 (1997), Nr. 2 — ISBN 1051-8223 VO - 7
- [Wood06] WOODS, LESLIE C.: *Theory of Tokamak Transport*, 2006 — ISBN 9783527406258
- [Xu16] XU, YUHONG: A general comparison between tokamak and stellarator plasmas. In: *Matter and Radiation at Extremes* Bd. 1 (2016), Nr. 4, S. 192–200
- [YHKK82] YOUNG, J.L. ; HEYNE, C.J. ; KOMAREK, P. ; KRAUTH, H. ; MARINUCCI, C. ; VECSEY, G.: The forced flow cooled coils for the International Energy Agency Large Coil Task. In: *Advances in Cryogenic Engineering* Bd. 27 S. 11–2 (1982)
- [YJYG77] YASKIN, L.A. ; JONES, M.C. ; YEROSHENKO, V.M. ; GIARRATANO, P.J. ; ARP, V.D.: A correlation for heat transfer to superphysical helium in turbulent flow in small channels. In: *Cryogenics* Bd. 17, Elsevier (1977), Nr. 10, S. 549–552
- [ZaGM06] ZANINO, R. ; GIORIS, S. ; MONDINO, R.: CFD modeling of ITER cable-in-conduit superconductors. Part II. Effects of spiral geometry on the central channel pressure drop. In: *Fusion Engineering and Design* Bd. 81 (2006), Nr. 23–24, S. 2605–2610

Appendix A

Annexure 1

EFFI sample code for DEMO

DEMO Case 1

UNITS

ANGLE=DEGREE CURRENT=A/M**2

LENGTH=M

TCURVE

NAME=N1

TOLLEN=0.5

TOLAN=0.5

**

RAD=48.898 R=54.050 T=0.000 ANG=6.28

**

RAD=3.0896 R=8.430 T=4.548 ANG=77.277

**

RAD=4.5785 R=8.372 T=3.060 ANG=55.61

**

RAD=10.3275 R=3.504 T=0.000 ANG=32.16

**

TCOIL

NAME=TFIT CURVE=N1 DR=1.595 DA=1.595 CURD=728300 NUMC=16

\$\$\$

B-CON 1.0 2.0 3.0 4.0 5.0 6.0 7.0 8.0 9.0 10.0 11.0 12.0 13.0 14.0\$

XZY

-15.000 0.500 15.000

-10.000 0.500 10.000

0.0 0 \$

XYZ

-15.000 0.500 15.000

-15.000 0.500 15.000

0.0 0 \$

Annexure 2

Modified solids.f file to run quench simulations in THEA

```

c
#####
##
c #
c # This set of functions define the properties of solid materials for
c # thermal components. They are called when in the Thermal block the
c # Model = user, or when a thermal material name is user's defined.
c #
c
#####
##
    function UserMaterialType(MaterialName)
c
#####
##
c #
c # Compute the electrical material type of a user's defined material
c #
    implicit none
c *
    character*(*) MaterialName
c *
    character*72 UserMaterialType
c *
c *   call WriteErrorMessage('UserMaterialType','WARNING - std called')
c *   UserMaterialType = ' '

    if (MaterialName.eq.'Bi2223') then
        UserMaterialType = 'SuperConductor'
    elseif (MaterialName.eq.'YBCO') then
        UserMaterialType = 'SuperConductor'

```

```

elseif (MaterialName.eq.'AgAu') then
  UserMaterialType = 'Alloy'
elseif (MaterialName.eq.'AgAuMg') then
  UserMaterialType = 'Alloy'
elseif (MaterialName.eq.'Constantan') then
  UserMaterialType = 'Metal'
elseif (MaterialName.eq.'Alumina') then
  UserMaterialType = 'Metal'
elseif (MaterialName.eq.'Epoxy_Resin') then
  UserMaterialType = 'Insulator'
elseif (MaterialName.eq.'Hastelloy') then
  UserMaterialType = 'Alloy'
elseif (MaterialName.eq.'Copper_new') then
  UserMaterialType = 'Metal'
elseif (MaterialName.eq.'Silver_new') then
  UserMaterialType = 'Metal'
else
  call WriteErrorMessage('UserMaterialType','WARNING - std called')
end if
c  WRITE(1,*) 'UserMaterialType: ', UserMaterialType
c  WRITE(1,*) 'UserMaterialName: ', MaterialName
c *
  return
end
c
#####
##
  function UserConductivity(MaterialName,X,T,B,RRR)
c
#####
##
c #
c # Compute the thermal conductivity of a user's defined solid material
c #
  implicit none
c *
  character*(*) MaterialName

```

```

real  X,T,B,RRR
c *
real  UserConductivity

real  Conductivity
integer MatId_Kapton,MatId_Epoxy,MaterialId
c *
c *  call WriteErrorMessage('UserConductivity','WARNING - std called')
c *  UserConductivity = 0.0
c *
if (MaterialName.eq.'Bi2223') then
  if (T.le.25) then
    UserConductivity = - 9.363929146591340E-06*T**4 +
&  3.418357487948720E-04*T**3 - 3.770813204576730E-03*T**2 +
&  8.829830917866000E-02*T + 1.165901771343890E+00
  elseif(T.gt.25.AND.T.le.110) then
    UserConductivity = 2.686135044008640E-09*T**5 -
&  7.274797347061920E-07*T**4 + 7.143703891228950E-05*T**3 -
&  3.894099867770100E-03*T**2 + 1.644530856919180E-01*T +
&  1.654292383055510E-01
  elseif(T.gt.110.AND.T.le.1000) then
    UserConductivity = - 1.119776724898080E-11*T**4 +
&  2.657008985129860E-08*T**3 - 2.229014971319300E-05*T**2 +
&  9.188156783093810E-03*T + 2.179840946397580E+00
  else
    call WriteErrorMessage('UserConductivity','T > 1000 K, K
& Bi2223 not defined')
    UserConductivity = 0.0
  endif
c *  UserConductivity = 10 * UserConductivity
c -----
c  if (X.lt.1e-4) then
c    WRITE(3,*) 'X =',X,'T =',T,'K Bi2223 =',UserConductivity
c  endif
c -----
elseif (MaterialName.eq.'AgAu') then
  if (T.le.30.2) then

```

```

    UserConductivity = 4.704470354610630E-05*T**4 -
& 3.071987725469680E-03*T**3 + 5.299859362132690E-02*T**2 +
& 1.220191039413780E+00*T - 5.552231372735610E-02
elseif(T.gt.30.2.AND.T.lt.352.9) then
    UserConductivity = - 5.168565137370710E-09*T**4 +
& 6.891378786858130E-06*T**3 - 3.421215329947760E-03*T**2 +
& 9.820953190115200E-01*T + 1.362236093767050E+01
else
    call WriteErrorMessage('UserConductivity','T > 352.9 K, K
& AgAu not defined')
    UserConductivity = 0.0
endif
UserConductivity = 100 * UserConductivity / 60.2
c *   UserConductivity = 10 * UserConductivity
c -----
c   if (X.lt.1e-4) then
c     WRITE(4,*) 'X =',X,'T =',T,'k AgAu =',UserConductivity
c   endif
c -----
elseif (MaterialName.eq.'Constantan') then
  if (X.le.0.00125) then
    if (T.lt.39.0) then
      UserConductivity =
& 1.61359e-08*T**6 -1.88525e-06*T**5
& +9.09209e-05*T**4 -2.61918e-03*T**3
& +4.65135e-02*T**2 +7.50680e-02*T -2.67721e-02
    elseif (T.ge.39.0.and.T.lt.79.0) then
      UserConductivity =
& 5.30104e-08*T**6 -1.92640e-05*T**5
& +2.87906e-03*T**4 -2.26208e-01*T**3
& +9.83880e+00*T**2 -2.24123e+02*T +2.10077e+03
    else
      UserConductivity =
& 6.69356e-13*T**6 -6.96715e-10*T**5
& +2.87675e-07*T**4 -5.94531e-05*T**3
& +6.27563e-03*T**2 -2.69821e-01*T +2.11991e+01
    endif

```

```

else
  MatId_Kapton = MaterialId('Polyimide')
  UserConductivity = Conductivity(MatId_Kapton,T,0,0)/1000
endif

c -----
c   if (X.lt.1e-4) then
c     WRITE(1,*) 'X =',X,'T =',T,'k_constantan =',UserConductivity
c   endif
c -----

elseif (MaterialName.eq.'Alumina') then
  if (X.le.0.00125) then
    if (T.lt.39.0) then
      UserConductivity =
&    1.61359e-08*T**6 -1.88525e-06*T**5
&    +9.09209e-05*T**4 -2.61918e-03*T**3
&    +4.65135e-02*T**2 +7.50680e-02*T -2.67721e-02
    elseif (T.ge.39.0.and.T.lt.79.0) then
      UserConductivity =
&    5.30104e-08*T**6 -1.92640e-05*T**5
&    +2.87906e-03*T**4 -2.26208e-01*T**3
&    +9.83880e+00*T**2 -2.24123e+02*T +2.10077e+03
    else
      UserConductivity =
&    6.69356e-13*T**6 -6.96715e-10*T**5
&    +2.87675e-07*T**4 -5.94531e-05*T**3
&    +6.27563e-03*T**2 -2.69821e-01*T +2.11991e+01
    endif
  else
    MatId_Kapton = MaterialId('Polyimide')
    UserConductivity = Conductivity(MatId_Kapton,T,0,0)/1000
  endif

c -----
c   if (X.lt.1e-4) then
c     WRITE(1,*) 'X =',X,'T =',T,'k_constantan =',UserConductivity
c   endif
c -----

elseif (MaterialName.eq.'Epoxy_Resin') then

```

```

if (X.le.0.00125) then
  MatId_Epoxy = MaterialId('Epoxy_Resin')
  UserConductivity = Conductivity(MatId_Epoxy,T,0,0)
else
  MatId_Epoxy = MaterialId('Epoxy_Resin')
  UserConductivity = Conductivity(MatId_Epoxy,T,0,0)/1000
endif
c -----
c   if (X.lt.1e-4) then
c     WRITE(2,*) 'X =',X,'T =',T,'k_epoxy =',UserConductivity
c   endif
c -----
elseif (MaterialName.eq.'AgAuMg') then
  call WriteErrorMessage('UserConductivity','WARNING-std called')
  call WriteErrorMessage('Conductivity of AgAuMg not defined
&           yet')
  UserConductivity = 0.0
elseif (MaterialName.eq.'YBCO') then
  call WriteErrorMessage('UserConductivity','WARNING-std called')
  call WriteErrorMessage('Conductivity of YBCO not defined yet')
  UserConductivity = 0.0
elseif (MaterialName.eq.'Hastelloy') then
  call WriteErrorMessage('UserConductivity','WARNING-std called')
  call WriteErrorMessage('Conductivity of Hastelloy not defined
&           yet')
  UserConductivity = 0.0
elseif (MaterialName.eq.'Silver_new') then
  call WriteErrorMessage('UserConductivity','WARNING-std called')
  call WriteErrorMessage('Conductivity of Silver not defined
&           yet')
  UserConductivity = 0.0
end if
c *   WRITE(3,*) 'UserConductivity: ', UserConductivity
c *
return
end

```

```

c
#####
##
    function UserCriticalCurrent(MaterialName,X,T,B,Epsilon)
c
#####
##
    c #
    c # Compute the critical current of a user's defined superconductor
    c #
    implicit none
c *
    character*(*) MaterialName
    real  X,T,B,Epsilon
c *
    real  UserCriticalCurrent
c *
c *   call WriteErrorMessage('UserCriticalCurrent',
c *   &   'WARNING - std called')
    UserCriticalCurrent = 1.0
c *
    return
    end
c
#####
##
    function UserCriticalTemperature(MaterialName,X,B,Epsilon)
c
#####
##
    c #
    c # Compute the critical temperature of a user's defined superconductor
    c #
    implicit none
c *
    character*(*) MaterialName
    real  X,B,Epsilon

```

```

c *
  real  UserCriticalTemperature
c *
c *   call WriteErrorMessage('UserCriticalTemperature',
c *   &   'WARNING - std called')
  UserCriticalTemperature = 1.0
c *
  return
  end

c
#####
##
  function UserCurrentSharing(MaterialName,X,B,Jop,Epsilon)
  c
#####
##
  c #
  c # Compute the current sharing temperature of a user's defined
  c # superconductor
  c #
  implicit none
c *
  character*(*) MaterialName
  real  X,B,Jop,Epsilon
c *
  real  UserCurrentSharing
c *
c *   call WriteErrorMessage('UserCurrentSharing',
c *   &   'WARNING - std called')
  UserCurrentSharing = 1.0
c *
  return
  end

c
#####
##
  function UserDensity(MaterialName,X,T)

```

```

c
#####
##
c #
c # Compute the density of a user's defined solid material
c #
    implicit none
c *
    character*(*) MaterialName
    real    X,T
c *
    real    UserDensity
c *
c *    call WriteErrorMessage('UserDensity','WARNING - std called')
c *    UserDensity = 0.0
c *
    if (MaterialName.eq.'Bi2223') then
        UserDensity = 5400.0
    elseif (MaterialName.eq.'AgAu') then
        UserDensity = 10633.0
    elseif (MaterialName.eq.'AgAuMg') then
* For the moment I took the same as AgAu
        UserDensity = 10633.0
    elseif (MaterialName.eq.'Constantan') then
        UserDensity = 8900
    elseif (MaterialName.eq.'Alumina') then
        UserDensity = 4025
    elseif (MaterialName.eq.'Epoxy_Resin') then
        UserDensity = 1150
    elseif (MaterialName.eq.'YBCO') then
        UserDensity = 6380.0
    elseif (MaterialName.eq.'Hastelloy') then
c * Hastelloy
        UserDensity = 8890.0
c * NiW
c *    UserDensity = 8800.0d0
c * Copper_new

```

```

elseif (MaterialName.eq.'Copper_new') then
  UserDensity = 8960.0
c * Silver_new
elseif (MaterialName.eq.'Silver_new') then
  UserDensity = 10630.0
else
  call WriteErrorMessage('UserMaterialType','WARNING - std called')
end if
c  WRITE(4,*) 'UserDensity:', UserDensity

return
end

c
#####
##
function UserResistivity(MaterialName,X,T,B,RRR)
c
#####
##
c #
c # Compute the electrical resistivity of a user's defined material
c #
implicit none
c *
character*(*) MaterialName
real  X,T,B,RRR
c *
real  UserResistivity
c *
c * call WriteErrorMessage('UserResistivity','WARNING - std called')
UserResistivity = 1.0
c *
return
end

c
#####
##

```

```
function UserSpecificHeat(MaterialName,X,T,B,Tcs,Epsilon)
```

```
c
```

```
#####
```

```
##
```

```
c #
```

```
c # Compute the specific heat of a user's defined solid material
```

```
c #
```

```
implicit none
```

```
c *
```

```
character*(*) MaterialName
```

```
real X,T,B,Tcs,Epsilon
```

```
c *
```

```
c * real UserSpecificHeat
```

```
c *
```

```
c * call WriteErrorMessage('UserSpecificHeat','WARNING - std called')
```

```
c * UserSpecificHeat = 0.0
```

```
c *
```

```
C * fit variables
```

```
REAL T0
```

```
REAL TMIN,TMAX
```

```
DATA T0 / 40.0 /
```

```
DATA TMIN / 4.0/, TMAX / 400.0/
```

```
REAL A,BB,C,D,E,F
```

```
DATA A /-7.56748553820916E-10/, BB /6.3514526420169E-7/
```

```
DATA C /-1.9479757865476E-4/ , D /2.3616673974415E-2/
```

```
DATA E /2.39331954284042E-1/ , F /-1.09619172128011E+0/
```

```
SAVE
```

```
C * local variables
```

```
REAL TT
```

```
INTEGER i,j
```

```
REAL Temp(360), Integral(360)
```

```
REAL N, k_b, D_Ef, theta
```

```
REAL cp_e, cp_ph
```

```
REAL ind_Temp, Integral_val
```

```
REAL beta,gam,cp_low,cp_300
```

```
REAL g1,h1,i1,l1,m1,n1,a1,a2,a3,a4
```

```
c * -----
```

```

c * THERE IS A PROBLEM WITH THE E+44, WHICH IS TOO BIG !!!
c * FOR THE MOMENT I COMMENTED THE 2 FOLLOWING LINES :
c *   DATA N / 9.47739156704746E+24/, k_b / 1.38054E-23 /,
c *   &   D_Ef / 2.1211684621511E+44/, theta / 371 /
c * -----
      DATA Integral   /2.469550E+001, 2.451510E+001, 2.432210E+001,
&          2.411700E+001, 2.390010E+001, 2.367220E+001,
&          2.343380E+001, 2.318550E+001, 2.292810E+001,
&          2.266220E+001, 2.238860E+001, 2.210810E+001,
&          2.182120E+001, 2.152890E+001, 2.123170E+001,
&          2.093040E+001, 2.062560E+001, 2.031790E+001,
&          2.000810E+001, 1.969650E+001, 1.938390E+001,
&          1.907080E+001, 1.875750E+001, 1.844470E+001,
&          1.813260E+001, 1.782180E+001, 1.751250E+001,
&          1.720520E+001, 1.690010E+001, 1.659760E+001,
&          1.629780E+001, 1.600100E+001, 1.570750E+001,
&          1.541740E+001, 1.513080E+001, 1.484800E+001,
&          1.456910E+001, 1.429410E+001, 1.402320E+001,
&          1.375640E+001, 1.349380E+001, 1.323550E+001,
&          1.298150E+001, 1.273180E+001, 1.248640E+001,
&          1.224540E+001, 1.200880E+001, 1.177650E+001,
&          1.154860E+001, 1.132490E+001, 1.110560E+001,
&          1.089050E+001, 1.067960E+001, 1.047290E+001,
&          1.027030E+001, 1.007180E+001, 9.877390E+000,
&          9.686900E+000, 9.500350E+000, 9.317650E+000,
&          9.138750E+000, 8.963600E+000, 8.792130E+000,
&          8.624280E+000, 8.459980E+000, 8.299170E+000,
&          8.141780E+000, 7.987760E+000, 7.837030E+000,
&          7.689530E+000, 7.545200E+000, 7.403970E+000,
&          7.265780E+000, 7.130570E+000, 6.998270E+000,
&          6.868830E+000, 6.742170E+000, 6.618250E+000,
&          6.497000E+000, 6.378370E+000, 6.262290E+000,
&          6.148720E+000, 6.037580E+000, 5.928840E+000,
&          5.822430E+000, 5.718300E+000, 5.616400E+000,
&          5.516680E+000, 5.419100E+000, 5.323590E+000,
&          5.230120E+000, 5.138630E+000, 5.049080E+000,
&          4.961430E+000, 4.875630E+000, 4.791640E+000,

```

& 4.709410E+000, 4.628910E+000, 4.550100E+000,
& 4.472930E+000, 4.397360E+000, 4.323370E+000,
& 4.250910E+000, 4.179950E+000, 4.110450E+000,
& 4.042390E+000, 3.975710E+000, 3.910400E+000,
& 3.846420E+000, 3.783740E+000, 3.722330E+000,
& 3.662170E+000, 3.603210E+000, 3.545440E+000,
& 3.488820E+000, 3.433340E+000, 3.378960E+000,
& 3.325660E+000, 3.273410E+000, 3.222190E+000,
& 3.171980E+000, 3.122750E+000, 3.074490E+000,
& 3.027160E+000, 2.980750E+000, 2.935240E+000,
& 2.890600E+000, 2.846820E+000, 2.803880E+000,
& 2.761760E+000, 2.720440E+000, 2.679900E+000,
& 2.640130E+000, 2.601110E+000, 2.562810E+000,
& 2.525240E+000, 2.488360E+000, 2.452170E+000,
& 2.416640E+000, 2.381780E+000, 2.347550E+000,
& 2.313950E+000, 2.280960E+000, 2.248570E+000,
& 2.216770E+000, 2.185550E+000, 2.154880E+000,
& 2.124770E+000, 2.095190E+000, 2.066140E+000,
& 2.037600E+000, 2.009570E+000, 1.982040E+000,
& 1.954980E+000, 1.928400E+000, 1.902290E+000,
& 1.876620E+000, 1.851410E+000, 1.826620E+000,
& 1.802270E+000, 1.778330E+000, 1.754800E+000,
& 1.731670E+000, 1.708930E+000, 1.686580E+000,
& 1.664600E+000, 1.642990E+000, 1.621740E+000,
& 1.600850E+000, 1.580310E+000, 1.560100E+000,
& 1.540230E+000, 1.520680E+000, 1.501460E+000,
& 1.482540E+000, 1.463940E+000, 1.445640E+000,
& 1.427630E+000, 1.409920E+000, 1.392480E+000,
& 1.375330E+000, 1.358450E+000, 1.341840E+000,
& 1.325490E+000, 1.309400E+000, 1.293560E+000,
& 1.277970E+000, 1.262620E+000, 1.247520E+000,
& 1.232640E+000, 1.218000E+000, 1.203580E+000,
& 1.189390E+000, 1.175410E+000, 1.161640E+000,
& 1.148090E+000, 1.134740E+000, 1.121590E+000,
& 1.108640E+000, 1.095880E+000, 1.083310E+000,
& 1.070940E+000, 1.058740E+000, 1.046730E+000,
& 1.034890E+000, 1.023230E+000, 1.011740E+000,

& 1.000410E+000, 9.892560E-001, 9.782590E-001,
& 9.674220E-001, 9.567410E-001, 9.462140E-001,
& 9.358380E-001, 9.256100E-001, 9.155280E-001,
& 9.055890E-001, 8.957910E-001, 8.861310E-001,
& 8.766070E-001, 8.672160E-001, 8.579570E-001,
& 8.488270E-001, 8.398230E-001, 8.309450E-001,
& 8.221880E-001, 8.135530E-001, 8.050350E-001,
& 7.966350E-001, 7.883480E-001, 7.801750E-001,
& 7.721120E-001, 7.641580E-001, 7.563110E-001,
& 7.485700E-001, 7.409320E-001, 7.333960E-001,
& 7.259600E-001, 7.186230E-001, 7.113830E-001,
& 7.042380E-001, 6.971880E-001, 6.902290E-001,
& 6.833620E-001, 6.765840E-001, 6.698940E-001,
& 6.632900E-001, 6.567720E-001, 6.503380E-001,
& 6.439860E-001, 6.377160E-001, 6.315260E-001,
& 6.254140E-001, 6.193800E-001, 6.134220E-001,
& 6.075390E-001, 6.017300E-001, 5.959940E-001,
& 5.903300E-001, 5.847370E-001, 5.792120E-001,
& 5.737570E-001, 5.683680E-001, 5.630460E-001,
& 5.577900E-001, 5.525980E-001, 5.474690E-001,
& 5.424030E-001, 5.373980E-001, 5.324540E-001,
& 5.275700E-001, 5.227440E-001, 5.179760E-001,
& 5.132660E-001, 5.086120E-001, 5.040130E-001,
& 4.994680E-001, 4.949780E-001, 4.905410E-001,
& 4.861560E-001, 4.818220E-001, 4.775390E-001,
& 4.733060E-001, 4.691230E-001, 4.649880E-001,
& 4.609010E-001, 4.568610E-001, 4.528680E-001,
& 4.489210E-001, 4.450190E-001, 4.411610E-001,
& 4.373480E-001, 4.335770E-001, 4.298500E-001,
& 4.261650E-001, 4.225210E-001, 4.189180E-001,
& 4.153560E-001, 4.118340E-001, 4.083510E-001,
& 4.049060E-001, 4.015000E-001, 3.981320E-001,
& 3.948000E-001, 3.915060E-001, 3.882480E-001,
& 3.850250E-001, 3.818380E-001, 3.786850E-001,
& 3.755670E-001, 3.724820E-001, 3.694310E-001,
& 3.664120E-001, 3.634270E-001, 3.604730E-001,
& 3.575510E-001, 3.546600E-001, 3.518000E-001,

```

&      3.489700E-001, 3.461700E-001, 3.434000E-001,
&      3.406590E-001, 3.379470E-001, 3.352630E-001,
&      3.326080E-001, 3.299800E-001, 3.273790E-001,
&      3.248060E-001, 3.222590E-001, 3.197390E-001,
&      3.172440E-001, 3.147750E-001, 3.123320E-001,
&      3.099130E-001, 3.075190E-001, 3.051500E-001,
&      3.028050E-001, 3.004830E-001, 2.981850E-001,
&      2.959100E-001, 2.936580E-001, 2.914290E-001,
&      2.892220E-001, 2.870370E-001, 2.848740E-001,
&      2.827320E-001, 2.806110E-001, 2.785120E-001,
&      2.764330E-001, 2.743750E-001, 2.723370E-001,
&      2.703190E-001, 2.683200E-001, 2.663420E-001,
&      2.643820E-001, 2.624410E-001, 2.605200E-001,
&      2.586170E-001, 2.567320E-001, 2.548650E-001/
C      % Integral part of the phonon contribution from 41 to 400 K with Delta_T =
1 K
  SAVE
  c *
  real  UserSpecificHeat,SpecificHeat
  integer MatId_Kapton,MatId_Epoxy,MaterialId
  c *
  c * call WriteErrorMessage('UserSpecificHeat','WARNING - std called')
  C *
  DO 10, i=1,360
    Temp(i) = i+40
10 CONTINUE

  TT=T
  TT=MAX(TT,TMIN)
  TT=MIN(TT,TMAX)

  if (MaterialName.eq.'Bi2223') then
    if (T.le.200) then
      UserSpecificHeat = -6.916672678274560E-09*T**5 +
&  3.889910000612640E-06*T**4 - 8.005849754884250E-04*T**3 +
&  7.212439094688730E-02*T**2 - 3.366884731715880E-01*T +
&  2.898264121468130E-02

```

```

elseif(T.gt.200.AND.T.lt.300) then
  UserSpecificHeat = - 4.062499999999860E-03*T**2 +
& 2.675535714285670E+00*T + 5.092857142857450E+01
  else
    call WriteErrorMessage('UserSpecificHeat','T > 300 K, Cp
& Bi2223 not defined')
    UserSpecificHeat=0.0
  endif
c   UserSpecificHeat = UserSpecificHeat / 10
c -----
c   if (X.lt.1e-4) then
c     WRITE(3,*) 'X =',X,'T =',T,'Cp Bi2223 =',UserSpecificHeat
c   endif
c -----
elseif (MaterialName.eq.'AgAu') then
  if (T.le.50) then
    UserSpecificHeat = 1.151014273836900E-06*T**5 -
& 1.669388838156370E-04*T**4 + 7.580236622236280E-03*T**3 -
& 6.875293827061390E-02*T**2 + 2.888357884384530E-01*T -
& 3.043552459555570E-01
  elseif(T.gt.50.AND.T.lt.300) then
    UserSpecificHeat = 6.04641400560E-10*T**5 -
& 6.55419968950E-07*T**4 + 2.80828657560E-04*T**3 -
& 6.03487450540E-02*T**2 + 6.77049021750E+00*T -
& 1.12101992760E+02
  else
    call WriteErrorMessage('UserSpecificHeat','T > 300 K, Cp
& AgAu not defined')
    UserSpecificHeat=0.0
  endif
c   UserSpecificHeat = UserSpecificHeat / 10
c -----
c   if (X.lt.1e-4) then
c     WRITE(4,*) 'X =',X,'T =',T,'Cp AgAu =',UserSpecificHeat
c   endif
c -----
elseif (MaterialName.eq.'Constantan') then

```

```

if (X.le.0.00125) then
  if (T.lt.49.0) then
    UserSpecificHeat =
&    4.60481e-08*T**6 -6.80894e-06*T**5
&    +3.42956e-04*T**4 -6.23154e-03*T**3
&    +5.69572e-02*T**2 -7.42851e-02*T +1.52765e-01
  elseif (T.ge.49.0.and.T.lt.99.0) then
    UserSpecificHeat =
&    1.64998e-08*T**6 -7.94692e-06*T**5
&    +1.56282e-03*T**4 -1.61193e-01*T**3
&    +9.19556e+00*T**2 -2.70884e+02*T+3.25752e+03
  else
    UserSpecificHeat =
&    4.34459e-11*T**6 -5.47291e-08*T**5
&    +2.80367e-05*T**4 -7.43307e-03*T**3
&    +1.06458e+00*T**2 -7.62130e+01*T+2.35439e+03
  endif
else
  MatId_Kapton = MaterialId('Polyimide')
  UserSpecificHeat = SpecificHeat(MatId_Kapton,T,0,
&    Tcs,Epsilon) / 1000
endif

c -----
c   if (X.lt.1e-4) then
c     WRITE(1,*) 'X =',X,'T =',T,'Cp consta =',UserSpecificHeat
c   endif
c -----

elseif (MaterialName.eq.'Alumina') then
  if (X.le.0.00125) then
    UserSpecificHeat = 1000 * (
&    -3.011359441447570e-15*T**6
&    +4.155892525668420e-12*T**5
&    -2.052840726929160e-09*T**4
&    +3.999433040371980e-07*T**3
&    -1.545516798717730e-05*T**2
&    +4.030366857534770e-04*T
&    +8.321270763644860e-05)

```

```

else
  MatId_Kapton = MaterialId('Polyimide')
  UserSpecificHeat = SpecificHeat(MatId_Kapton,T,0,
&          Tcs,Epsilon) / 1000
endif
c -----
c   if (X.lt.1e-4) then
c     WRITE(1,*) 'X =',X,'T =',T,'Cp Alumina =',UserSpecificHeat
c   endif
c -----
elseif (MaterialName.eq.'Epoxy_Resin') then
  if (X.le.0.00125) then
    MatId_Epoxy = MaterialId('Epoxy_Resin')
    UserSpecificHeat = SpecificHeat(MatId_Epoxy,T,0,Tcs,Epsilon)
  else
    MatId_Epoxy = MaterialId('Epoxy_Resin')
    UserSpecificHeat = SpecificHeat(MatId_Epoxy,T,0,
&          Tcs,Epsilon) / 1000
  endif
c -----
c   if (X.lt.1e-4) then
c     WRITE(2,*) 'X =',X,'T =',T,'Cp epoxy =',UserSpecificHeat
c   endif
c -----
elseif (MaterialName.eq.'AgAuMg') then
  call WriteErrorMessage('UserSpecificHeat','WARNING-std called')
  UserSpecificHeat=0.0
elseif (MaterialName.eq.'YBCO') then
  UserSpecificHeat = A*TT**5 + BB*TT**4 + C*TT**3 +
&          D*TT**2 + E*TT + F
elseif (MaterialName.eq.'Hastelloy') then
c * Hastelloy
  IF(TT.GT.TMAX) THEN
    UserSpecificHeat=429.34
  ELSEIF (TT.LE.T0) THEN
    cp_ph = 5.99E-4 * TT**3
    cp_e = 1.33E-1 * TT

```

```

ELSEIF (TT.GT.T0) THEN
  cp_e = 1.33E-1 * TT
  do 20, j = 1,360
    if (Temp(j) .eq. TT) then
      ind_Temp = j
      integral_val = Integral(j)
      exit
    elseif (Temp(j) .gt. TT) then
      ind_Temp = j
      integral_val = Integral(j-1) + (Integral(j) -
&          Integral(j-1))
&          /(Temp(j) - Temp(j-1)) * (TT - Temp(j-1))
      exit
    endif
20  continue
  cp_ph = 9*N*k_b*(TT/theta)**3 * integral_val
ENDIF
UserSpecificHeat = cp_e + cp_ph
c * NiW
c *   IF (T.le.100) THEN
c *     UserSpecificHeat = (5.305223E-06)*T**4 - (1.819265E-03)*T**3 +
c * &     (2.171073E-01)*T**2 - 7.399751*T + 8.964978E+01
c *   ELSE
c *     UserSpecificHeat = (-2.275717E-08)*T**4 + (4.273496E-05)*T**3-
c * &     (2.433487E-02)*T**2 + 6.147619*T - 1.787338E+02
c *   ENDIF
c * Copper database
  elseif (MaterialName.eq.'Copper_new') then
    beta = 0.0011
    gam = 0.011
    cp_300 = 3.454d6
    cp_low = beta * T ** 3 + gam * T
    UserSpecificHeat = 1/((1/cp_300+1/(cp_low*8960))*8960)
c * Silver database
  elseif (MaterialName.eq.'Silver_new') then
    g1 = 7.32004351555293e-10
    h1 = -7.70491558847795e-07

```

```
i1 = 0.000322580551281146
l1 = -0.0680507660128324
m1 = 7.45462336836355
n1 = -131.433647503242
a1=0.00155058200152750
a2=1.32544504052410e-06
a3=0.00595103979776042
a4=5.91469832756015e-05

if (T.lt.30) then
  UserSpecificHeat = a1*T**3+a2*T**2+a3*T+a4
elseif(T.ge.30.AND.T.lt.300) then
  UserSpecificHeat = g1*T**5+h1*T**4+i1*T**3+l1*T**2+m1*T+n1
else
  UserSpecificHeat = 227.1761
end if
else
  call WriteErrorMessage('UserSpecificHeat','WARNING - std called')
end if
c *  WRITE(3,*) 'UserSpecificHeat: ', UserSpecificHeat
c *
return
end
```

Annexure 3

Input file for THEA

Begin Model

```

ModelName      'DEMO PROCESS JULY 2012'
Length         39.0

;
; setting the CurrentModel to "user" triggers a call to the user routine
; UserCurrent
;
CurrentModel   constant
InitialCurrent 50000

;
; setting the MagneticFieldModel to "user" triggers a call to the user
; routine userMagneticField
;
MagneticFieldModel constant
MagneticFieldSS      13.5    13.5

end

```

Begin Thermals

```

Components     2

Model          constant      constant
NrMaterials    2              1

; note the reference to standard materials "Copper" and "AISI304_Steel"
; in contrast to the reference to a material name that is not in the
; material database "PFCI_NbTi". This triggers calls to user defined
; solid material properties

Materials      Copper      YBCO              Hastelloy

```

```

Area          555.0e-6    1.826e-6          91.3e-6
RRR           100.0      0.0                0.0
E0            1.0e-4          0.0
nPower        30

```



```

QModel        window      none
Q             7.1409351E3    0.0
Q_Tau        1e-1          0.0
Q_XBegin     19.0           0.0
Q_XEnd       20.0           0.0
; Q=4.965 when thermal resistance is 2.0e-3

```



```

InitialCondition  constant      constant
TInitial         4.5                4.5

```



```

BoundaryType    heat          heat
                heat          heat
BoundaryConditions  constant      constant
                constant      constant
qBoundary       0.0           0.0
                0.0           0.0

```



```

Links_Model     constant
ThermalResistance  2.0e-3

```

end

Begin Hydraulics

```

Components      1
Fluid           Helium
Model           constant
Area            272.209e-6
Dh              5.3903E-03

```

```

fModel      user
hModel      DB

Links_Model  none

InitialCondition  constant
TInitial        4.5
pInitial        10.0e5
mdotInitial     2.0e-3

QModel        none
; Q           1.8
; Q_XBegin    0
; Q_XEnd      721.0

BoundaryType   reservoir   reservoir
BoundaryConditions  constant   constant
TBoundary     4.5          4.5001
pBoundary     10.0e5       9.9993E5
; mdotBoundary      2.0e-3   2.0e-3
; DP for 100 W using Hess was 0.06822 bar so the pressure drop per unit
; length was calculated and used for 39 meters

end

Begin Links
; The S_H_Links_Model determines that the wetted perimeter is a constant
; along the length. The order matters, the links are in the following
; sequence:
;
; Thermal 1 <---> Hydraulic 1
; Thermal 2 <---> Hydraulic 1
; Thermal 3 <---> Hydraulic 1
;
; The wetted perimeter is then defined for each link, in the same sequence

```

S_H_Links_Model constant

 constant

WettedPerimeter 0.202

 0.0

; wetted perimeter is of 11 super strands ($2\pi r$) and due to compaction it is reduced to 65%.

; the second component is hastloy to helium which is 0 in this case.

end

Begin Simulation

MeshType uniform

NrElements 100

ElementOrder 1

ElementNodes 2

StartTime 0.0

EndTime 20.0

OutputStep 1.0E-1

TimeMethod EulerBackward

MinimumStep 1.0e-6

MaximumStep 1.0e-1

StepEstimate smooth

ErrorEstimate change

ErrorControl none

Tolerance 1.0e-2

LogFile DEMO_ht5.log

StorageFile DEMO_ht5.store

end

Appendix 4

Sample output file of THEA

THEA Version 2.1

file created at 13/08/2015 10:59:56

Storage file: DEMO_ht5.store

Model

=====

Name..... DEMO PROCESS JULY 2012
 Length [m]..... 3.900E+01
 Current flag..... constant
 Initial Current [A]..... 5.000E+04
 Tau Detection [s]..... 0.000E+00
 Tau Dump [s]..... 0.000E+00
 Magnetic Field flag..... constant
 B Steady State [T]..... 1.350E+01 1.350E+01
 B Transient [T]..... 0.000E+00 0.000E+00
 Strain flag..... None
 Strain Steady State [-]..... 0.000E+00 0.000E+00
 Strain Transient [-]..... 0.000E+00 0.000E+00

Simulation

=====

Mesh..... uniform
 Nr of Elements..... 100
 Nr of Nodes..... 101
 Nr of Nodes per Element..... 2
 Order of Element..... 1
 Mesh Adaptivity..... None
 TimeMethod..... EulerBackward
 Tolerance..... 1.000E-02
 ErrorEstimate..... change
 ErrorControl..... none
 StepEstimate..... smooth
 ArtificialViscosity..... Upwind
 Start Time [s]..... 0.000E+00

End Time [s]..... 2.000E+01
 Minimum Step [s]..... 1.000E-06
 Maximum Step [s]..... 1.000E-01
 Output Step [s]..... 1.000E-01

Thermals

=====

Nr of Components..... 2
 Link Model..... constant
 Thermal Resistance [K m/W]..... 2.000E-03
 Component..... 1
 Nr of Materials..... 2
 Materials..... Copper YBCO
 Initial Conditions..... constant
 Initial Temperature [K]..... 4.500E+00
 Boundary..... 1
 Boundary Condition..... constant
 Boundary Type..... heat
 Boundary Temperature [K].... 0.000E+00
 Boundary Heat [W]..... 0.000E+00
 Boundary..... 2
 Boundary Condition..... constant
 Boundary Type..... heat
 Boundary Temperature [K].... 0.000E+00
 Boundary Heat [W]..... 0.000E+00
 Model flag..... constant
 Area [m**2]..... 5.550E-04 1.826E-06
 RRR [-]..... 1.000E+02 0.000E+00
 E0 [V/m]..... 1.000E-04
 n-power [-]..... 30
 Heat source model..... window
 Heating [W/m]..... 7.141E+03
 XBegin [m]..... 1.900E+01
 XEnd [m]..... 2.000E+01
 Tau [s]..... 1.000E-01
 Component..... 2

Nr of Materials..... 1
 Materials..... Hastelloy
 Initial Conditions..... constant
 Initial Temperature [K]..... 4.500E+00
 Boundary..... 1
 Boundary Condition..... constant
 Boundary Type..... heat
 Boundary Temperature [K].... 0.000E+00
 Boundary Heat [W]..... 0.000E+00
 Boundary..... 2
 Boundary Condition..... constant
 Boundary Type..... heat
 Boundary Temperature [K].... 0.000E+00
 Boundary Heat [W]..... 0.000E+00
 Model flag..... constant
 Area [m**2]..... 9.130E-05
 RRR [-]..... 0.000E+00
 E0 [V/m]..... 0.000E+00
 n-power [-]..... 0
 Heat source model..... none

Hydraulics

=====

Nr of Components..... 1
 Fluid..... Helium
 Initial Conditions..... constant
 Initial Temperature [K]..... 4.500E+00
 Initial Pressure [Pa]..... 1.000E+06
 Initial massflow [Kg/s]..... 2.000E-03
 Boundary..... 1
 Boundary Condition..... constant
 Boundary Type..... reservoir
 Boundary Temperature [K]..... 4.500E+00
 Boundary Pressure [Pa]..... 1.000E+06
 Boundary massflow [Kg/s]..... 0.000E+00
 Boundary..... 2

Boundary Condition..... constant
 Boundary Type..... reservoir
 Boundary Temperature [K]..... 4.500E+00
 Boundary Pressure [Pa]..... 9.999E+05
 Boundary massflow [Kg/s]..... 0.000E+00
 Model flag..... constant
 Area [m**2]..... 2.722E-04
 Dh [m]..... 5.390E-03
 Friction Factor [-]..... 0.000E+00
 Heat Transfer Coeff. [W/m**2 K] 0.000E+00
 fModel..... user
 hModel..... DB
 Heat source model..... none
 Heating [W/m]..... 0.000E+00
 XBegin [m]..... 0.000E+00
 XEnd [m]..... 0.000E+00
 Tau [s]..... 0.000E+00
 Link Model..... none

Thermals-Hydraulics Links

=====

Links Model

| Hydraulic
Thermal	1
 1 | constant
 2 | constant

Wetted Perimeter [m]

| Hydraulic
Thermal	1
 1 | 0.202E+00
 2 | 0.000E+00

thermal 1

Time	Resistance
[s]	[Ohm]
0.0000E+00	0.0000E+00
1.0000E-01	2.9503E-07
2.0000E-01	2.9427E-07
3.0000E-01	2.9255E-07
4.0000E-01	2.8534E-07
5.0000E-01	2.6847E-07
6.0000E-01	2.1931E-07
7.0000E-01	1.6043E-07
8.0000E-01	1.1569E-07

Appendix C: Designations and abbreviations

ABAD - Alternating-Beam-Assisted-Deposition
AC - Altering Current
Ag - Copper
AMSC - American Superconductor
ASDEX – Axially Symmetric Divertor Experiment
BiSSCO - bismuth-strontium-calcium-copper oxide
CAD – Computer Aided Design
CASTOR – Czech Academy of Sciences TORus
CICC - Cable-In Conduit Conductors
COMPASS - COMPact ASSEMBly
CORC - Conductor on Round Core
CSD - Chemical Solution Deposition
DDD - Design Description Document
EFFI - electromagnetic fields, forces and inductance calculation
EU DEMO – European Demonstration
EURATOM - European Atomic Energy Community
HTS – High Temperature Superconductor
IBAD - Ion-Beam-Assisted-Deposition
ITEP - Institute for Technical Physics
ITER - International Thermonuclear Experimental Reactor
ISD - Inclined-Substrate-Deposition
ISTEC - International Superconductivity Technology Center
JET - Joint European Torus
KERI - Korea Electrotechnology Research Institute
KIT - Karlsruhe Institute of Technology
LCT – Large Coil Task
LHD - Large Helical Device
LTS – Low Temperature Superconductors
MAGLEV - Magnetically Levitated
MgB₂ - Magnesium diboride
MgO - Magnesium Oxide
MHD - Magneto Hydrodynamic
MOD - Metal Organic Decomposition

MOCVD - Metal Organic Chemical Vapour Decomposition
NbTi - Niobium-titanium
Nb₃Sn - Niobium–tin
PDE - partial differential equation
PLD - Pulsed Later Decomposition
PVD - Physical Vacuum Deposition
RABiTS - Rolling Assisted Biaxially Textured Substrates
RACC - Roebel Assembled Coated Conductor
RCE-CDR - Reactive Co-Evaporation and Cyclic Deposition Reaction
RCE-DR - Reactive Co-Evaporation and Deposition Reaction
REBCO - Rare-Earth-Barium-Copper-Oxide
SC – Superconductor
SMES - Superconducting Magnetic Energy Storage
SS – Stainless Steel
SS316LN - Stainless Steel Grade 316LN
STORAC - Spherical Torus Reactor Analysis Code
SWCC - Showa Cable Systems Co., Ltd
TETRA - TOKAMAK Engineering Test Reactor Analysis
TF – Toroidal Field
TFC - Toroidal Field Coil
TFTR - Tokamak Fusion Test Reactor
THEA - Thermal, Hydraulic and Electric Analysis
TOKEF - tokamak input generator for EFFI
TSTC - Twisted Stacked Tape Cables
USA – United States of America
USSR – Union of Soviet Socialist Republics
UK – United Kingdom
Y₂O₃ - Yttria
YBCO - Yttrium-Barium-Copper oxide
YSZ - Yttria-Stabilized Zirconia

Appendix D: Index of Symbols

μm – Micrometer
 ρ_{he} - helium density
 u - helium dynamic viscosity
 $\Omega\text{-m}$ – electrical resistivity
 Δp - pressure drop
 $^{\circ}\text{C}$ – degree centigrade
 Bar - Pressure
 B_c - Critical Magnetic Field
 C_p - Helium Specific Heat
 C_{he} - Heat Capacity of Helium
 D_{he} - Hydraulic Diameter of Helium
 f_{he} - Friction Factor of Helium
 GPa – Giga Pascal
 GJ – Giga Joule
 h - Heat Transfer Coefficient
 H – Thermal Resistance
 H_c - single critical magnetic field
 H_{c1} - lower critical magnetic field
 H_{c2} - higher critical magnetic field
 I - current
 J_c - critical current density
 K - thermal conductivity
 K - Kelvin
 kA - Kilo Ampere
 kV - Kilovolts
 L_0 - Lorenz number
 \dot{m} - mass flow
 m - meter
 mm - millimeter
 MA- Miga Ampere
 MN – Mega newton
 MPa – Mega pascal
 ms - milliseconds
 mV – milli volts

N/m² - Pressure

p_{he} – pressure of helium

R - interstrand resistance

t_{del} – Time Delay

T – Tesla

T_c - Critical Temperature

T_{co} - temperature of the conductor

T_{he} - temperature of helium

s - seconds

QD – Discharge Voltage

v_{he} - velocity of helium

W – Watts